MATHEMATICAL MODELLING OF MULTIPLE PULSED LASER PERCUSSION DRILLING

A thesis submitted to The University of Manchester
for the degree of
Doctor of Philosophy (PhD)
in the Faculty of Engineering and Physical Sciences

2011

MATUROSE SUCHATAWAT

School of Mechanical, Aerospace and Civil Engineering

TABLE OF CONTENTS

LIST OF FIGURES

CHAPTER 4 LITERATURE REVIEW-LASER DRILLING MOELS

CHAPTER 5 MATHEMATICAL FORMULATION

CHAPTER 6 EXPERIMENTAL PROCEDURES FOR MODEL
VERIFICATION

CHAPTER 7 RESULTS AND DISCUSSION

LIST OF TABLES

ABSTRACT

Name of the University: The University of Manchester
Submitted by: Maturose Suchatawat
Degree Title: Doctor of Philosophy
Thesis Title: Mathematical Modelling of Multiple Pulsed Laser Percussion Drilling
Date: 30-09-2011

In laser percussion drilling, a series of laser pulses with specified energies and durations irradiate the workpiece surface to gradually heat, melt, and vaporise material until a hole with required depth and diameter is achieved. Despite being the quickest technique for producing small diameter holes, laser percussion drilling regularly suffers from difficulties in controlling the hole quality such as hole circularity, hole taper and recast layer. Therefore, in order to produce holes to a specific requirement at minimum cost and time, it is crucial to fully understand the effects of each parameter on hole quality.

In this research, a new mathematical model for multiple pulsed laser drilling is developed to predict the hole depth, hole taper, and recast layer thickness, and to investigate the effects of key laser parameters on hole dimensions. The new model accounts for recoil pressure, melt ejection, O_2 assist gas effects, as well as solidification of the melt. The development of the new model is divided into two stages; pulse on stage where interaction between laser beam-material takes place, and pulse off stage where solidification of the melt is modelled. Governing equations are established from heat conduction, energy, and mass equations at the solid-liquid and liquid-vapour interfaces with appropriate boundary and initial conditions. Analytical solutions are derived by using Mathematica 7 software as a tool to solve the system of non-linear equations.

To validate the model, experimental work has been conducted and the measured results are compared to those calculated from the model. It is shown that the new model gives a good prediction of the hole depth and acceptable prediction of the recast layer thickness. Laser peak power and pulse width are shown to have a significant influence over the drilled hole quality whereas the changes due to pulse frequency are less pronounced.

DECLARATION

I hereby declare that no portion of the work referred to in the thesis has been submitted in support of an application for another degree or qualification of this or any other university, or other institute of learning.

<div align="right">

Maturose Suchatawat

September 2011

</div>

COPYRIGHT STATEMENT

ACKNOWLEDGEMENTS

First and foremost, I would like to express my sincerest gratitude to my supervisors, Dr.Mohammad Sheikh and Prof.Lin Li, who have supported me throughout my thesis with their patience and knowledge whilst allowing me the room to work in my own way. Without their kind supervision and encouragement, the completion of this thesis would not have been possible.

Besides my supervisors, I wish to acknowledge the contributions, advice, and suggestions of Dr.Andrew Pinkerton, who has devoted his time in reviewing my modelling work and helping in derive those complicated equations. My special thanks also go to Dr.Kursad Sezer and Dr.David Whitehead for their generous support throughout my lab works. Whenever I have difficulties in the lab, they are always more than welcome to assist.

I am indebted to the wonderful staffs and colleagues at the Laser Processing Research Centre (LPRC) for sharing all the limitless knowledge and experiences, tough comments, friendly smile, and cheerful moments. Without these people, my PhD student life would never been completed.

My parents receive my deepest gratitude and love for their dedication, understanding, and years of support. I also thanks to my sister and brother for their endless encouragement.

Finally, I am thankful to the Royal Thai Government for continuous funding me throughout my course.

DEDICATION

I would like to dedicate this thesis to

Mom & Dad

NOMENCLATURES

a	melt depth (m)
a'	dimensionless melt depth
A	absorptivity
A_b	Laser spot area (m^2)
A_l	absorptivity of liquid
A_{eff}	effective area of gas entering the hole (m^2)
A_{rl}	cylindrical area of radial loss of gas pressure (m^2)
A_s	absorptivity of solid
A_0	numerical coefficient
B_0	vaporisation constant
c_{eff}	effective heat capacity (J kg^{-1} K^{-1})
c_{pl}	specific heat of liquid (J kg^{-1} K^{-1})
c_{ps}	specific heat of solid (J kg^{-1} K^{-1})
C_c	a constant for forced convection
d_b	beam diameter (m)
d_{ent}	hole entrance diameter (m)
d_{exit}	hole exit diameter (m)
d_f	minimum spot diameter (m)
d_n	nozzle exit diameter (m)
E	laser energy (J)
f	frequency (Hz)
f_l	focal length (m)
Δf	depth of focus (m)
g	gravitational acceleration (m s^{-2})
h	Plank's constant (6.63×10^{-34} J s^{-1})
h_g	heat transfer coefficient of assist gas (W m^{-2} K^{-1})

H_{ox}	enthalpy of oxidation (J kg^{-1})
I_0	incident laser intensity (W m^{-2})
I_{abs}	absorbed laser intensity (W m^{-2})
k	thermal conductivity (W m^{-1}K^{-1})
k_b	Boltzmann's constant (1.38×10^{-23} J/K)
k_g	thermal conductivity of gas (W m^{-1}K^{-1})
k_l	thermal conductivity of liquid (W m^{-1}K^{-1})
k_s	thermal conductivity of solid (W m^{-1}K^{-1})
l	workpiece thickness (m)
L_m	latent heat of melting (J kg^{-1})
L_v	latent heat of vaporisation (J kg^{-1})
m_v	mass of vapour (kg)
$\dot{m}_m$	molten liquid ejection rate (kg s^{-1})
$\dot{m}_s$	solid melting rate (kg s^{-1})
$\dot{m}_v$	vaporisation rate (kg s^{-1})
M_m	molar mass (kg mol^{-1})
n_c	a constant for forced convection
N_a	Avogadro's number (6.02×10^{23} mol^{-1})
p_0	atmospheric pressure (Pa)
p_c	gas pressure at the nozzle exit (Pa)
p_{eff}	effective gas pressure (Pa)
p_g	gas pressure inside the nozzle (Pa)
p_r	recoil pressure (Pa)
p_{vap}	vapour pressure (Pa)
P_{heat}	power required for heating an melting the solid material (W)
P_0	incident laser power (W)
P_p	laser peak power (W)
Pr	Prandtl number

r	radial distance (m)
r_b	beam radius (m)
r_m	radial distance of the melting front (m)
r_{m0}	melt front radius at the hole entrance (m)
r_v	radial distance of the vaporisation front (m)
r_{v0}	vapour front radius at the hole entrance (m)
R	specific gas constant (J kg^{-1} K^{-1})
R_u	universal gas constant (8.314 J mol^{-1} K^{-1})
Re	Reynolds number
R_f	reflectivity
sc	surface area correction factor
S_c	surface area of a conical profile (m^2)
S_p	surface area of a paraboloid profile (m^2)
S_m	surface area of the melt ejection (m^2)
S_{lv}	surface area of the liquid-vapour interface (m^2)
S_{sl}	surface area of the solid-liquid interface (m^2)
t	time (s)
t_{int}	laser-material interaction time (s)
t_m	time required to initiate melting (s)
t_{on}	pulse on time (s)
t_{off}	pulse off time (s)
t_{th}	threshold time (s)
T_b	boiling temperature (K)
T_f	freezing temperature (K)
T_g	temperature of assist gas (K)
T_l	temperature of liquid (K)
T_{l0}	melt surface temperature (K)
T_m	melting temperature (K)

$T_{on,i}$	surface temperature during laser heating of pulse i (K)
$T_{off,i}$	surface temperature during pulse off i (K)
T_r	temperature distribution in the radial direction (K)
T_s	temperature of solid (K)
T_0	ambient temperature (K)
U	interface velocity (m s^{-1})
U'	dimensionless interface velocity
v_g	flow velocity of assist gas (m s^{-1})
V_m	melt ejection velocity (m s^{-1})
x	vertical distance from the solid-liquid interface (m)
x_m	solidification front (m)
x_0	liquid-vapour interface location (m)
z	vertical distance from the workpiece surface (m)
z_f	freezing front (m)
z_m	melting front (m)
z_{m0}	melting front at the hole centre (m)
z_v	vaporisation front (m)
z_{v0}	vaporisation front at the hole centre (m)
z_n	nozzle-workpiece distance (m)
α	thermal diffusivity (m^2 s^{-1})
α_l	thermal diffusivity of liquid (m^2 s^{-1})
α_s	thermal diffusivity of solid (m^2 s^{-1})
γ	specific heat ratio
δ_0	recast layer thickness at the hole entrance (m)
η_{ox}	oxidation efficiency
θ	beam divergence angle (degree)
θ_T	tapering angle (degree)
μ_g	viscosity of assist gas (N s m^{-2})
ν	photon frequency (s^{-1})

ξ	a constant in the solidification model
ρ_g	density of assist gas (kg m^{-3})
ρ_l	density of liquid (kg m^{-3})
ρ_s	density of solid (kg m^{-3})
σ	surface tension (N m^{-1})
τ_0	transmission coefficient
τ	time scale during pulse off (s)

CHAPTER 1

INTRODUCTION

1.1 RESEARCH BACKGROUND

Since the introduction of ruby laser in 1960 [2], applications of lasers have increased dramatically. They can be found in numerous areas ranging from entertainment, information technology, electronics, material processing, medical to military devices. Of particular interest is the case of material processing where utilization of lasers tends to provide some outstanding benefits over traditional methods. The continuous growing of the laser applications in this area is mainly because of its high precision, non-contact process, and flexibility to a wide range of requirements. The applications of laser material processing may range from macroscopic scale including laser cutting, machining, and drilling of rock, to microscopic level including micro-hole drilling for jet engine turbine blades and precision machining, for instance [3, 4].

Laser drilling is one of the most extensively used applications of lasers in material processing. Its ability to produce small diameter and high aspect ratio holes in a wide variety of materials, including difficult-to-machine materials such as superalloys, ceramics and composites, make laser drilling an attractive option for modern industries. One of the most important applications is laser drilling of a large number of closely spaced cooling holes in turbine blades of aerospace engines. These tiny holes (ranging from 0.25 to 1 mm in diameter [5]) are required to provide sufficient cooling without reducing the structural integrity of the blade. The conventional method used for producing such holes is electro-discharge machining (EDM) which, although gives excellent hole quality, the process is comparatively slow and expensive compared with laser drilling. Laser percussion drilling is a drilling technique which provides an alternative option to EDM due to its high production rate. It employs a series of short laser pulses to produce a hole in the workpiece. Despite being continuously improved over the past few years, laser percussion drilling still suffers from some defects including hole taper, splatter (resolidified material at the hole entrance) and dross (resolidified material at the hole exit). Therefore, it is essential to conduct more studies in order to precisely define the

optimum setting of laser parameters which produces the desired hole with least defects.

Laser drilling is a complex process accompanied by various laser beam-material interactions. When the laser beam impinges onto the workpiece, it is absorbed and conducted into the workpiece. Solid substrate is then heated to the melting or boiling temperature depending on the laser intensity. This leads to changing of the phase from solid to liquid, liquid to vapour or solid to vapour. The hole is subsequently formed by melt ejection and/or vaporisation. The ejected melt may oxidise with oxygen and add more heat to the process. In some cases, plasma may be formed in the process which traps part of the laser energy resulting in less energy delivered to the workpiece. Moreover, the laser beam targeted to the hole bottom may reflect repeatedly along the hole wall leading to the variation of laser intensity inside the hole.

Research on laser percussion drilling may be carried out by following two approaches: experimental and numerical or analytical. The experimental approach although provides actual results of the process, it normally requires higher cost and time. The numerical (or analytical) approach is by far more time and cost effective. Using this approach, a large number of costly and time consuming experimental tests can be reduced tremendously. Moreover, unlike the experiments, the mathematical model also has less restriction on the input parameters such as laser power and wave length, which is frequently a problem in the experiments. This approach can be conveniently used to obtain the ideal laser parameters setting for any particular laser hole drilling requirement.

To date, numerous laser percussion drilling models have been developed with an attempt to describe the role of each phenomenon in the drilling process and to determine the optimum laser settings for a particular application. Literature review shows that most laser percussion drilling models previously developed are typically based on heat conduction, melting and vaporisation equations with a set of defined assumptions. However, most works either ignore the effects of the additional heat generated from exothermic reaction between metals and oxygen assist gas, or disregard the solidification during pulse off which in fact have great influence on the

drilling mechanisms. This indicates that the accuracy of the available models can be improved by reducing the number of assumptions and incorporating more related phenomena into the calculations.

In this present research, a new mathematical model for multiple pulsed laser drilling is developed. The model accounts for the recoil pressure, O_2 assist gas, as well as the solidification of the melt. The governing equations are set up from heat conduction, energy, and mass equations at the solid-liquid and liquid-vapour interfaces. Solutions are obtained using Mathematica 7 as a tool to solve the system of non-linear equations.

1.2 RESEARCH AIMS AND OBJECTIVES

This study aims to develop a mathematical model for multiple pulsed laser percussion drilling of metals or their alloys. Effects of the recoil pressure, assist gas pressure, additional heat added due to exothermic reaction between the melt particles and oxygen assist gas, and pulse repetition frequency will be included in the new model.

The new model enables the prediction of hole geometry, hole taper, and recast layer thickness, as well as the optimal parameters setting for a required hole dimension. In addition, the derived equations will be used to explain the laser drilling mechanisms for a better understanding of the process.

The specific objectives of this work are listed as follows:

1. To develop a mathematical model of laser percussion drilling of metals and their alloys. The model developed would be able to predict the breakthrough pulse, hole depth, hole profile, hole taper, and recast layer thickness.
2. To conduct experimental work to validate the new model.
3. To investigate the effects of laser parameters on the laser percussion drilled hole quality.

1.3 THESIS STRUCTURE

CHAPTER 2 LITERATURE REVIEW - LASER FUNDAMENTALS

Chapter 2 gives a brief summary of basic laser fundamentals including the basic operating principles and components of a laser. Types of laser generally used for material processing is also summarised with particular attention being addressed to the Nd:YAG laser as it is the dominant laser used for metal drilling.

CHAPTER 3 LITERATURE REVIEW-LASER DRILLING

Chapter 3 reviews state-of-the art and comprehensive fundamentals of laser drilling. Techniques commonly used and the complex mechanisms involved in the laser drilling process are addressed. Defects typically associated in the laser percussion drilled hole are also defined. Finally, parameters affecting laser drilled hole quality are summarised.

CHAPTER 4 LITERATURE REVIEW –LASER DRILLING MODELS

Chapter 4 focuses exclusively on the previously developed mathematical modelling of laser drilling. The mathematical formulation and solution approaches are addressed for laser heating, melting, and vaporisation.

CHAPTER 5 MATHEMATICAL FORMULATION

Chapter 5 presents a development of the new mathematical model of laser percussion drilling. Formulation of the model is divided into two steps i.e. pulse on analysis; when the laser beam-matter interaction takes places, and the pulse off analysis; when solidification occurs. The recoil pressure, exothermic reaction, and assist gas pressure are also accounted for in the model.

CHAPTER 6 EXPERIMENTAL PROCEDURES FOR MODEL VERIFICATION

Chapter 6 provides details of the experimental set up for model verification. Experimental apparatus, sample preparation, hole quality measurement procedure, and the process parameters employed are explained.

CHAPTER 7 RESULTS AND DISCUSSION

Chapter 7 presents and discusses the results obtained from the model currently developed. In the first section, the new model is validated by comparing the hole depth and hole profiles to those obtained experimentally. The second section reports on the predicted hole profile, hole taper, and recast layer thickness. Lastly, the effects of laser parameters on the hole quality are discussed.

CHAPTER 8 CONCLUSIONS AND RECOMMENDATION FOR FUTURE WORK

Chapter 8 draws the conclusion from the results obtained from the new model of laser percussion drilling. Effects of laser parameters on the drilled hole quality are summarised. Recommendations for possible future work to improve the model accuracy are also addressed.

CHAPTER 2
LITERATURE REVIEW - LASER FUNDAMENTALS

2.1 INTRODUCTION

This chapter gives a brief review of laser fundamentals. Basic operating principles and components are explained. Types of the lasers used in material processing and their applications are also summarized.

2.2 BASIC PRINCIPLES OF LASER OPERATING

Laser stands for Light Amplification by Stimulated Emission of Radiation according to its operating characteristics. The process may be simply described as the amplification of light signals which have been previously produced by the stimulation process [6]. The output beam is high intensity, highly directional and has almost identical wavelength.

There are basically three processes involved in producing the laser beam: population inversion, stimulated emission, and amplification.

2.2.1 Population inversion

For a material in thermal equilibrium, number of electrons orbiting around a nucleus of an atom varies from one energy level to other energy levels. In the outer most orbit, where the energy level is the highest, the electron population is the smallest compared to other orbits with lower energy levels. Population inversion is a process that excites electrons in the lower energy levels to the higher energy levels. This leads to the non-equilibrium state where number of the electrons in higher energy level is greater than that in the lower energy state [7].

As shown in Figure 2.1 (a), electrons initially at energy level E0 are pushed to E2 level by the absorption of energy from photons (light particles) generated by a pumping source. Energy of the pumped photon is essentially equal to the energy difference between E0 and E2 levels, i.e.

$$hv = E2 - E0$$

(2.1)

where h is Plank's constant (6.63×10^{-34} J s) and ν is the photon frequency (s^{-1}).

| (a) | (b) |
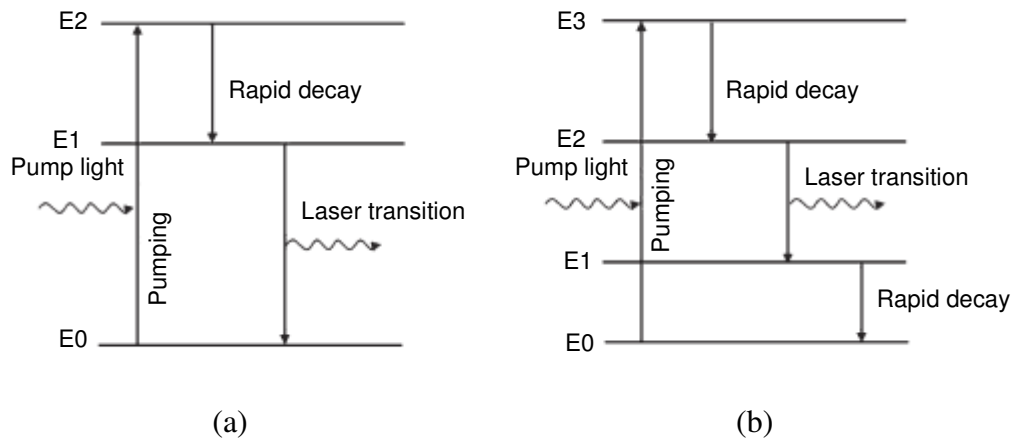
Figure 2.1 Population inversion (a) three-level system (b) four-level system [7].

At this level, the excited electrons are not stable and are able to sustain in E2 level only for a very short lifetime. The electrons consequently decay into a metastable energy level E1 and emit photons which travel in any random direction. This process which does not generate laser radiation is referred to as 'spontaneous emission' [7].

2.2.2 Stimulated emission

The electrons decay from E2 to E1 level in Figure 2.1 (a) may further interact with other incoming photons resulting in the transition from E1 to E0 level. During this transition, photons of the same wavelength, phase and direction as that of the stimulating photons are released resulting in more photons in the system. This process is known as the stimulated emission [6, 8-10].

In addition to a three-level system, as shown in Figure 2.1 (a), lasers may also operate with a four-level system, as shown in Figure 2.1 (b) where the stimulated emission (laser transition) takes place between energy level E2 and E1 [7, 11].

2.2.3 Amplification

As explained earlier, the population inversion and the stimulated emission produce intense photons with the same phase and wavelength in the cavity. These photons therefore add constructively to each other giving rise to the amplitude of the photons.

A basic laser device consists of a total reflective mirror and a partial transparent mirror placed in parallel to each other to form an optical cavity. Between these two mirrors is an active laser medium. The stimulation occurs repeatedly as the light oscillates back and forth between the two mirrors before escaping from the partial transparent mirror as an output laser beam. The pumping sources typically used to initiate the population inversion are flash lamp and diode laser for solid-state lasers while in gas lasers, DC or RF voltage supply is employed. Figure 2.2 illustrates the components of a basic laser [12].
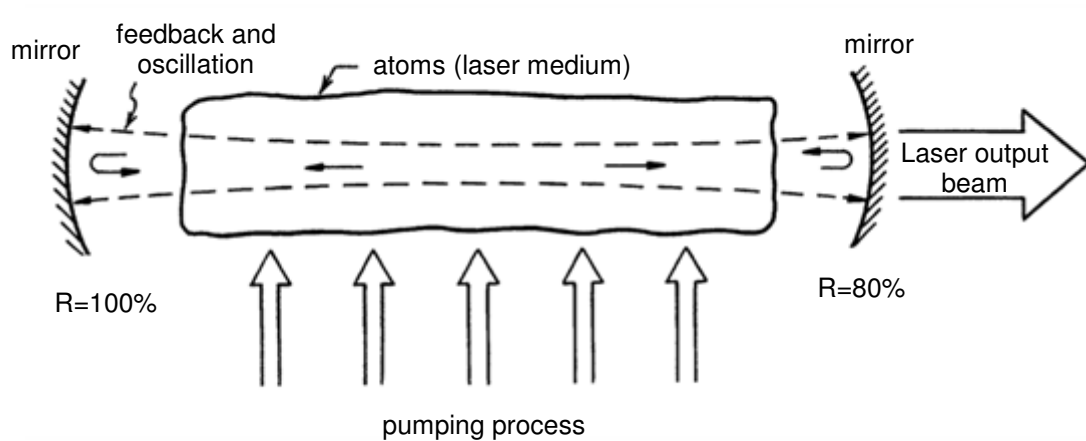
Figure 2.2 Components of a basic laser [12].

2.3 INDUSTRIAL LASERS

Laser research has progressed continuously since the introduction of the first ruby laser by Maiman in 1960 [2]. In order to specialize and optimize laser capacity for a specific requirement, various types of lasers have been developed. These lasers may be divided into several categories depending on the basis of consideration. Table 2.1 lists examples of the laser classification based on the physical characteristics of the laser active medium, i.e. solid-state lasers, gas lasers, semiconductor lasers and liquid dye lasers.

Table 2.1 Types of lasers [7].

Basis of consideration	Laser active medium
Solid-state lasers	Nd:YAG*
	Ruby*
	Nd:Glass*
	Alexandrite
	Ti-sapphire*
	Er:YAG
	Nd:YLF*
Gas lasers	HeNe
	Argon
	Krypton
	HeCd
	CO_2*
	ArF*
	KrF*
	XeCl*
	XeF*
	Copper vapour*
	Gold vapour
Semiconductor lasers	InGaAs
	AlGaInP
	InGaAsP
	AlGaAs
Liquid dye lasers	Rhodamine 6G
	Coumarin 102
	Stilbene

* These lasers are commonly used for laser material processing.

Some lasers commonly used in materials processing and applied research are briefly summarized as follows.

2.3.1 Solid-state lasers

Solid state lasers work by doping a crystalline solid host with ions that provide the required energy states. The ions are particularly the rare earth (RE) or transition-metal ions whereas the host crystals generally used are oxides or fluorides.

Nd:YAG laser is the most widely used solid state laser. The wavelength of the beam produced is 1064 nm which is in the infrared region. The combination of the YAG host crystal and the Nd^{3+} ion generates the laser beam which is favourable for laser processing. Undoped pure yttrium aluminium garnet has high thermal conductivity and good optically isotropic property; that is the reflectivity does not vary with the direction of the light nor the beam polarization. The concentration of the Nd^{3+} ions also has a role on the laser efficiency. It is estimated that 1.2% doping concentration is suitable for the Q-switched lasers to generate the high energy whereas the lower doping concentration, 0.6-0.8%, is generally selected for the continuous wave operating mode to achieve a good beam quality [13].

Nd:YAG lasers may operate in either continuous wave or pulsed modes with the pumping source being lamp or semiconductor diode laser. For lamp pumping, the efficiency is approximately 3% for both pulsed and continuous wave modes, with the average output ranging from 1-3 kW. For diode pumping, although the output power may be lower, the efficiency can exceed 10% which is much higher compared with the lamp pumping [13].

The Nd:YAG lasers are broadly used for material processing such as drilling, welding and cutting. In case of drilling, Nd:YAG laser is widely used for drilling shaped holes of aircraft turbine blades to improve the cooling efficiency [14]. A repetitive pulsed laser is delivered to the material surface typically with the average powers of 50-100 W, pulse duration 1-10 ms and pulse frequency 100 Hz [13]. In welding applications, the pulsed beam with the average output power of typically up to 2 kW is delivered to the workpiece through an optical fibre. This improves the system flexibility compared with CO_2 laser normally used for welding.

For cutting, Nd:YAG lasers are generally less cost effective compared with the conventional CO_2 lasers. However, there are some applications for which Nd:YAG

lasers are preferred. These include high precision cutting of reflective materials or cutting process where the delivery of the laser beam through an optical fibre is required [15-17]. Comparing with the CO_2 gas laser, Nd:YAG laser, in general, gives lower beam power but higher peak power when operating in pulsed mode [18]. This allows the Nd:YAG laser to machine thicker workpiece.

In addition to material processing, Nd:YAG lasers are also employed in medical treatment. For example, a 50 W continuous wave Nd:YAG laser is used in coagulation and tissue evaporation by delivering the beam through a small optical fibre inserted into the human body. Moreover, the Q-switched photodisruptor laser is becoming an essential tool for ophthalmology. It provides consistently accurate, high precision surgery on delicate ocular tissue [13].

2.3.2 Gas lasers

Examples of this laser type are helium-neon lasers (HeNe), carbon dioxide (CO_2) lasers, Argon-ion lasers and metal ion lasers. Among these gas lasers, CO_2 laser generating a 10.6 μm radiation is the most successful in material processing due to its high average beam power, high efficiency, good beam quality and the possibility of convection cooling [16, 18]. The power of generated continuous wave can be up to tens of kilowatts [19]. The main applications of CO_2 laser are in cutting and welding of metals [18, 20].

Excimer laser is another gas laser generally used for material processing. It operates in pulsed mode and produces light in the ultraviolet range with high peak power but fairly low average power. A unique characteristic of the excimer laser is the excellent beam quality which is close to the diffraction limit [21]. They are generally used for producing micron-size structures where Nd:YAG lasers are not applicable. Excimer lasers are finding their application chiefly in ablation, micro-fabrication medicine and microelectronics industries [9, 17, 22]. Drilling with excimer lasers show some improvements over the lasers emitting with visible and infrared wavelength. The shorter wavelength of ultraviolet beam allows focusing to a smaller area with less thermal effect to the surrounding material. Moreover, each pulse of the excimer laser removes only a thin layer of the substrate resulting in an accurate control of the drilling depth [17]. Examples of the excimer lasers include ArF, KrF, and XeCl [11].

2.3.3 Semiconductor lasers

Due to some limitations of the traditional gas and solid-state lasers, semiconductor lasers have been developed to overcome the constraints. Diode laser is a well known example of semiconductor lasers. Comparing with gas and solid-state lasers, it has compact size and a shorter wavelength so that it can work with reflective metals and some plastics. However, due to lower beam quality, the beam divergence is quite large resulting in larger spot diameter [20]. Diode lasers with high power are employed in manufacturing for cutting and welding while lower power ones are used in CD/DVD players and printers. In addition, diode lasers have also been recently used as pumping source for Nd:YAG lasers typically excited by either flash or arc lamps. This gives the improvement in laser efficiency, longer operating hours and less thermal losses [20, 23].

2.3.4 Liquid dye lasers

In liquid dye lasers, liquid solution consisting of an organic dye dissolved in liquid solvent acts as the laser active medium. The most important feature of the dye lasers is that, unlike other types of lasers, the dye molecules in the solvent absorbs energy at a certain range of wavelength and release the laser energy over other range at longer wavelength [24, 25].
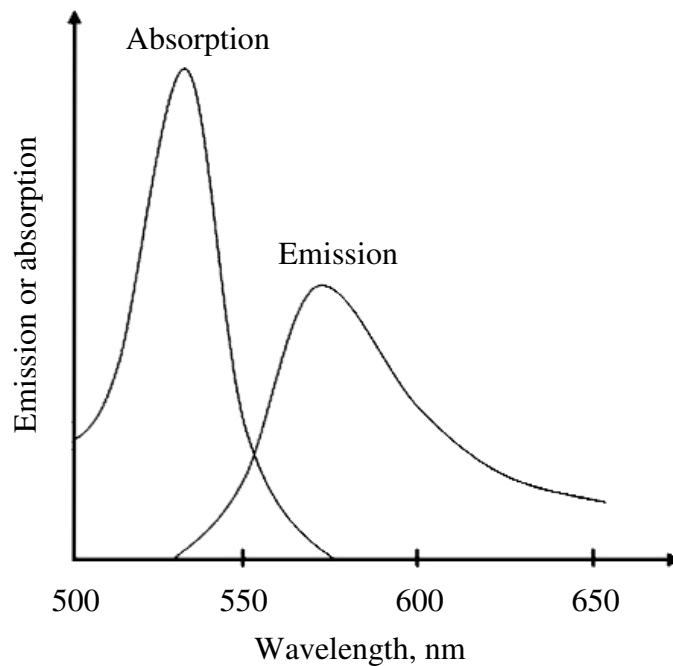
Figure 2.3 Absorption and emission bandwidth of the rhodamine 6G dye laser [7].

The wavelength of the output beam is tunable and can be varied from near-ultraviolet to near-infrared. This flexibility makes liquid dye laser a good candidate for applications where the available solid-state and gas lasers cannot offer the required wavelength, such as spectroscopy, molecular dissociation, chemical reactions and isotope separation [25]. Other advantages of liquid dye lasers include the ease of variation in the laser active medium concentration, the active medium is relatively cheap and damage-free, and offers ease of cooling.

CHAPTER 3

LITERATURE REVIEW - LASER DRILLING

3.1 INTRODUCTION

Laser drilling is becoming a reliable option for a variety of applications. Of particular interest is the laser drilling of cooling holes for aircraft engine components. This is due to the laser's ability to precisely produce shaped holes for the difficult-to-machine materials [26, 27]. Compared with other conventional methods such as mechanical drilling, electrochemical drilling (ECD), and electrical-discharge machining (EDM), laser drilling has many advantages over these methods as follows [7, 9, 23, 28-31]:

1. There is no tool wear and damage from mechanical contact.
2. Laser drilling offers high precision and repeatability,
3. Small beam divergence makes it possible to drill very small holes with high aspect ratio (hole depth to hole diameter).
4. Shaped and angled holes, which are difficult to drill by conventional methods, can be laser drilled with high accuracy.
5. Programming for automation control of the drilling process is easy and fast.
6. Comparing with the ECD and EDM techniques, laser drilling cost is competitive while the production time is shorter. However, the tooling and operating cost is higher compared to mechanical drilling except for mass production level.
7. There is a wide range of available laser specifications to suit any particular applications and materials. The difficult-to-machine materials such as ceramics, superalloys and composites can be drilled with less difficulty.
8. One laser machine may be employed for more than one process. In other words, laser machine is flexible. For example, a specially designed laser can be used for both welding and cutting.

Some restrictions of laser drilling which have to be taken into consideration are listed below [20, 29].

1. High initial tooling cost comparing to mechanical drilling. It was reported that the capital cost of laser drilling of silicon nitride and polyimide was approximately 115 k$ higher than that of mechanical drilling [32].

2. Hole taper is often found during direct drilling (single pulse and percussion drilling).

3. Some difficulties arise in drilling of the blind hole with exact depth requirement.

4. Thickness of materials to be drilled is limited. It is recommended that the thickness to be laser drilled should not exceed 50mm.

5. Debris at the hole exit needs to be removed.

6. Regular maintenance is required especially for the optics and optics alignment.

Due to the increasing applications of laser drilling, understanding of the laser drilling process is therefore essential. This chapter gives a brief summary on the basic knowledge of laser drilling process. Four laser drilling techniques commonly used, namely: single pulse, percussion, trepanning, and helical drilling, are reviewed. The related thermal and physical phenomena taking place during the laser beam-material are also presented. These include absorption of laser radiation, heating, melting and vaporisation, recoil pressure effects, plasma formation, and multiple reflection of the laser beam.

3.2 LASER DRILLING TECHNIQUES

There are three common techniques to laser drilling namely single pulse, percussion and trepanning drilling. In addition to these, helical drilling technique (Figure 3.1) has been recently developed with the improvement in the drilled hole accuracy [33-35].

3.2.1 Single pulse drilling

In single pulse or single-shot drilling, a single pulse with high energy is used to drill a hole on the workpiece surface. The hole diameter can be smaller or greater than laser beam diameter and depends primarily on temporal and spatial intensity profiles of the focused laser beam, and material thickness [36].

This technique is typically applied to small diameter hole drilling of thin sheet material where the production time is more important than the hole quality [37]. Examples of its application are drilling of the sieves and filters. Drilling on-the-fly process, in which laser beam or workpiece or both are moved relatively, may be

incorporate into the single pulse drilling technique in order to increase the production rate.

single pulse   percussion   trepanning   helical drilling

Pulse energy, pulse duration

accuracy
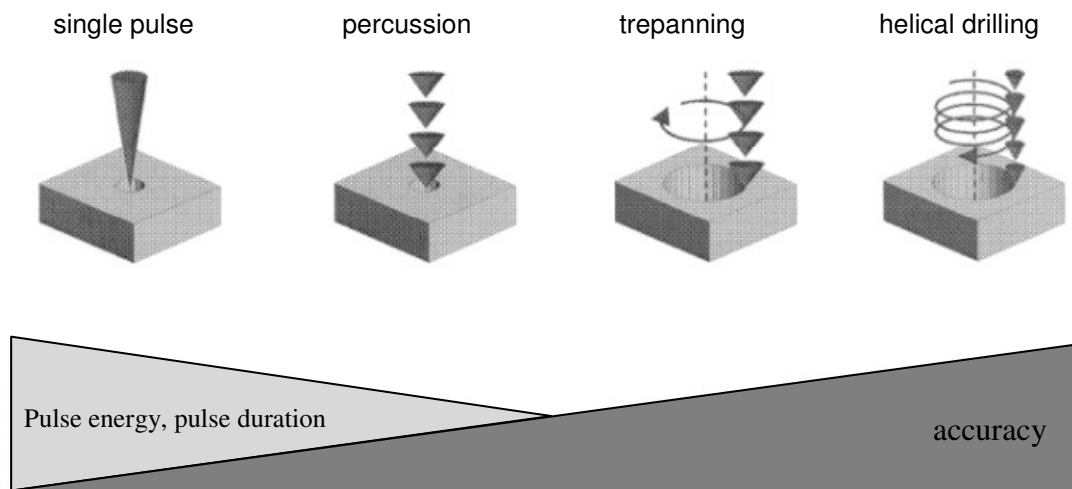
Figure 3.1 Laser drilling techniques [34].

3.2.2 Percussion drilling

In laser percussion drilling, a series of laser pulses is delivered onto the same spot on the workpiece surface to produce a hole. Between each successive pulse is a pulse off duration, which is typically longer than the pulse on [38]. This drilling technique is becoming favourite especially with the applications where a large numbers of hole are to be precisely positioned in a highly reproducible manner. One of the most important applications is drilling of cooling holes in aerospace engine components, such as turbine blades, combustion chamber, and guide vanes [39-42]. Other applications of the laser percussion drilling technique include blind hole in a surgical needle and most kind of the lubrication holes [36]. Compared to single pulse drilling, the percussion drilling can operate at lower beam energy [43] whilst enables drilling of the high aspect ratio holes i.e. up to approximately 1:100 for through holes and 1:20 for blind holes [36]. Although a recommended maximum thickness of material to be laser drilled is 50 mm, this aspect ratio implies that laser percussion drilling can produce a hole in material with thickness greater than 50 mm.

3.2.3 Trepanning drilling

When large diameter holes are to be drilled on a thin plate, trepanning drilling technique is often employed. The process begins by percussion drilling of a central

hole followed by contour cutting to achieve the desired hole diameter. The hole diameter drilled with this technique is typically larger than 25 mm and material thickness is between 0.25 to 20 mm [1]. Also noted that, this technique is applicable to the production of the through holes only [36].
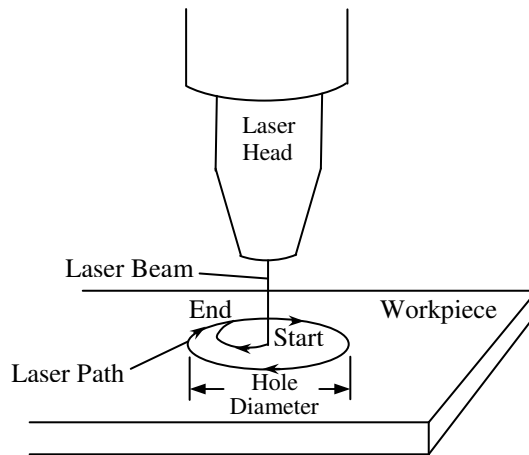
Figure 3.2 Trepanning drilling contour [1].

Trepanning technique has significant benefits in providing good hole circularity with less metallurgical defects. Moreover, the hole taper is considerably smaller comparing with those obtained from the percussion drilling [28]. This is because this technique requires low energy per pulse and the hole dimension is controlled mainly by the rotating movement of the beam. In other word, it might be possible to say that the quality of the hole drilled by trepanning drilling is independent of the laser parameters [37].

3.2.4 Helical drilling

Recently, helical drilling technique which enhances the drilling accuracy has been developed [34, 35]. It operates by spiral ablation of the laser beam into the workpiece at several small steps. The hole drilled by this technique shows significant reduction in the recast layer and good hole circularity [44]. However, the processing time is comparatively slow and the technique therefore requires further development.

3.3 LASER DRILLING MECHANISMS

In laser drilling, a high intensity laser beam is delivered to a workpiece by being focused into a small spot. The laser energy is then absorbed and conducted into the workpiece resulting in heating, melting and vaporisation of material. A hole is subsequently created due to mass removal in the form of liquid or vapour. Moreover, further irradiation of laser beam may cause ionization of the vapour trapped in the cavity and eventually leads to the formation of the plasma.

Because laser drilling is a complex process involving several thermal and physical mechanisms as mentioned above, in order to properly define the capability and limitation of the process, knowledge of the relative mechanism is thereby greatly essential.

3.3.1 Beam absorption by materials

When a laser beam impinges onto the workpiece surface, it is absorbed, reflected and in case of transparent materials, transmitted. However, because this research deals mostly with metals which are opaque material, the transmissivity is negligible. Hence, the absorptivity, *A*, can be expressed as

$$A = 1 - R_f \tag{3.1}$$

where R_f is the reflectivity of material.

Absorptivity or reflectivity is an important parameter indicating the ability to absorb laser energy of material. This parameter depends not only on material properties but also on characteristic of electromagnetic radiation. Factors affecting the absorptivity are laser wavelength, incident angle and polarization of the laser beam, temperature of material, surface roughness of material, and oxide formed on the surface. Figure 3.3 shows variation of the reflectivity with the incident laser wavelength for five metals [11]. It can be seen that, in general, metals reflect less and thus absorb more laser energy at shorter wavelength. This means that an Nd:YAG laser, which produces a beam with 1.064 μm wavelength, will have its energy absorbed in the material more efficiently than a CO_2 laser, which produces a beam with 10.6 μm wavelength.

37
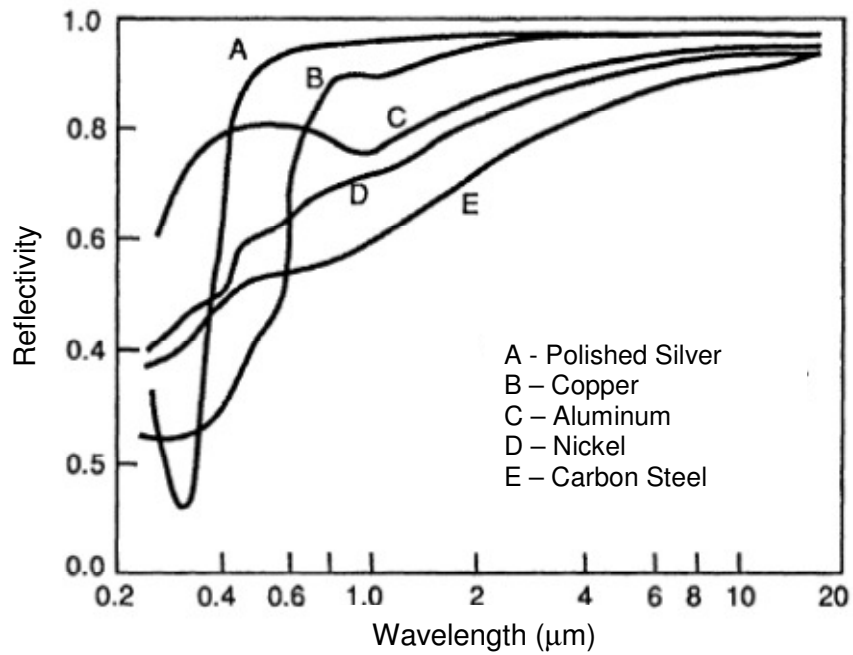
Figure 3.3 Variation of reflectivity with light wavelength for several metals [11].
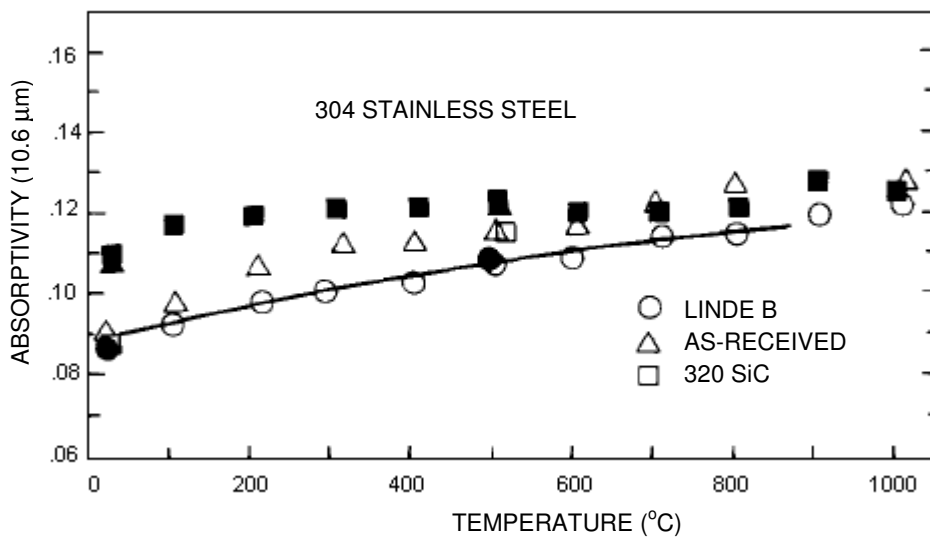
Figure 3.4 Absorptivity of 304 stainless steel at 10.6 μm. The black data points were recorded while increasing the furnace temperature from 25 to 1000 ^{o}C; the other data points were obtained from the return half of the temperature cycle [45].

Figure 3.4 shows the effects of temperature and surface roughness of material on the absorptivity [45]. It can be seen that absorptivity increases with the increase in temperature and surface roughness. It was found that rough surfaces tended to

38

promote the multiple reflections within the rough surface topography, hence resulting in more laser energy being absorbed [36, 46].

Oxide layer formed at the material surface also influences the absorptivity of the metals. Table 3.1 compares the absorptivity of some metals with unoxidised and oxidised surfaces [47]. It is clear that the oxidized surface appreciably increases the absorptivity of these metals. It should be noted that this effect is apparent only when the oxidised layer is sufficiently thick, which is the case of oxidation under high temperature i.e. furnaces, laser heating, etc. Normal oxidation of metals under room temperature produces quite a thin film of oxide layer which is found to have insignificant impact on the absorptivity [36].

Table 3.1 Absorptivity of some metals at 10.6 µm radiation [47].

	Absorptivity	
Metal	Unoxidised surface	Oxidised surface
Au	0.010	-
Al	0.034	0.25-0.50
Fe	0.050	0.33-0.74
Zr	0.083	0.45-0.56
Ti	0.094	0.18-0.25

3.3.2 Heating, melting, and vaporisation

When the laser beam impinges onto the workpiece surface, laser energy is rapidly converted into heat and conducted into solid substrate. This is followed by the phase transition mechanisms; melting and vaporisation. Material may be removed from the hole in the form of liquid or vapour or both in various proportions depending on the material properties and laser intensity. Once the vapour is formed during the process, it absorbs energy from the subsequent laser beam irradiating and hence plasma may exist. Figure 3.5 shows the interaction between laser beam and material [48].

By focusing on the interaction zone between laser beam and material, the process can be divided into four distinct stages [49-51]:

      1. surface heating,

2. surface melting,

3. vaporisation, and

4. melt ejection.

heats

melts

boils

plasma
formation
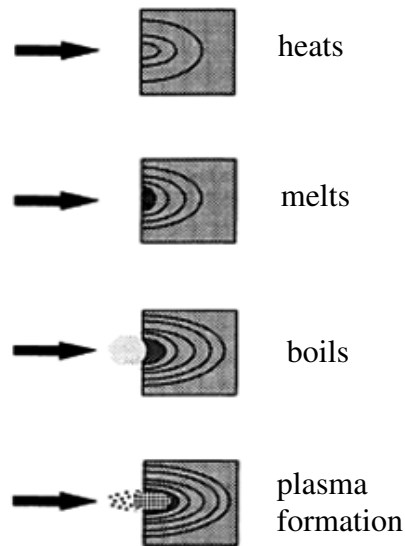
Figure 3.5 Laser-material interaction [48].

3.3.3 Material removal mechanisms

Due to the complexity of the process, material removal during laser drilling has been discussed widely to date [48, 50-60]. Basically, there are two mechanisms associated with material removal during laser-material interaction: vaporisation and melt ejection. Vaporisation takes place when temperature of the material reaches the boiling point. The vapour formed subsequently escapes from the molten material surface. As the vaporisation proceeds, a crater is formed and the vapour pressure rises to a very high level. Chen and Wang [61] has shown that for laser processing of titanium, the recoil pressure was found to be from 0.25 to 0.5 MPa corresponding to 1 to 3.3 MW/cm^2 laser intensity. As high pressure vapour leaves the molten liquid surface, it exerts 'recoil pressure' on the molten liquid underneath. If the pressure is high enough to overcome the molten liquid surface tension, liquid is pushed up along the hole wall and ejected as small droplets [51, 54]. The average diameter of the droplets is approximately the same as the thickness of the melt layer [58]. Figure 3.6 sketches the material removal through vaporisation and melt ejection.

Wei et al.[59] proposed an axisymmetric, quasi-steady model of the liquid metal flow in the cavity generated due to the laser beam penetration process. It was concluded that effective pressure; which consists of gas pressure near the surface, vaporisation pressure, and the force due to surface tension, was responsible for driving up the liquid layer. In addition, the model also showed that the mass removal due to vaporisation was only 0.5% of that due to melt ejection. Thus, the melt ejection was considered as the dominant process for creating the cavity. This result is consistent with that reported by Yilbas [57].
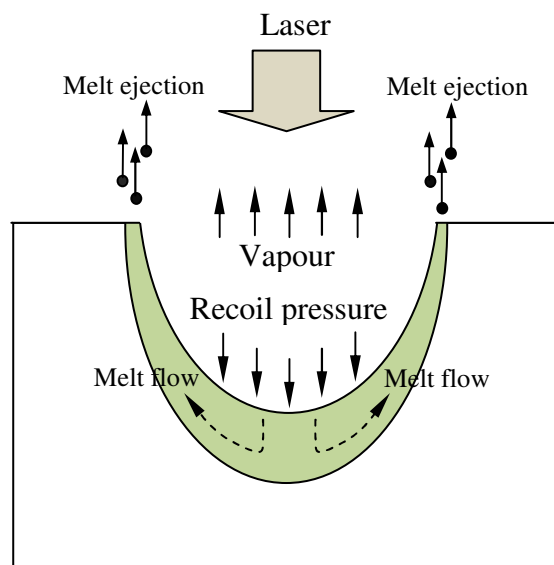
Figure 3.6 Schematic diagram of the material removal mechanism in laser drilling.

In addition to the melt removal due to recoil pressure, the liquid particles may be ejected from the melt pool due to nucleation boiling of the vapour bubbles [54, 58, 62, 63]. Yilbas [63] reported that temperature of the molten liquid layer rises from the surface to some point before decaying to zero at the infinity position. Hence, superheating may occur causing a rapid liquid-vapour phase change inside this layer. This leads to the formation of small vapour bubbles just below the surface which subsequently expand immediately resulting in a bubble explosion. Following such an explosion, the liquid particles surrounding the exploding vapour are consequently ejected from the cavity. Although comparing with the recoil pressure based-melt ejection, laser drilling based on the nucleation boiling tends to be more efficient, it is, nevertheless more difficult to control the process parameters to achieve the required hole dimension [63-65].

Laser intensity is one of the key parameters controlling the dynamics of material removal. Previous studies have reported that at laser intensity below 10^7 W/cm^2, melt ejection has a significant role in controlling the drilling velocity whereas for laser intensity beyond this value, vaporisation dominates the process [52, 53]. However, laser drilling due to melt ejection tends to be a more energy efficient mechanism than a purely vaporisation process. This is because no additional energy is required to change from molten liquid to vapour [66-68].

Another criteria to determine the key removal mechanism is proposed by Semak and Matsunawa [69]. It is suggested that the laser beam-material interaction time, t_{int} can be employed to define the key process:

(i) if $t_{int} \ll t_{th} = r_b / V_m$, vaporisation removal dominates the process, and

(ii) if $t_{int} \gg t_{th} = r_b / V_m$, melt ejection dominates the process,

where t_{th} is the threshold time, which is the minimum time required to initiate the melt ejection-dominated process, r_b is the beam radius and V_m is the melt ejection velocity.

In some cases, if very high laser intensity impinges on the solid material for a very short period of time, femtosecond scale for instance, only vaporisation occurs without melting. This method has the obvious benefits of producing no-spatter and no heat affected zone [70]. It is also possible to have vaporisation dominating the material removal even at low laser intensity (of magnitude in kW/cm^2). A very short interaction time is necessary for this situation to take place. However, the drilling speed has been found to be comparatively low [52]. Low et al. [52] reported that at the absorbed intensity of 0.5 MW/cm^2, the threshold time was found to be approximately 0.3 ms. To ensure the vaporisation-dominated material removal, the laser beam-material interaction time; or pulse width in case of pulsed drilling, must be less than 0.3 ms. The smaller interaction time means that for a given material thickness, more pulses are required to drill a hole, hence lower drilling speed.

3.3.4 Recoil pressure

Due to its significant influence on the melt ejection mechanism, extensive studies have been conducted on the effects of recoil pressure on laser beam-material interaction [61, 69, 71, 72]. Semak and Matsunawa [69] presented an energy balance analysis of the laser beam-material interaction incorporating the effects of the recoil pressure in the model. The correlation employed was [73, 74]:

$$p_r = A_0 B_0 T_{l0}^{-1/2} \exp\left(-\frac{U}{T_{l0}}\right) \tag{3.2}$$

where p_r is the recoil pressure, A_0 is a numerical coefficient and is taken to be 0.55 [74], B_0 is a vaporisation constant (3.9×10^{13} and 2.05×10^{13} g/cm.s^2 for iron and aluminium, respectively), and T_{l0} is the liquid surface temperature. Here, U is a parameter defined by

$$U = \frac{M_a L_v}{N_a k_b} \tag{3.3}$$

where M_a, L_v, N_a, and k_b are the atomic mass, latent heat of vaporisation, Avogadro's number, and Boltzmann's constant, respectively. In their analysis, Semak and Matsunawa assumed values of the melt surface temperature from slightly above the melting point up to some value beyond the vaporisation point. It was found that once the recoil pressure was built up, it played a significant role even when the melt surface temperature was just slightly above the melting temperature.

Chen and Wang [61] developed a model for predicting the recoil pressure based on mass and kinetic energy equations of the vapour. The recoil pressure was expressed in terms of the melt surface temperature and laser power as:

$$p_r = \frac{P_0 \tau_0 (1 - R_f) - P_{heat}}{A_b L_v} \sqrt{\frac{\pi k_b T_{l0}}{2 m_v}} \tag{3.4}$$

where P_0 is the incident laser power, m_v is the mass of the vapour, P_{heat} is the power required for heating and melting the solid material, τ_0 is the transmission coefficient of the laser beam in the plasma plume, R_f is the reflectivity of material, A_b is the laser spot area and L_v is the latent heat of vaporisation. Comparison with experiments show that Eq.(3.4) gives satisfactory prediction if the reflectivity R_f

varies inversely with the laser beam intensity. Chen and Wang [61] therefore introduced two empirical correlations to correct the reflectivity in their model, one for the case 10^5 Pa ambient pressure and the other for 1 Pa ambient pressure.

3.3.5 Laser induced plasma

As mentioned earlier in section 3.3.2, interaction between laser beam and material leads to the formation of the molten liquid layer and vaporisation. The vapour formed in the cavity expands rapidly into the surrounding ambient air, absorbs laser energy, and consequently leads to the formation of laser induced plasma.

Numerous works have been carried out to investigate the effects of laser induced plasma on laser drilling process [61, 75-85]. Although the actual role of plasma on laser drilling process is somewhat unclear for metals, it is generally accepted that the presence of plasma in the cavity reduces the process efficiency [61, 75-77]. This is because the plasma absorbs part of the incident laser energy, thereby resulting in beam scattering and hence less laser energy transmitted to the workpiece surface. However, there is a critical point when the plasma formed reflects the entire incident laser beam. This occurs when frequency of the irradiating laser is equal to that of the plasma[78].

Pandey et al. [75] investigated the behaviour of plasma generated during laser percussion drilling. It was found that at the beginning of the process, plasma absorbed and blocked laser energy from the workpiece surface. Further absorption of laser energy thereby heated up the plasma causing it to expand and become transparent. At this stage, the energy absorption coefficient of the plasma plume decreased, allowing more laser energy to reach the material surface. Consequently, the vaporisation rate increased again. Just before breakthrough, high density plasma plume was observed along with the melt and vapour expulsion.

Despite the shielding effect, some studies have argued that plasma may be considered as a secondary tool in laser drilling [79-84]. Previous studies have revealed that temperature and density of plasma at the hole exit are typically higher than those at the hole entrance [81, 82]. Therefore, more heat was conducted into the hole wall. This eventually led to the widening of the sidewall [79-82].

Primary drilling tool: Secondary drilling tool:
Laser beam   Plasma
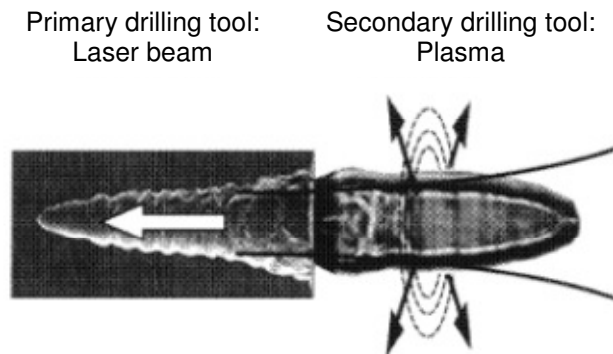
Figure 3.7 Plasma plume as a second drilling tool [79].

Although plasma plays some role in laser-material processing, these effects, nevertheless, are comparatively small if pulsed laser is employed. With pulsed laser processing, each successive pulse is separated by a longer pulse off period. It has been found that plasma is diminished during the pulse off duration as a result of cooling [86-89]. Lacroix et al. [90] also reported that absorption of laser energy in the plasma is less when Nd:YAG laser was used for producing the beam.

3.3.6 Multiple reflections of the laser beam

When a shallow cavity is formed on the workpiece, laser beam impinges on the cavity and undergoes a series of reflections causing an increase in laser intensity at the hole bottom [91]. As the hole gets deeper, effect of the multiple reflections becomes more significant. At the reflecting point, part of the laser energy is absorbed while the rest is reflected. This phenomenon occurs repeatedly in the hole giving rise to the amount of the laser energy being absorbed. Previous studies have reported that once the hole reaches a sufficient depth, the absorbed intensity due to multiple reflections could go up to about ten times or more than that in direct irradiation [92-94].

Researchers have attempted to incorporate the effects of multiple reflections inside the cavity in laser drilling models [89, 91, 95]. Kar et al. [89] proposed a two-dimensional model for laser-induced material damage including the effect of the multiple reflections. Their results showed that the model with multiple reflections predicted a deeper hole than the one predicted by the model without multiple reflections.

Modest [95] proposed a model of laser hole drilling including the effects of multiple reflections. It was concluded that with multiple reflection, laser energy exhibited a dual peak profile with high peak at the beam centre. The second peak was located away from the hole centre causing a bulge at the sidewall. Figure 3.8 illustrates the effect of multiple reflections inside the cavity [95].

8 pulses 16 pulses 19 pulses
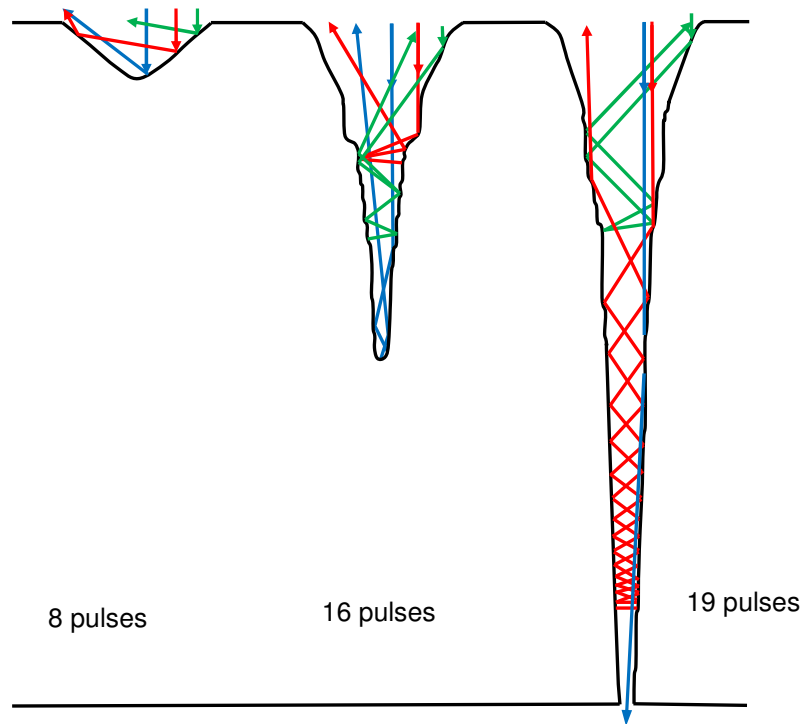
Figure 3.8 Multiple reflections inside the hole wall [95].

From the above review of laser drilling mechanism, it can be concluded that each stage of the process has a close relationship with the another. These interrelations are presented in the block diagram in Figure 3.9 [96].
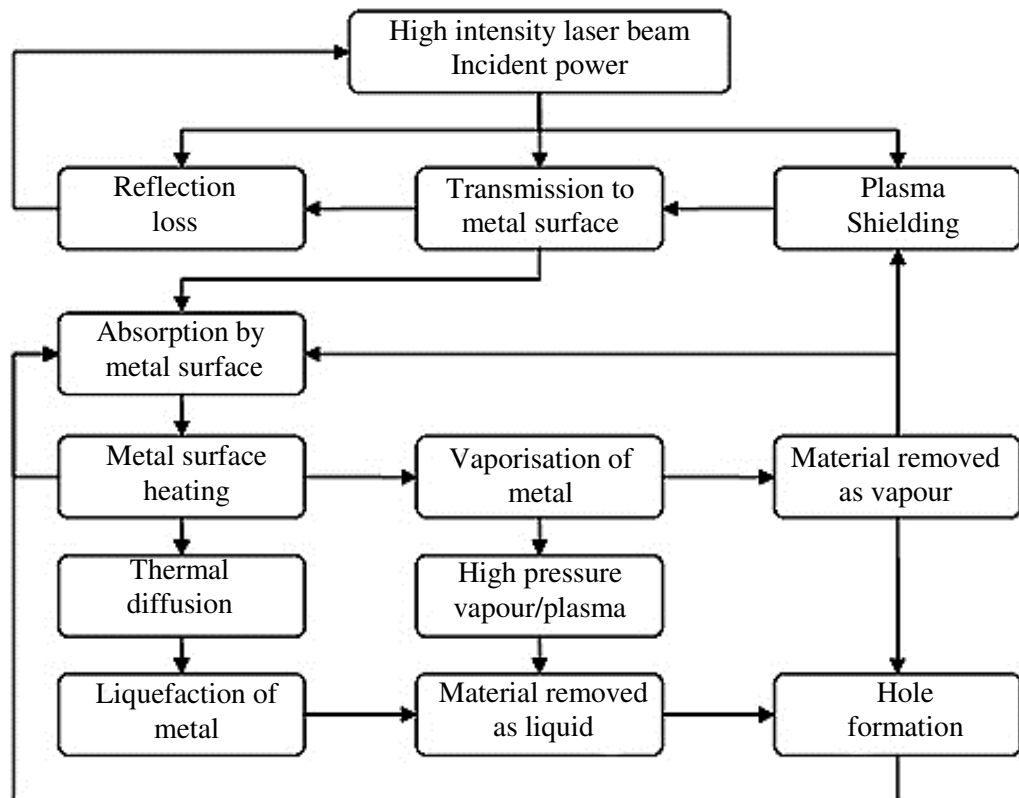
Figure 3.9 Block diagram of the laser drilling process [96].

3.4 DEFECTS IN LASER PERCUSSION DRILLING

Laser percussion drilling offers the outstanding advantages of high processing speed, high tolerance, and repeatability [60]; however, a percussion drilled hole regularly suffers from some drawbacks including resolidified material, hole taper, and noncircularity of the hole [97-102]. An illustration of a drilled hole geometry normally obtained from the actual drilling process is presented in Figure 3.10 [102].

The resolidified material may be further named according to the location adhered. If the resolidified material deposits to the hole wall, it is normally called recast layer. However, if it is found at the hole entrance and exit, it is generally called spatter and dross, respectively.

Hole taper, which represents the decrease of hole diameter with hole depth, is another defect regularly found in laser percussion drilled holes. Nevertheless, it may not be necessarily considered as a defect if the degree of tapering angle and

reproducibility is controllable. Ghoreishi et al. [102] and Li et al. [103] calculated the hole taper using the following equations:
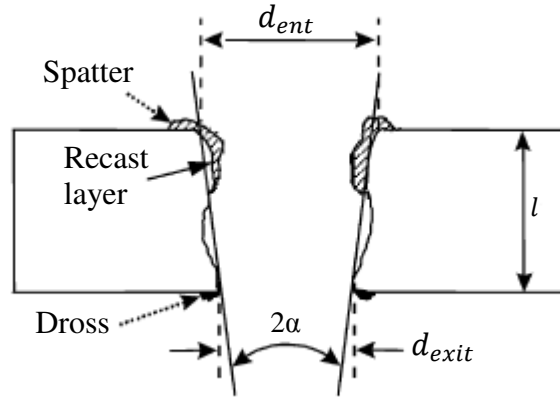
Figure 3.10 Illustration of laser drilled hole, here α is the hole taper [102].

$$Taper(^\circ) = \frac{d_{ent} - d_{exit}}{2l} \frac{180}{\pi} \qquad (3.5)$$

where d_{ent}, d_{exit}, and l are entrance diameter, exit diameter, and thickness of material, respectively.

It is also possible to express the hole taper by [104, 105]:

$$Taper(^\circ) = \tan^{-1}\left(\frac{d_{ent} - d_{exit}}{2l} \right) \qquad (3.6)$$

The hole circularity is another factor indicating the percussion drilled hole quality. In an attempt to define the hole circularity, researchers have generally focused on the correlation between the minimum and the maximum hole diameters [29, 106-109]. Ng and Li [108, 109] and Okasha et al. [105] estimated the equivalent hole diameter based on the total area of the irregular diameter and defined the average circularity as the ratio of the minimum to maximum hole diameter. Ghoreishi et al. [106, 110]; on the contrary, defined the hole circularity as the ratio of the maximum to minimum diameters of the hole.

In addition to the resolidified material, hole taper, and noncircularity mentioned above, barrelling, heat affected zone (HAZ), and microcracking may occasionally be

observed in pulsed drilled holes [49, 99, 100, 111]. These defects, although unavoidable, can be minimised by selecting the appropriate operating conditions. Several parameters are found to have influence on the laser drilled hole characteristics. Amongst these parameters, it is well known that laser parameters play the most important role.

3.5 PARAMETERS AFFECTING LASER DRILLED HOLE QUALITY

Laser applications for material processing have been growing continuously due to its vast advantages as explained earlier. In order to achieve the maximum drilling efficiency with the best hole quality and at the minimum cost, it is extremely important to have the laser machine run at optimum operating parameters.
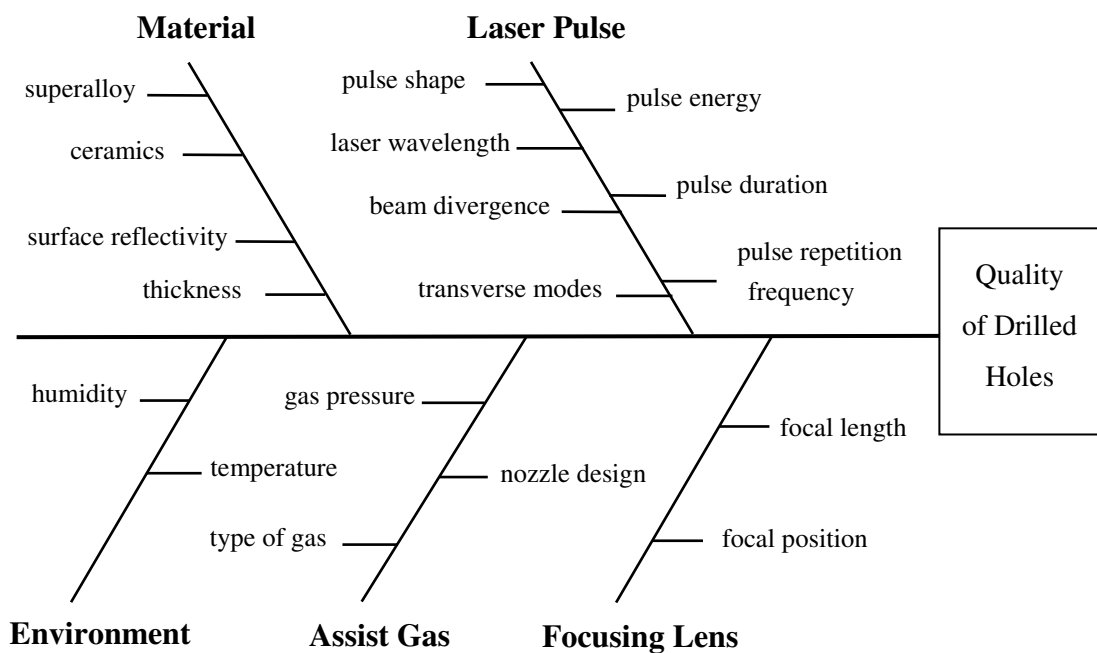
Figure 3.11 Parameters affecting laser drilled hole quality [29].

To date, several studies have been conducted in an effort to relate the operating parameters to the drilling efficiency and the drilled hole quality [107, 112-118]. For example, Yilbas [107] has demonstrated that the hole taper and recast layer formed inside the drilled hole can be effectively reduced by selecting the appropriate focal position, pulse energy, pulse width and pulse frequency. According to Yeo et al.

[29], these parameters may be divided into five categories, as shown in Figure 3.11, including: material properties, laser pulse parameters, focusing lens setting, assist gas and environment conditions.

3.5.1 Assist gas

In laser drilling, assist gas is normally used coaxially to the laser beam for the purpose of facilitating the material removal, blowing out the spatter and recast layer deposited on top and inside the cavity, preventing the optics from the debris ejected from the interaction zone and providing additional cooling to the substrate. At low laser intensity, where melting governs the melt removal mechanism, the assist gas enhances the melt removal and reduces the recast layer by increasing the shear forces on the liquid surface. At high laser intensity, where vaporisation dominates, the assist gas improves the drilling efficiency by expelling the vapour and debris that can prevent the laser beam from reaching the workpiece surface [7, 119].

Because assist gas flows coaxially in tandem with the laser beam, it is obvious that pressure of the assist gas would disturb the laser beam profile irradiating the workpiece. Up to ten percent of the incident energy may be scattered or blocked from material surface due to assist gas pressure, resulting in a non-linear profile of the drilling rate. However, the dissipated energy does not leave the interaction area and is later coupled into the cavity, resulting in the enlargement of the drilled hole [120].

Type of assist gas used also has influence on the final drilled hole quality. To date, oxygen is widely used as an assist gas to increase the material removal rate due to the exothermic energy added to the process [7, 119, 121-123]. Oxide formed at the surface also reduces the viscosity of the liquid metal thereby promoting the melt ejection [7]. In addition to the melt removal enhancement, oxygen assist gas also causes two important changes to the material surface; a change in the absorptivity, and a change in the melting temperature of the material. It has been reported that the absorptivity of the workpiece increased if oxidation occurred in the process [124, 125]. However, if the melting temperature of the oxide formed was higher than that of the parent material, longer time was needed to melt and expel the oxide and liquid material [119].
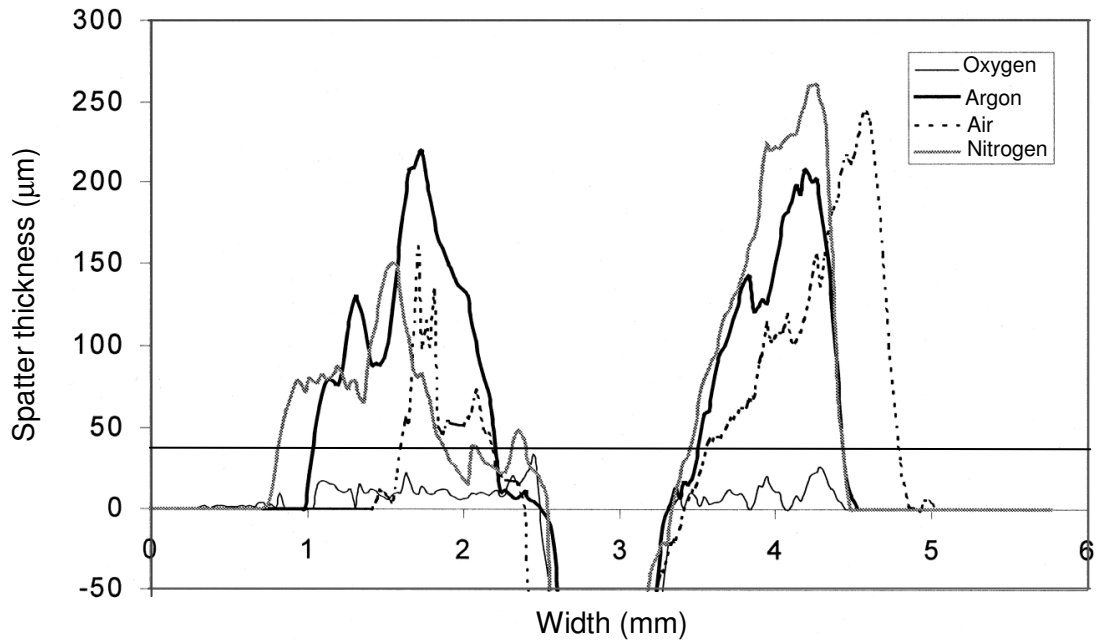
Figure 3.12 Effect of assist gas type on spatter thickness and shape [114].

In addition to the material removal and drilling rate, assist gas also has an impact on the hole quality. Low et al. [114] investigated the influence of assist gas on spatter accumulated during laser percussion drilling of Nimonic 263 alloy. Four gases considered were argon, nitrogen, compressed air and oxygen. It was found that oxygen assist gas gave the lowest spatter thickness with the weakest spatter bonding strength. Figure 3.12 shows the spatter thickness obtained from the four different assist gases used [114].

Rodden et al. [126] experimentally investigated the effects of assist gas with single pulse Nd:YAG laser drilling of titanium. They found that as the percentage of oxygen in the assist gas increases, larger entrance diameter and larger hole taper were observed. They also noted that assist gas could either promote or hinder the breakthrough percentages in drilling. The hindering effect was probably generated by the assist gas pressure exerted on the workpiece surface.

Khan et al. [127] conducted an experimental study on the effects of the assist gas type and nozzle size on the nanosecond laser percussion drilling of 316L stainless steel. The experiments were performed using oxygen, air and also with no assist gas in the system. The results showed a reduction in the drilling velocity when assist gas was employed. The lowest drilling rate existed when oxygen was used. However, the

51

diameter and taper of the hole drilled with the assist gas were larger compared to those obtained from drilling without assist gas. In addition to the type of assist gas, nozzle diameter was also found to have impact on hole quality. Khan et al. [127] reported that drilling with the smallest gas nozzle produced the thinnest recast layer.

Yilbas and Aleem [99] conducted experiments to study the impact of various parameters on the drilled hole quality. Compared with laser energy, focal plane position and workpiece thickness, assist gas pressure were shown to have the most significant impact on hole taper and surface debris characteristics.

3.5.2 Laser parameters

As laser drilling is based on thermal interaction between the laser beam and the material, it is obvious that the laser beam, acting as a heat source, is crucial for the drilled hole quality. In laser percussion drilling, a series of laser pulses is delivered onto the same spot and therefore the energy transferred is normally considered in terms of each pulse. These laser parameters which have significant influence on the hole characteristics are peak power, pulse width, pulse frequency, pulse shape and laser beam properties including the laser wavelength, beam divergence and transverse modes.

3.5.2.1 Peak power, pulse width, pulse frequency, and number of pulses

Numerous experimental and mathematical data confirm the pivotal relationship between the pulse variables, hole geometry, and metallurgical quality [96, 100, 113, 115, 128-131]. For any laser machine, pulse peak power, pulse width and pulse energy are normally interdependent. For a laser beam with rectangular temporal beam profile, the relation between these variables can be expressed as:

$$P_p = \frac{E}{t_{on}}$$
(3.7)

where P_p is the peak power, E is the pulse energy, and t_{on} is pulse width.

Pulse peak power:

Pulse peak power has significant impact on the material removal mechanism. As peak power increases, more energy is transferred into the material creating more

vapour above the workpiece surface. The large amount of vapour then causes a large recoil pressure above the melt liquid layer and enhances the liquid removal from the crater. Eventually, this lowers the formation of the recast layer [29, 128, 129, 132]. Figure 3.13 shows variation of the average recast layer thickness with the peak power obtained from the experiment performed on a high-nickel alloy [132].
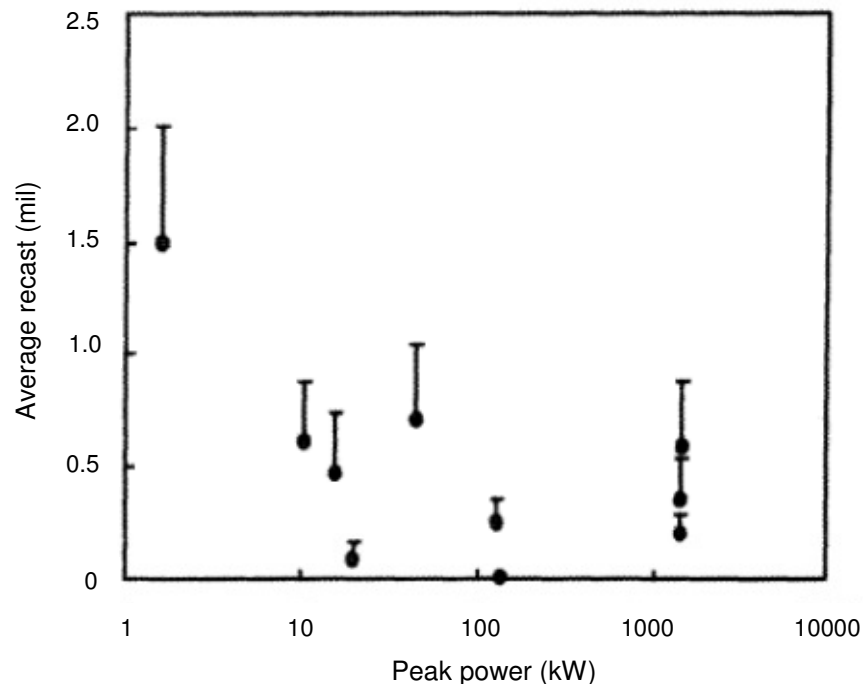
Figure 3.13 Variation of the average recast layer thickness with peak power [132].

According to Eq.(3.7), it can be seen that high peak power can be achieved by either increasing the pulse energy or by reducing the pulse width. However, if a lower peak power is required, then it is recommended to adjust pulse energy rather than pulse width. This is because pulse with too long width may result in excess melting and hence widen the entrance diameter [130, 131].

Figure 3.14 shows the effects of peak power on drilled hole diameter [100]. The three plots show entrance, exit and minimum diameters of the hole. It can be seen that higher peak power gives larger hole diameter at all three positions. There is a slightly decrease in the exit and minimum hole diameter at 16 kW peak power. This is because at high peak power, plasma plume may be formed and part of the laser

energy is trapped in the plasma resulting in less laser energy reaching the cavity and hence a smaller hole diameter [100].
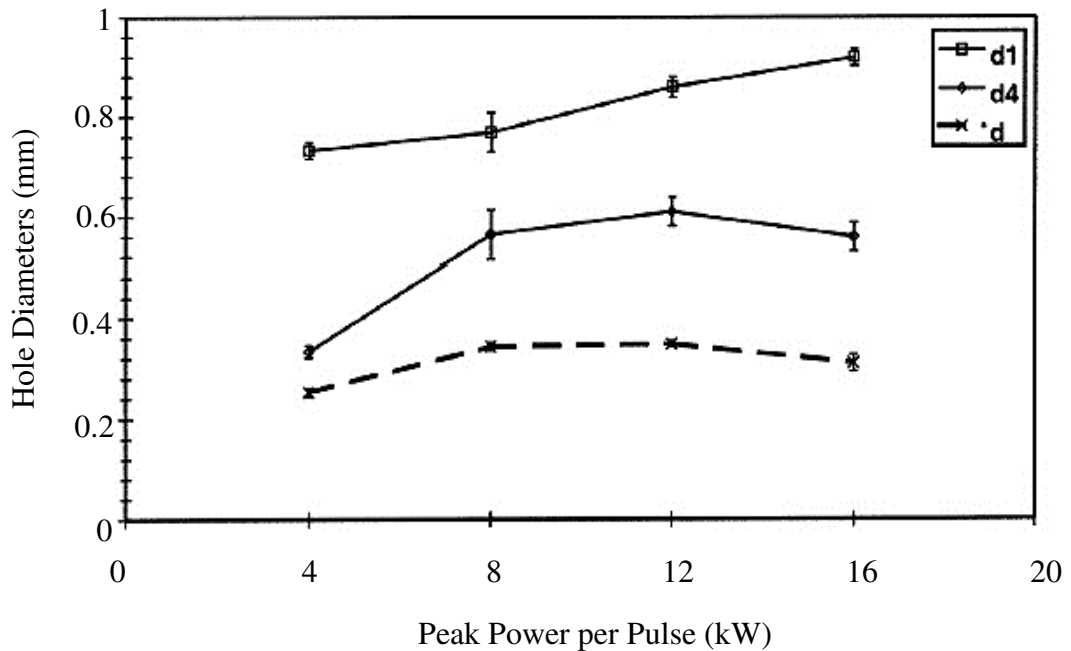
Figure 3.14 Effects of peak power on drilled hole diameter [100],
d1: entrance diameter, d4: exit diameter, d: minimum diameter.

Han and Pryputniewicz [96] have also reported on the variation of hole diameter with peak power and have concluded that the increasing in peak power has a more noticeable influence on minimum and exit diameters than the inlet diameter.

Low et al. [115] studied the effects of peak power on spatter formation and reported a larger spatter deposited at high peak power. This was due to more melt removal taking place at high peak power, resulting in more solidified liquid deposited around the hole entrance. Lowering the peak power reduced the spatter but the drilling time was increased accordingly.

Pulse width:
Pulse width has been found to have a significant influence on mean hole diameter and inlet cone [107]. From Eq. (3.7), it can be seen that, for a fixed pulse peak power, as the pulse width increases, energy per pulse is increased accordingly. This

leads to more vapour being generated, higher recoil pressure, and more subsequent liquid removal.

In general, longer pulse results in larger diameter and the deeper holes [15, 96, 115, 133]. However, Han and Pryputniewicz [96] found that too long pulse duration may be unable to produce the through hole. As the pulse width was extended to more than 1.75 ms, a through hole was not achieved for 30 mm thick stainless steel 304. This was attributed to the occurrence of the laser-supported absorption (LSA) at high laser pulse energy.

Advantages of drilling with short, high intensity pulse have been recently reported [1, 128, 132-135]. Previous studies have revealed that drilling with a short pulse duration dramatically reduces the severity of microcracking and the recast layer thickness [1, 128, 132], improves hole circularity and process repeatability [133, 135], and causes less HAZ defects [15]. However, for nanosecond and femtosecond pulse drilling, it was found that HAZ does not depend on pulse width setting [84].
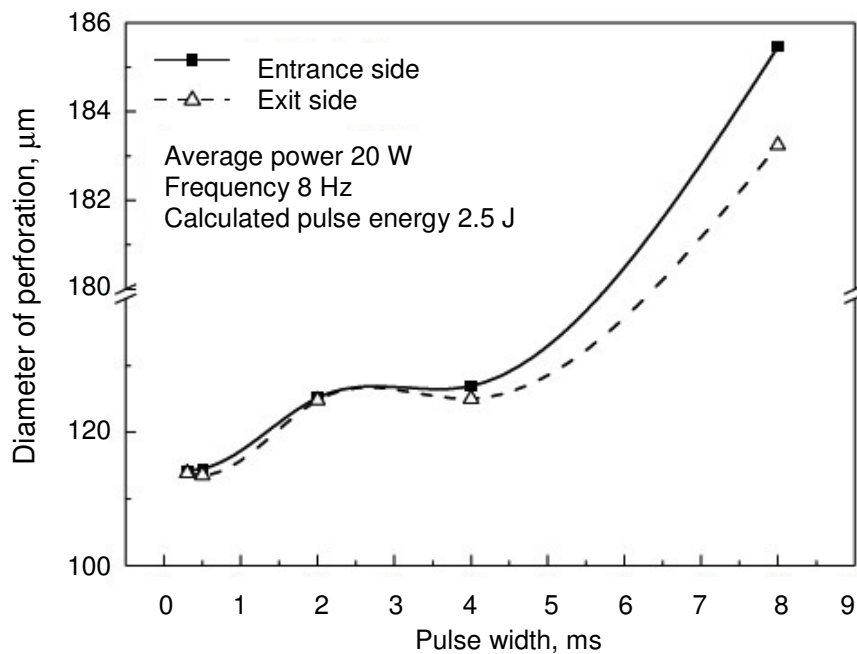
Figure 3.15 Effect of pulse width on drilled hole diameter [133].

Figure 3.15 shows the effects of the pulse width on the laser drilled hole diameter [133]. At the shortest pulse width, the difference in diameters at the entrance and exit sides is insignificant thereby indicating that the smallest hole taper can be produced at this point.

In conclusion, selecting a suitable pulse width is a compromising decision. A long pulse width is more energy efficient while a short pulse width gives better hole quality. It has been recommended that the pulse width for laser drilling should be in the range of 0.1-2.5 ms [29].

Pulse frequency:

Influence of pulse frequency on drilled depth and interaction time is shown in Figure 3.16 [136]. The collected data has indicated that pulse frequency has no meaningful effect on the maximum drill depth. However, the interaction time to reach the maximum drill depth varies depending on the pulse frequency.
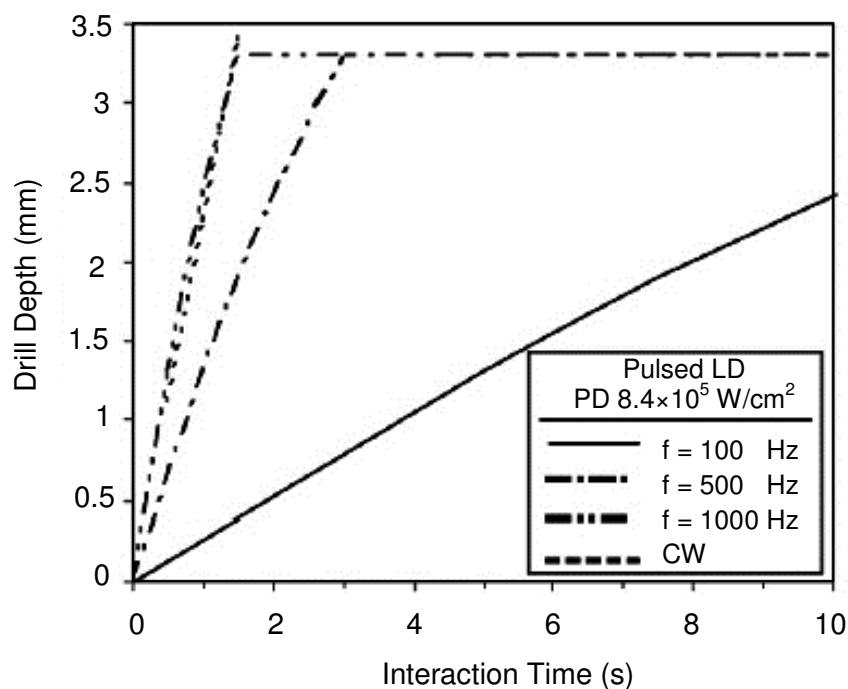
Figure 3.16 Effect of pulse frequency on maximum drill depth [136].

Number of pulses:

In laser percussion drilling, number of pulses has significant influence on the hole depth. During the initial pulses, drilling rate increases rapidly which may be due to

56

an effective mass removal mechanism. As the number of pulses increase, the drilling rate decreases. This is most-likely due to the defocusing effect of the laser beam at the bottom of the cavity [137].

3.5.2.2 Pulse shape

The importance of pulse shaping on laser drilling productivity and quality has been widely reported to date [138-147]. Similar studies have also been conducted in laser welding in order to improve the joint quality [148, 149]. Figure 3.17 illustrates example of various temporal pulse shapes, where τ_0 is the time when peak power is achieved and τ_p is the pulse on duration.
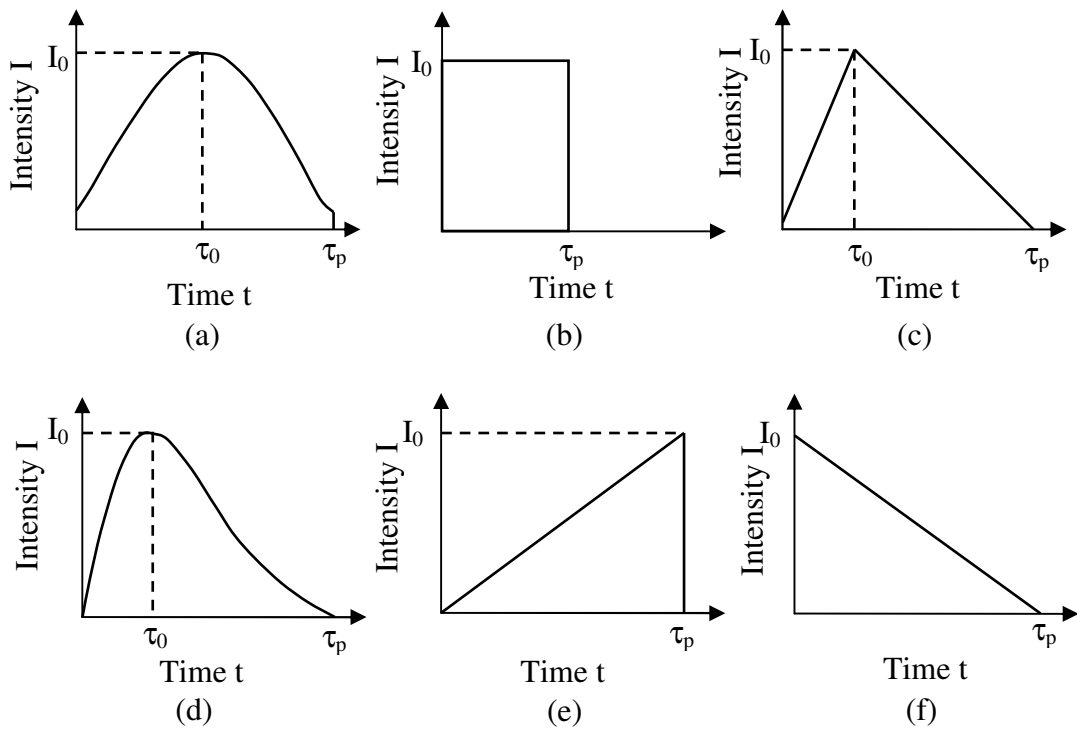
Figure 3.17 Examples of various laser pulse shapes: (a) Gaussian,
(b) rectangular, (c) triangular, (d) smooth, (e) ramp-up,
(f) ramp-down [149].

There are generally two types of laser pulse shaping: individual pulse modulating called 'intra-pulse' shaping and entire pulse train modulating called 'inter-pulse' shaping. Roos [138] compared the hole quality drilled by the normal continuous pulse and the short spiked pulse train with the same laser energy. It was found that the pulse train configuration provides a better hole quality without clogging due to

molten material. A similar conclusion was recently reported by Tan [81]. In an attempt to improve the hole wall deformation, Tan employed the pulse train, called 'multi-bursts' in his work for drilling a silicon workpiece with an aspect ratio up to 1:10. Initially, a series of low energy pulses interacted with the workpiece and produced a through hole with minimal deformation. After that, a series of high energy pulses were delivered to enlarge the hole diameter until the required dimension was obtained. The results showed that using a pulse train with increasing laser energy for each successive pulse improved the straightness of the wall.

Further studies confirmed that laser pulse shaping strongly affects material removal mechanism [141-143]. Low et al. [141] compared the hole drilled by a linearly increasing inter-pulse (see Figure 3.18 (b)) with that produced by a normal pulse delivery pattern. It was found that the spatter accumulated around the hole entrance was reduced while the material ejected from the hole exit was increased when a modulated pulse train was used. Improvements in the hole taper using a linearly increasing inter-pulse train was also reported later by Low and Li [142]. This was attributed to the attenuation of laser intensity at the hole exit which resulted from multiple reflections and better absorption along the hole wall.

Low and Li [142] also studied the influence of the ramp-up intra-pulse shaping (see Figure 3.18 (a)) on the laser drilled hole quality. Their results showed that this type of intra-pulse alone has no significant impact on the hole wall taper.

Chen et al. [140] compared a hole drilled by a rectangular pulse in comparison with that drilled by a sharp-spiked intra-pulse. The results showed that with the same average power and drilling time, the hole penetration by the latter was deeper.

Mazhukin et al. [143] compared temperatures and melting front velocity profiles obtained from rectangular, Gaussian, rising triangular and falling triangular pulses. It was suggested that if hole depth was the most important factor, then Gaussian or falling triangular pulses should be employed. In cases where absence of the effects of melting was required, rectangular or rising triangular pulses were recommended.

Laser Peak Power

Initial Laser Pulse (n=1)

Initial Laser Pulse (n^{th} pulse)

P_p

Intra-pulse shaping within each pulse (ramp-up pulse shown).

Time

$P_p = P_{p1} = P_{p2}$
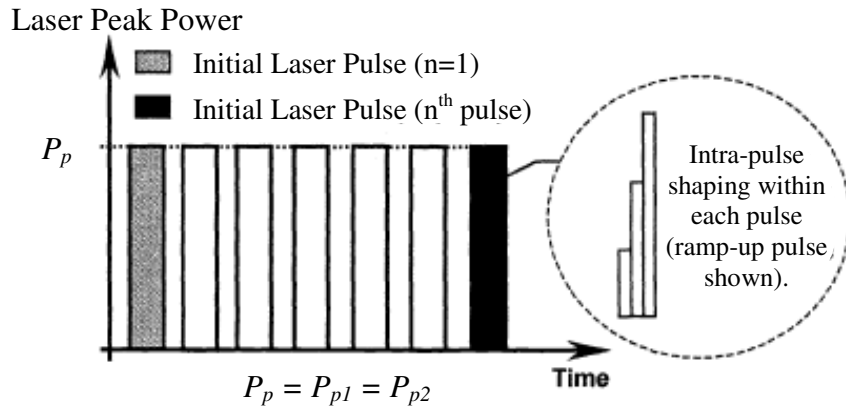
(a) Ramp-up rectangular intra-pulse delivered by normal delivery pattern

Laser Peak Power

Initial Laser Pulse (n=1)

Final Laser Pulse (n^{th} pulse)

P_{p2}

P_{p1}

$P_{p2} > P_{p1}$

Time
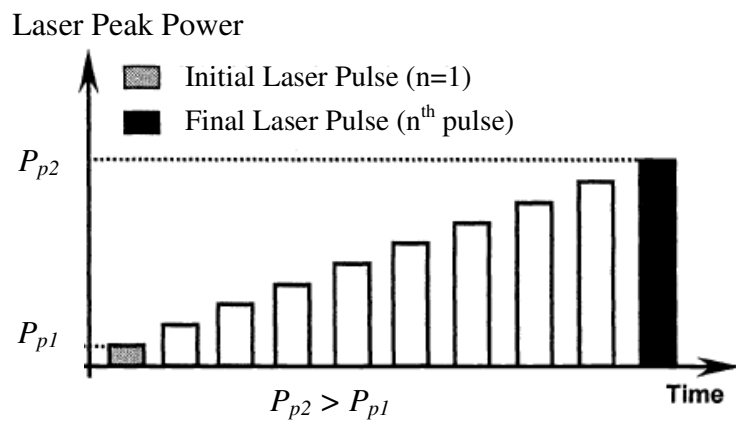
(b) Linearly increasing rectangular inter-pulse pattern

Figure 3.18 Intra-pulse and inter-pulse shaping [142].

% Height*

Ramp-up   Treble   Ramp-down
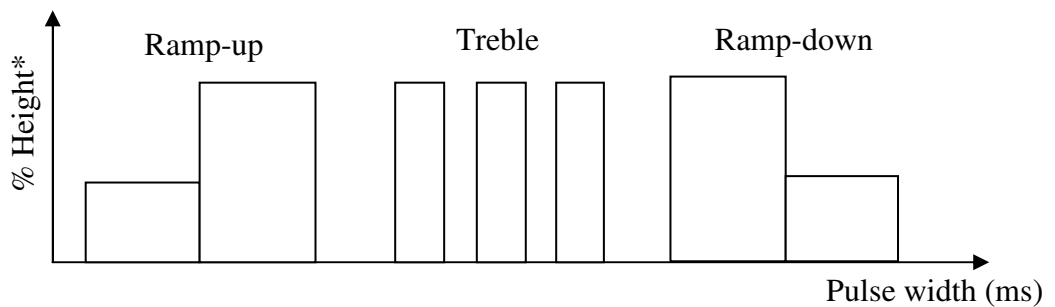
Pulse width (ms)

Figure 3.19 Pulse shapes considered in Corcoran et al.[1]'s study. (% Height is an adjustable function on the JK704 laser. %Height coupled with pulse width identifies the energy content of the laser pulse.)

Corcoran et al. [1] investigated the influence of pulse shape on percussion drilling of Rene80 coated with a thermal barrier coating. Rectangular ramp-up, ramp-down and treble pulses, as shown in Figure 3.19, were studied. It was concluded that a ramp-up pulse gives a reduction of the delaminating defect while a treble pulse shape generates least microcracking.

3.5.2.3 Laser wavelength, beam divergence and transverse mode

Laser wavelength:

Effects of the laser wavelength on laser operating performance are normally considered from the point of view of reflectivity which depends on the material type and the incident wavelength [16, 29]. As explained earlier in section 3.3.1, the following correlation between the reflectivity and the absorptivity [48] holds:

for opaque materials: reflectivity = 1- absorptivity ,

for transparent materials: reflectivity = 1 – (transmissivity+absorptivity).

It clearly indicates that with a more reflected laser beam, less energy is absorbed. Table 3.2 lists the reflectivity of various materials at laser operating wavelengths. Amongst these wavelengths, a CO_2 laser with 10.6 µm wavelength results in the highest reflection of all metals. Ruby and glass lasers are recommended for metal processing [150].

Table 3.2 Reflectivity of metals at normal incident [150].

Wavelength (µ)	Au	Cu	Mo	Ag	Al	Cr	Fe	Ni
0.4880 (Ar ll)	0.415	0.437	0.455	0.952	-	-	-	0.597
0.6943 (Cr^{3+})	0.930	0.831	0.498	0.961	-	0.555	0.575	0.676
1.06 (Nd3+)	0.981	0.901	0.582	0.964	0.733	0.570	0.650	0.741
10.6 (CO_2)	0.975	0.984	0.945	0.989	0.970	0.930	-	0.941
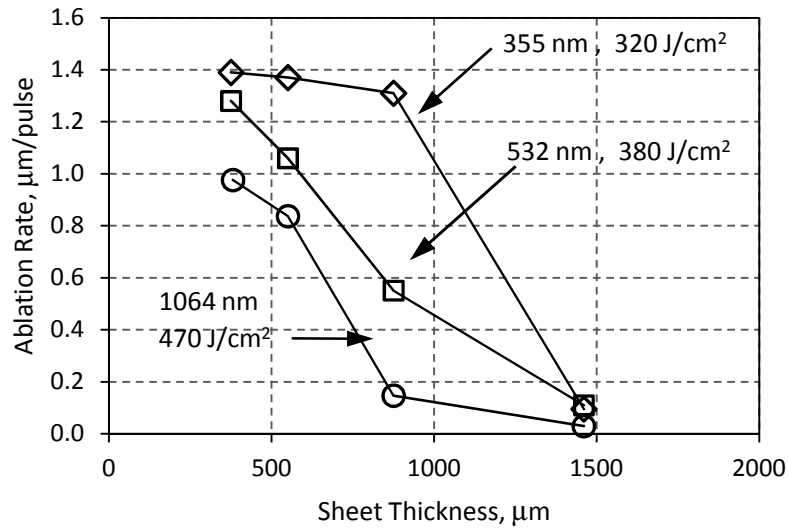
Figure 3.20 Effect of wavelength on drilling rate [151, 152].

Dependence of the ablation rate of stainless steel on laser wavelength can be seen in Figure 3.20. Although shorter wavelength gives the higher drilling rate, this effect disappears at the maximum sheet thickness used in this experiment.

Beam divergence:

Owing to the way nature of light, the emitted radiations from a laser machine are not perfectly parallel. However, the divergence angle for most laser beams is quite small. Therefore, it can be adjusted and focused to a small spot using a simple lens system.

One simple way to reduce beam divergence is to pass the beam through a 'reverse telescope' lens system arranged as shown in Figure 3.21 [153]. The original laser beam divergence θ_1 can be modified to give a smaller divergence angle θ_2 by a factor f_1 / f_2 whereas the beam diameter is enlarged by the factor f_2 / f_1 [153].
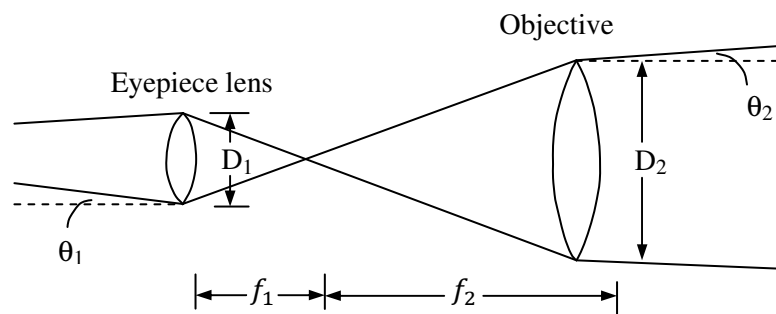
Figure 3.21 Reverse telescope arrangement used to reduce beam divergence [153].

61

Laser beam divergence during laser drilling also has impact on the hole geometry. From the experimental and mathematical data obtained for a Gaussian beam, it has been suggested that a conical hole can be produced with a collimated Gaussian beam and a bulbous hole can be drilled with a very rapid expanded beam [80, 154]. Lazare and Tokarev [155] recently developed a mathematical model for predicting the drill depth as a function of laser pulse energy and beam divergence. It was found that deeper holes can be drilled with a low divergence laser with high brilliance (laser pulse energy/divergence angle).

Transverse mode:

Laser resonators can be considered by two modes; transverse, and longitudinal. Transverse mode indicates the cross-sectional profile of the laser output while longitudinal mode relates to the resonance along the laser cavity. Basically, transverse mode has a more pronounced effect on beam quality in most applications [49].

As the waves travel along the laser axis, some waves travel on-axis but some may travel off-axis and are able to replicate themselves after covering a closed path [153]. This results in a number of 'light spots' in the laser output which is referred to as transverse mode or transverse electromagnetic mode (TEM). Samples of TEM patterns are given in Figure 3.22 [153].

TEM_{00} (uniphase) TEM_{01}

TEM_{10} TEM_{11}
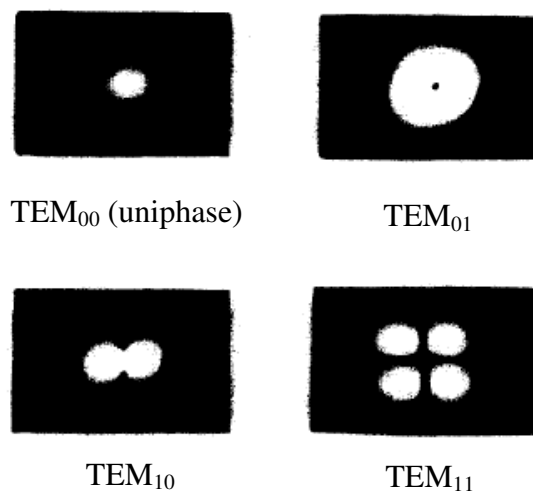
Figure 3.22 Samples of TEM patterns [153].

TEM$_{00}$ is the lowest order mode with minimum diffraction loss, minimum divergence and can be focused to the smallest spot. Although higher order modes give larger beam divergence, the beam output is more energy efficient as a larger volume is excited. For laser hole drilling, a combination of low-order modes is recommended to give low divergence but high energy output beam [29, 49].

3.5.3 Focusing lens: focal position and focal length

Focal position and focal length are two more parameters which influence laser drilled hole characteristics as these relate to the laser power intensity distribution and the spot size projected onto the material surface [156]. Focal length is related to the minimum spot size by the following equation:

$$d_f = f_l \, \theta \tag{3.8}$$

where d_f is the minimum spot diameter (waist diameter), f_l is the focal length, and θ is the total beam divergence angle.

The depth of focus or the depth of field (Δf) is the distance over which the focused spot diameter changes by 5% [157]. The following equation can be used to estimate the depth of focus [157]:

$$\Delta f = \frac{2 d_f \, f_l}{d_b} \tag{3.9}$$

where d_b is the unfocused beam diameter.

Eq.(3.9) suggests that a lens with long focal length gives larger depth of focus.
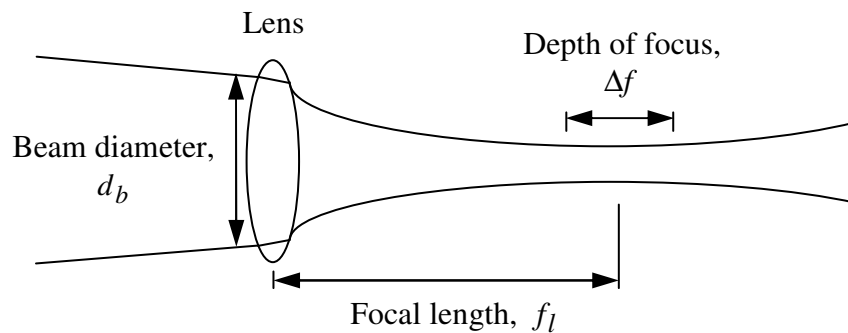
Figure 3.23 The depth of focus [7].

In case of laser drilling, the common requirements corresponding to these factors are beam with low divergence, long focal length and negative focal plane [29].

Focal plane position may be divided into three groups based on relative position to the workpiece surface [115]:

1. zero focal plane position: the focal plane position is located exactly on the workpiece surface,

2. positive focal plane position: the focal plane position is set above the workpiece surface, and

3. negative focal plane position: the focal plane position is set below the workpiece surface.

Research on the effects of focal plane position has revealed that in order to obtain a hole with small diameter, good circularity, and low taper, a negative focal plane position should be employed with a compromise made in the amount of spatter generated [29, 49, 115]. Owing to the reduction in laser intensity as the beam enlarges, the positive focal plane position tends to provide the hole with enlarged entrance, poor circularity and even a non-through hole [115].

3.5.4 Material properties and environment

When a laser beam is incident on the substrate, it is reflected, absorbed and transmitted depending on whether the material is opaque or transparent. In order to develop a laser model, absorptivity or reflectivity are required for calculating the actual laser power absorbed by the material. The correlation is expressed as:

$$I_{abs} = A.I_0 = (1 - R_f)I_0 \qquad (3.10)$$

where I_{abs} , I_0 , A and R_f *are* the absorbed laser intensity, laser intensity at the material surface, absorptivity, and reflectivity, respectively.

Despite low absorptivity of metallic materials at room temperature, some intrinsic mechanisms promote the absorption coefficient during the interaction time [158-162].

1. As the temperature of the substrate increases due to laser heating, absorptivity of materials rises accordingly. Experimental studies on laser drilling have shown

that the absorptivity can rise up to 80% for laser intensity in the range 10-20 MW/cm^2 [159]. As a result, strong vaporisation induced at the liquid-vapour interface enhances the beam scattering and hence absorption at the interface.

2. Dust, oxides and other impurities deposited on the surface also contribute to an increase in the absorption coefficient.

3. If plasma is formed in the process, it can absorb part of the laser energy and subsequently transfer it to the substrate.

In addition to absorptivity, thermal properties of the materials also have direct influence on the drilled hole quality [163, 164]. Shen et al. [163] compared the melt depth calculated from the mathematical model for four metals, as shown in Figure 3.24. As can be expected, the melt depth for the same interaction time for each material, varies according to the differences in material properties. Chmelickova and Polak [164] also obtained similar results from their experiments. It was found that for the same operating variables, aluminium can be drilled to a depth of 10 mm while copper to only 2 mm.
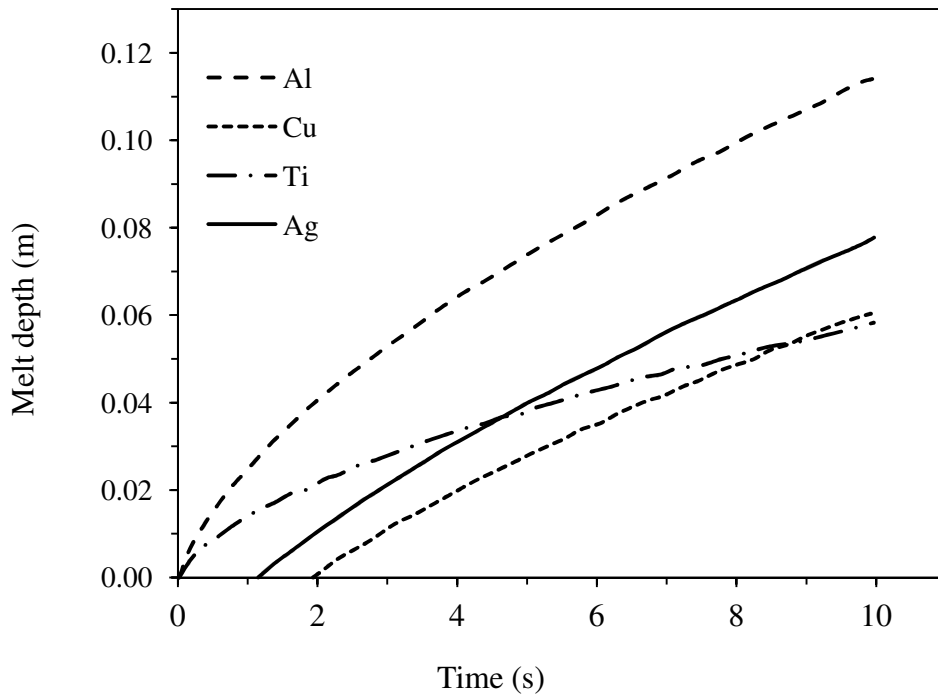
Figure 3.24 Comparison of calculated melt depth for four metals [163].
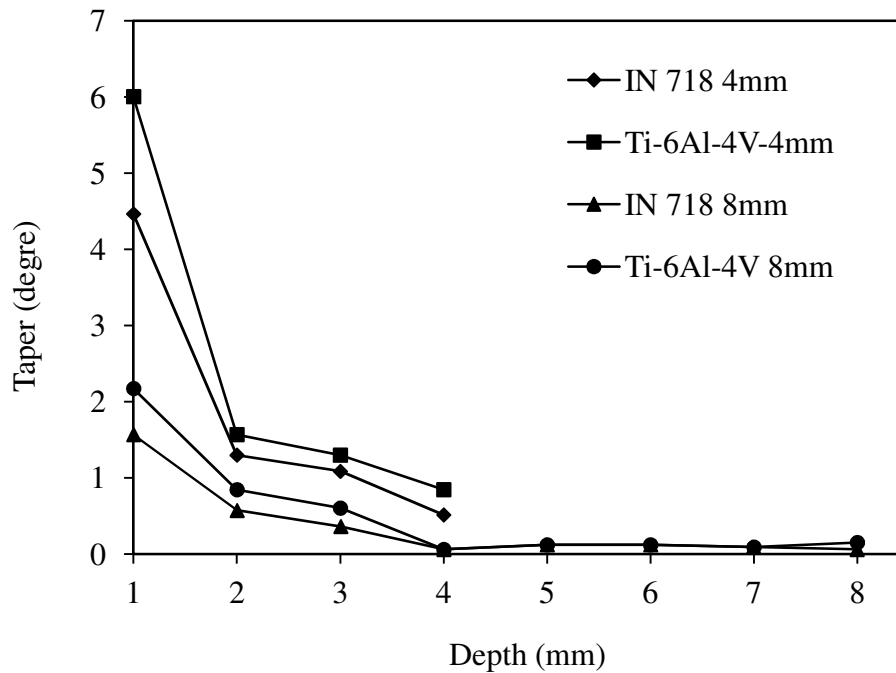
Figure 3.25 Influence of material thickness on hole taper at various depths [112].

In addition to material properties, workpiece geometry also affects the process performance. In case of laser drilling, the thickness of the material also plays a role on the final drilled hole quality. Bandyopadhyay et al. [112] concluded from their experimental study on laser drilling of IN718 and Ti-6Al-4V that material and its thickness have a remarkable influence on hole quality in terms of both geometrical and metallurgical aspects. It was found that increasing the material thickness leads to a lowering of the hole taper whereas spatter, recast layer and HAZ increase with material thickness. Figure 3.25 shows effects of material properties on hole taper [112].

Environmental variables such as dust, oil vapour, ambient temperature, humidity and vibration of the machine could also have impact on the laser performance. For example, in case of high power laser applications, oil vapour or dust may lead to serious damage of the optical system [29].

CHAPTER 4
LITERATURE REVIEW-LASER DRILLING MODELS

4.1 INTRODUCTION

Mathematical modelling has long been recognized as an effective tool for studying various phenomena involved in laser material processing. Based on the basic concept of thermal processing, the general model of laser beam-material interaction can be applied to most laser applications. Basically, heat conduction, fluid and vapour dynamics, and the corresponding boundary conditions are discussed. There are, however, differences in the detail of each particular application. Nevertheless, the formulation of these problems can be analysed in a very similar way.

Over the past two decades, modelling of laser drilling has continuously improved. The available models may range from the simple ones to the most sophisticated depending on the assumptions, problem setting and solving approaches. Nevertheless, similar to other mathematical models for laser processing, the governing equations for laser drilling models are typically established from heat conduction in solid and liquid, conservation of mass and energy, as well as the boundary conditions at the interfaces.

Development of the laser drilling model is normally divided into three stages namely solid heating, melting, and vaporisation. During solid heating, laser beam interacts with the solid substrate and raises the solid temperature to the melting point. The modelling of this stage is typically focused on determining the temperature profile in the solid substrate [136, 165-167]. Once melting begins, the solid-liquid interface is formed and propagates into the solid. Modelling of this stage is normally aimed to find the solid-liquid interface location, its moving speed, and the melt layer thickness [163, 168, 169]. Further irradiation of the laser beam not only leads to more melting at the solid-liquid interface, it also raises the surface temperature of the liquid layer. If laser energy is sufficiently high, vaporisation takes place and the liquid-vapour interface is formed. The vapour generated inside the cavity also exerts a recoil pressure on the liquid surface resulting in melt expulsion. The analysis of this stage is

generally focused on determining the solid-liquid and liquid-vapour interfaces locations, drilling speed and the hole profiles [166, 170-172].

In this chapter, mathematical models of laser drilling developed in the past are summarized. The content is divided into three sections namely solid heating, melting (and solidification), and vaporisation.

4.2 SOLID HEATING

During laser heating, laser energy heats up the solid substrate from room temperature to the melting point. To determine the temperature profile in the solid and the time required to initiate melting, one-dimensional transient heat conduction in a semi-infinite solid has been generally applied to the analytical modelling [165, 166, 173, 174]. Consider a solid plate subjected to a laser heat beam at the surface ($z = 0$) as illustrated in Figure 4.1:
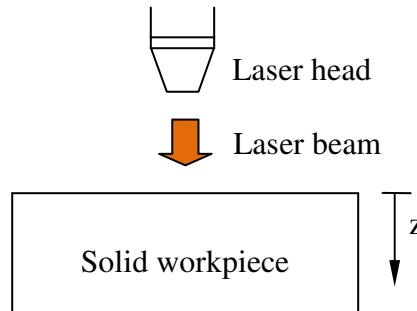
Figure 4.1 Schematic diagram of stage 1: solid heating.

The heat conduction equation can be written as:

$$\frac{\partial^2 T_s}{\partial z^2} = \frac{1}{\alpha_s} \frac{\partial T_s}{\partial t}$$

(4.1)

where T_s, t, z, and α_s are the temperature in solid, time, vertical distance, and thermal diffusivity of the solid, respectively.

The boundary and initial conditions are

$$T_s(z,0) = T_0$$

(4.2)

68

$$I_{abs} = -k_s \frac{\partial T_s}{\partial z}\bigg]_{z=0} \tag{4.3}$$

where k_s is the thermal conductivity of the solid workpiece, T_0 is the ambient temperature, and I_{abs} is the absorbed laser intensity defined by:

$$I_{abs} = (1 - R_f)I_0 = A_s I_0 \tag{4.4}$$

where I_0, A_s, and R_f are the incident laser intensity, absorptivity, and reflectivity of the solid, respectively.

Carslaw and Jaeger [165] assumed that there would be solutions to the above system of equations if the laser absorption profile was in the form:

$$I(z,t) = I_{abs} erfc \frac{z}{2\sqrt{\alpha_s t}} \tag{4.5}$$

where $erfc$ is the complimentary error function and is defined by [175]:

$$erfc(x) = 1 - erf(x) = \frac{2}{\sqrt{\pi}} \int_x^\infty e^{-u^2} du$$

where u is a temporal variable defined here for integrating.

The temperature profile in solid is then found to be:

$$T_s(z,t) = T_0 + \frac{2I_{abs}}{k_s}\left[\left(\frac{\alpha_s t}{\pi}\right)^{1/2} e^{-z^2/4\alpha_s t} - \frac{z}{2} erfc \frac{z}{2\sqrt{\alpha_s t}}\right] \tag{4.6}$$

Of particular interest is the temperature at the surface so that the time required to initiate the melting can be estimated. According to Eq.(4.6), for a single laser pulse heating, the temperature at the surface ($z = 0$) can now be determined from [165]:

$$T_s(0,t) = T_0 + \frac{2I_{abs}}{k_s}\left(\frac{\alpha_s t}{\pi}\right)^{1/2} \tag{4.7}$$

In case of laser percussion drilling, a series of multiple pulses are employed. As shown in Figure 4.2, each successive laser pulse is separated by a pulse off time where there is no laser beam-substrate interaction. The temperature drop takes place during this pulse off duration.
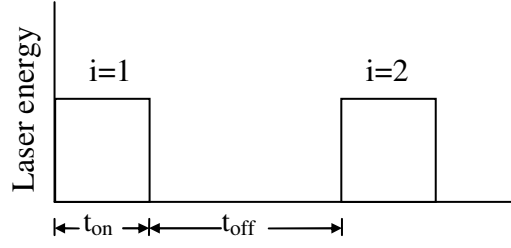
Figure 4.2 Time step in laser percussion drilling.

The rise and drop of the surface temperature during the ith cycle can be estimated from [51, 165]:

$$T_{on,i}(0,t) = T_{(i-1)/f} + \frac{2I_{abs}}{k_s}\sqrt{\frac{\alpha_s(t-(i-1)/f)}{\pi}} \quad ;$$

$$\text{for} \quad \frac{i-1}{f} \leq t \leq \frac{i-1}{f} + t_{on} \qquad (4.8)$$

$$T_{off,i}(0,t) = T_{(i-1)/f} + \frac{2I_{abs}}{k_s}\left[\sqrt{\frac{\alpha_s(t-(i-1)/f)}{\pi}} - \sqrt{\frac{\alpha_s(t-t_{on}-(i-1)/f)}{\pi}}\right] \quad ;$$

$$\text{for} \quad \left(\frac{i-1}{f}+t_{on}\right) \leq t \leq \frac{i}{f} \qquad (4.9)^*$$

where $T_{on,i}(0,t)$ and $T_{off,i}(0,t)$ are the surface temperatures during heating and pulse off duration, and $T_{(i-1)/f}$ is the surface temperature at the end of the $(i-1)th$ pulse, respectively.

It is worth noting that in Eq.(4.9), the effect of convective heat transfer between the heated surface and the surrounding gas is not included. Therefore, some errors can be expected. Figure 4.3 shows the temporal characteristics of the surface temperature during pulsed laser heating [51]. It can be seen that the surface temperature rises sharply during heating with each pulse and decays dramatically during the pulse off time.

---

* It is unclear why the laser source, I_{abs}, is included in the pulse off term as written in Eq.(4.9). To author, the laser source should appear in the pulse on term only.
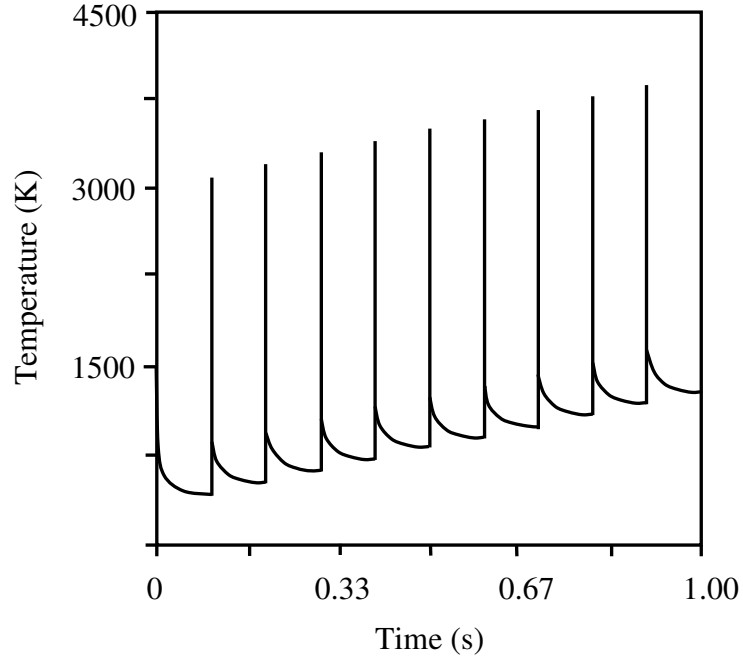
Figure 4.3 Temporal evolution of the surface temperature [51].

In order to include effects of the convective heat transfer into his analysis, Holman [173] derived an expression to predict the temperature change of a plate subjected to heat convection at the surface. By applying this equation to the case of cooling during laser pulse off, the change in surface temperature can be written as [136]:

$$T_{off,i}(0,t) = T_{on,i}(0,t) + [T_0 - T_{on,i}(0,t)]\left\{1 - \left[\exp\frac{h_g^2\alpha_s t_{off}}{k_s^2}\right]\left[1 - erf\left(\frac{h_g\sqrt{\alpha_s t_{off}}}{k_s}\right)\right]\right\}$$

(4.10)

where $erf(x)$ is the error function defined by

$$erf(x) = \frac{2}{\sqrt{\pi}}\int_0^x e^{-u^2}\,du$$

Figure 4.4 shows the surface temperature evolution calculated using Eq.(4.7) for laser heating and Eq.(4.10) for pulse off interval [136]. It can be seen that during laser beam-material interaction, the surface temperature rises sharply while the temperature drops very slightly during the pulse off duration.

71
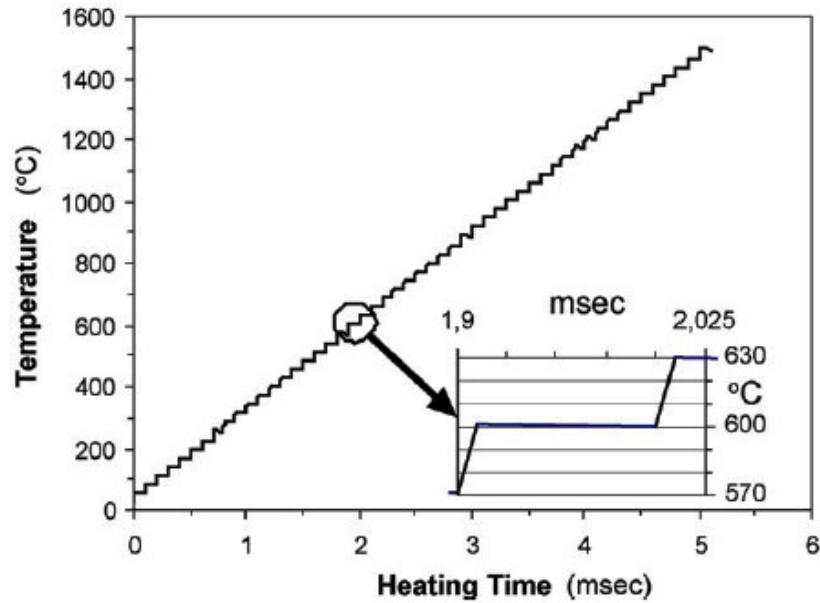
Figure 4.4 Surface temperature evolution calculated using Eqs.(4.7) an (4.10) [136].

By knowing the surface temperature during the laser beam-solid substrate interaction, number of pulses required to initiate melting can be predicted.

4.3 MELTING

If energy of the laser beam incident on the solid surface is sufficient, melting begins and the solid-liquid interface is formed and propagates into the solid. Analysis of melting can be described as the Stefan problem which deals with the phase change process with moving boundary [176].

Extensive works have been carried out to study the laser-induced melting of material, including analytical models [163, 168, 169, 177, 178] and numerical simulations [27, 179-181]. Consider a plate irradiated with the laser beam at the surface where a thin layer of molten liquid is formed, as shown in Figure 4.5. Because the melt pool diameter is much larger than the melt thickness, and because the melting occurs dominantly in the vertical direction , a one-dimensional approach may be assumed [140, 167].
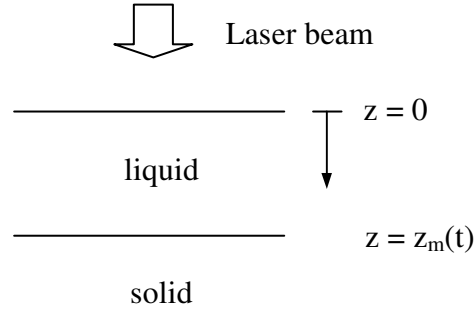
Figure 4.5 Schematic diagram of stage 2: melting.

Heat conduction equations in the liquid and solid can be described as [167, 169]

$$\frac{\partial^2 T_l(z,t)}{\partial z^2} = \frac{1}{\alpha_l} \frac{\partial T_l(z,t)}{\partial t} \qquad ; \qquad 0 \leq z < z_m \qquad (4.11)$$

$$\frac{\partial^2 T_s(z,t)}{\partial z^2} = \frac{1}{\alpha_s} \frac{\partial T_s(z,t)}{\partial t} \qquad ; \qquad z_m \leq z < \infty \qquad (4.12)$$

with boundary and initial conditions:

$$-k_l \frac{\partial T_l(z,t)}{\partial z} = A_l I_0 \qquad ; \qquad z = 0 \qquad (4.13)$$

$$T_s(z,t) = T_l(z,t) = T_m \qquad ; \qquad z = z_m(t) \qquad (4.14)$$

$$\rho_s L_m \frac{dz_m(t)}{dt} = k_s \frac{\partial T_s(z,t)}{\partial z} - k_l \frac{\partial T_l(z,t)}{\partial z} \qquad ; \qquad z = z_m(t) \qquad (4.15)$$

$$T_s(z,t) = T_0 \qquad ; \qquad z \to \infty \qquad (4.16)$$

$$z_m(t_m) = 0 \qquad ; \qquad t = t_m \qquad (4.17)$$

where $T_l(z,t)$ and $T_s(z,t)$ are the temperature profiles in liquid and solid, k_l, ρ_s and α_l are the thermal conductivity, density, and thermal diffusivity of the liquid, L_m, t_m, and $z_m(t)$ are the latent heat of melting, the time required to initiate melting, and the melting front location, respectively.

To date, solutions to the above set of nonlinear partial differential equations have been proposed by several authors [163, 165, 169, 177, 182, 183]. Carslaw and Jaeger [165] reported an approximated series solution for the solidification of a semi-infinite

large liquid mass. It must be noted that the proposed series solution is valid only for the case of low intensity laser irradiation. Cohen and Epperson [182] assumed the same thermal conductivity and diffusivity values in the solid and liquid, and obtained the melting front location as:

$$z_m(t) = \frac{0.16 I_0}{\rho_s L_m}(t - t_m)$$ (4.18)

where the time to start melting, t_m, is given by [182]

$$t_m = \frac{\pi k_s^2 T_m^2}{4 \alpha_s I_0^2}$$ (4.19)

Some researchers have developed the analytical models of laser melting by firstly assuming the temperature profiles in solid and liquid phases which satisfy the boundary and initial conditions, and heat conduction equations at some points, i.e. at $z = 0$, $z = z_m(t)$, and $z \to \infty$ [163, 169, 183]. Xie and Kar [169] assumed the temperature profile in the liquid layer to be:

$$T_l(z,t) = T_m - \frac{A_l I_0}{k_l}[z - z_m(t)] + f(t)[z^2 - z_m^2(t)]$$ (4.20)

where
$$f(t) = \frac{A_l I_0}{2 \alpha_l k_l \left(1 + \frac{z_m(t)}{\alpha_l}\frac{dz_m(t)}{dt}\right)}\frac{dz_m(t)}{dt} \; .$$

In the solid, an exponential function was assumed for the temperature profile, i.e.

$$T_s(z,t) = T_m - (T_m - T_0)\{1 - \exp[-b(t)(z - z_m(t))]\}$$ (4.21)

where $b(t) = \frac{1}{\alpha_s}\frac{dz_m(t)}{dt} \; .$

By substituting the assumed temperature profiles in the heat conduction equations, expressions for the melt depth and the melting front velocity were derived.

In addition to the profiles assumed by Xie and Kar [169], it is generally accepted that exponential forms can be approximated for the temperature profiles in the solid and liquid [163, 183, 184]. Shen et al.[163] assumed the following exponential temperature profiles in their laser melting model:

$$T_l(z,t) = T_{l0}(t) \exp\left[\frac{-z}{\delta_l(t)}\right] \tag{4.22}$$

$$T_s(z,t) = T_m \exp\left[\frac{-(z - z_m(t))}{\delta_s(t)}\right] \tag{4.23}$$

where $T_{l0}(t)$ is the melt surface temperature, and $\delta_l(t)$ and $\delta_s(t)$ are two temporal functions indicating the melt depth in liquid and solid, respectively.

It is worth noting that, in addition to the temperature profiles and melt layer thickness, Shen et al. [163, 183] also reported an expression for the melt surface temperature, $T_{l0}(t)$, i.e.

$$T_{l0}(t) = \left[\frac{2\alpha_l A_l^2 I_0^2}{k_l^2} t + C_0\right]^{1/2} \tag{4.24}$$

where $C_0 = T_m^2 - \dfrac{\alpha_l k_s^2 A_l^2}{\alpha_s k_l^2 A_s^2}(T_m - T_0)^2$.

As the irradiation proceeds, temperature of the melt rises until the melt surface temperature reaches the boiling point and vaporisation begins. Therefore, Eq.(4.24) can be used as a criteria for the transition from melting to vaporisation stage.

Figure 4.6 shows a comparison between the measured and predicted melt depths depicted from Shen et al.[163]. It can be seen that the melt depth increases sharply at the beginning of irradiation. After that, the melt depth increases gradually. It was found that the model over predicted the melt depth as the irradiation time increased. Shen et al. explained that, during the experiment, plasma and vapour may be formed with increasing irradiation time resulting in less laser beam energy delivered to the surface. Because the effects of plasma and vapour were not included in their model, hence the smaller melt depth.

Temperature profiles in the solid and liquid are also plotted as shown in Figure 4.7 for 40, 80, 100 and 120 ms irradiation time [163].
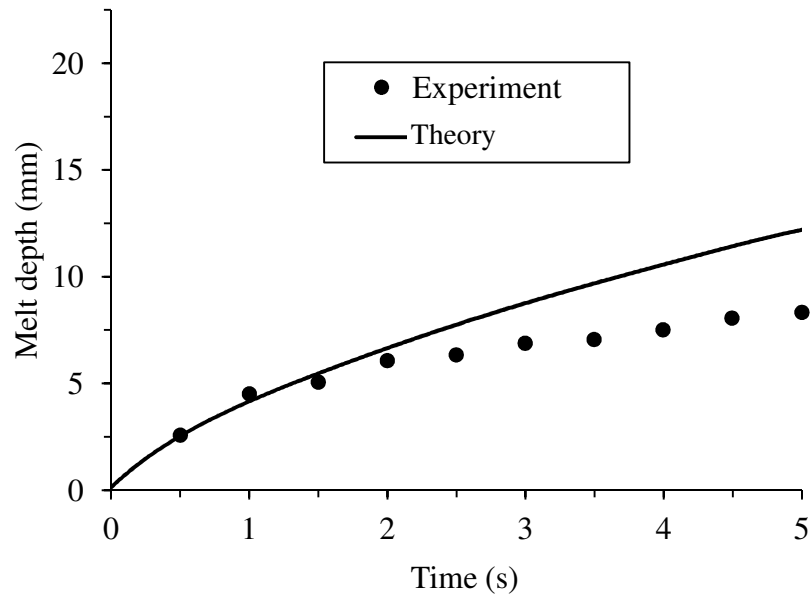
Figure 4.6 Melt depth evolution [163].
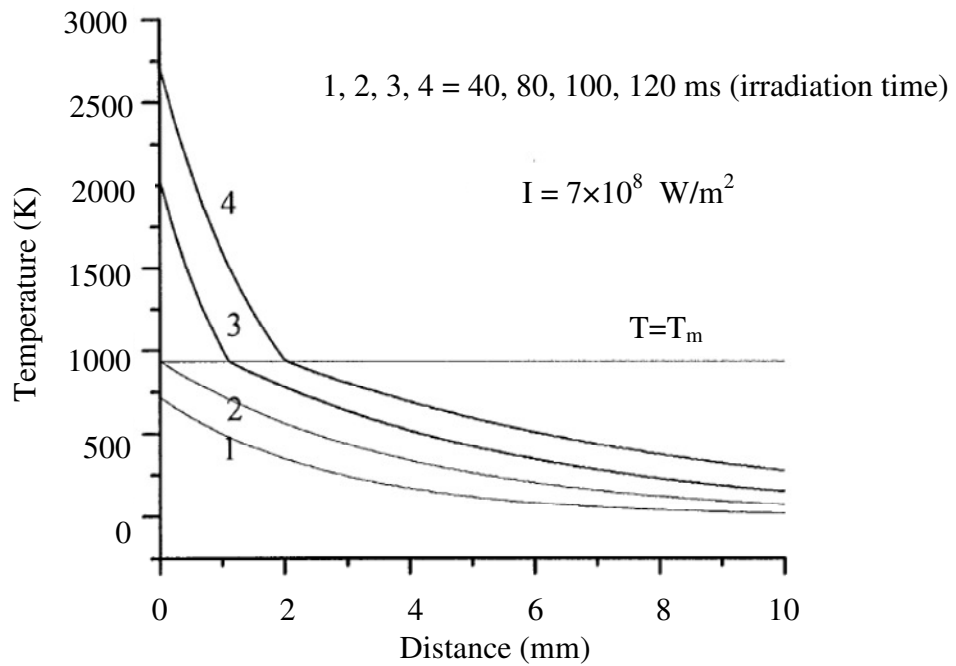
Figure 4.7 Temperature profiles in solid and liquid at different irradiation time [163].

In laser percussion drilling, melting occurs during the 'pulse on' duration while the solidification takes place during 'pulse off'. Basically, the melting model, addressed above, can also be applied to solidification; however, particular analysis for solidification has also been reported [176, 183].

Development of the solidification model is widely based on the Neumann's solution (given by F.Neumann in his lectures in the 1860's, see Dowden [183] , p.146), in which the error function is employed to solve the Stefan problem. Consider a system where there is a liquid in $x > 0$. The freezing front begins at $x = 0$ and is at $x = x_f(t)$ at time t. At $x = 0$, the temperature is constant at T_0 and as $x \to \infty$, the temperature in the liquid remains at T_2. Figure 4.8 illustrates the schematic diagram of the proposed solidification model.

$$T_s = T_0 \quad \text{————————} \quad \top \quad x = 0$$

solid

$$T_s = T_l = T_f \quad \text{——————} \quad x = x_f(t)$$

liquid

$$T_l = T_2 \quad \text{——————}$$

Figure 4.8 Schematic diagram for the solidification used in Dowden's model [183].

For a solidification process where no laser energy is provided at $x = 0$, by assuming the same density in solid and liquid phases [183], the boundary conditions at $x = 0$ and at $x = x_f(t)$ can be written as:

$$T_s(0,t) = T_0 \qquad\qquad ; \quad \text{at} \quad x = 0 \tag{4.25}$$

$$T_s(x_f(t),t) = T_l(x_f(t),t) = T_f \qquad\qquad ; \quad \text{at} \quad x = x_f(t) \tag{4.26}$$

$$\rho L_m \frac{dz_m(t)}{dt} = k_s \frac{\partial T_s(z,t)}{\partial z} - k_l \frac{\partial T_l(z,t)}{\partial z} \qquad\qquad ; \quad \text{at} \quad x = x_f(t) \tag{4.27}$$

The asymptotic condition is given by:

$$T_l \to T_2 \quad \text{as} \quad x \to \infty \tag{4.28}$$

with $\qquad\qquad x_f(0) = 0 \quad$, and $\quad T_l(x,0) = 0$. $\tag{4.29}$

Temperature profiles in the solid and liquid are typically assumed as [176, 183]:

$$T_s(z,t) = T_0 + a_1 \, erf \frac{x}{\sqrt{4\alpha_s t}} \tag{4.30}$$

$$T_l(z,t) = T_2 - a_2 \, erfc \frac{x}{\sqrt{4\alpha_l t}} \tag{4.31}$$

which satisfy the boundary conditions at $x = 0$ and at $x \to \infty$, respectively.

Temperature at the solid-liquid interface ($x = x_f(t)$) requires that there will be solutions in the forms of Eqs.(4.30) and (4.31) if $x_f(t)$ is proportional to $\sqrt{t}$. It is written as:

$$x_f(t) = \xi\sqrt{4t\sqrt{\alpha_l \alpha_s}} \tag{4.32}$$

Therefore, a_1 and a_2 are obtained as:

$$a_1 = \frac{T_f - T_0}{erf\left[\xi(\alpha_l / \alpha_s)^{1/4}\right]} \quad \text{and} \quad a_2 = \frac{T_2 - T_f}{erfc\left[\xi(\alpha_s / \alpha_l)^{1/4}\right]}$$

By substituting Eqs.(4.30) and (4.31) into the interface condition (4.27), ξ is determined.

Figure 4.9 shows the temperature distributions in solid and liquid at various intervals of elapsed time [183]. These plots indicate that moving speed of the freezing front decreases as time increases.
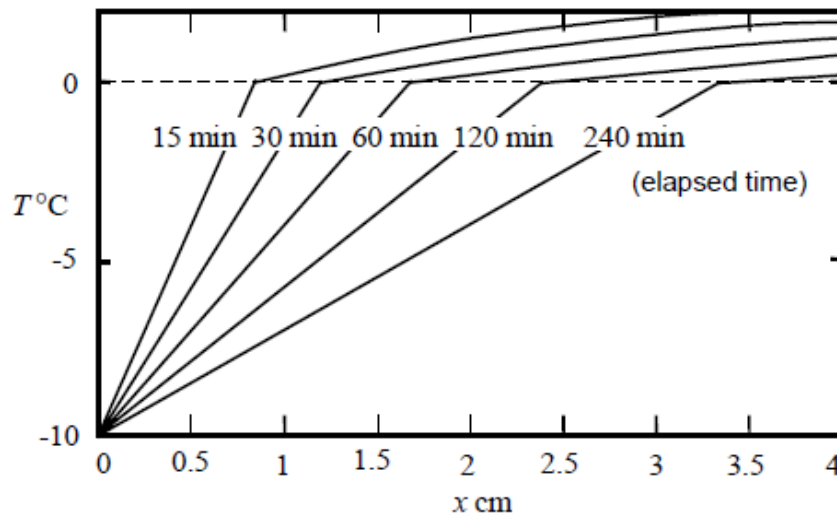
Figure 4.9 Temperature distribution during freezing of water [183].

4.4 VAPORISATION

Vaporisation takes place when temperature of the liquid layer reaches the boiling point. Consequently, the liquid-vapour interface is formed and propagates into the liquid layer whereas the solid-liquid interface created due to melting propagates into the solid. The cavity is then formed due to the combined effects of the vaporisation and liquid expulsion. Because various complex mechanisms are associated, modelling of the vaporisation therefore varies extensively. Theses may range from the one-dimensional steady-state model; where the analytical solutions are possible [53, 63, 143], to the more sophisticated two-dimensional transient models; where numerical methods are preferred [50, 97, 179, 185]. The numerical approach is beyond the scope of this work and a review of the previous vaporisation models emphasised here is based on the analytical approach.

Modelling of laser induced vaporisation is generally aimed to predict the melting and vaporisation front locations and speeds [140, 186, 187], hole shape and recast layer thickness [179, 184, 185], and temperature distribution in the liquid and solid [119, 188]. Similar to the case of laser induced melting, modelling of vaporisation is normally established from the heat conduction equations with Stefan conditions at the solid-liquid and liquid-front interfaces. A schematic diagram of the basic one-dimensional model of laser induced vaporisation is illustrated in Figure 4.10. The two moving boundaries; the solid-liquid and liquid-vapour interfaces, are formed at $z = z_m(t)$ and $z = z_v(t)$, respectively.
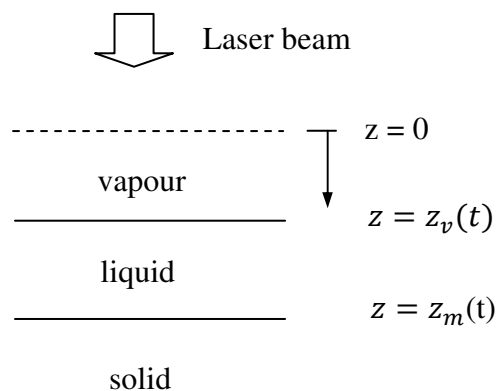
Figure 4.10 Schematic diagram of stage 3: vaporisation.

Heat conduction equations in the solid and liquid are given by:

$$\frac{\partial^2 T_l(z,t)}{\partial z^2} = \frac{1}{\alpha_l}\frac{\partial T_l(z,t)}{\partial t} \qquad ; \quad 0 \le z < z_m(t) \qquad (4.33)$$

$$\frac{\partial^2 T_s(z,t)}{\partial z^2} = \frac{1}{\alpha_s}\frac{\partial T_s(z,t)}{\partial t} \qquad ; \quad z_m(t) \le z < \infty \qquad (4.34)$$

Boundary conditions at the solid-liquid and liquid-vapour interfaces can be written as [140, 166, 170]:

$$\rho_s L_m \frac{dz_m(t)}{dt} = k_s \frac{\partial T_s(z,t)}{\partial z} - k_l \frac{\partial T_l(z,t)}{\partial z} \qquad ; \quad \text{at } z = z_m(t) \qquad (4.35)$$

$$T_s\ (z_m(t),t) = T_l\ (z_m(t),t) = T_m \qquad ; \quad \text{at } z = z_m(t) \qquad (4.36)$$

$$\rho_l L_v \frac{dz_v(t)}{dt} = I_{abs} + k_l \frac{\partial T_l(z,t)}{\partial z} \qquad ; \quad \text{at } z = z_v(t) \qquad (4.37)$$

$$T_l(z_v(t),t) = T_{l0} \qquad ; \quad \text{at } z = z_v(t) \qquad (4.38)$$

where L_v is the latent heat of vaporisation and T_{l0} is the melt surface temperature.

It is generally accepted that the melt surface temperature T_{l0} is a function of vapour pressure. This vapour pressure can be estimated from the well known Clasius-Clapeyron equation [189, 190]:

$$p_{vap} = p_0 \exp\left[\frac{L_v}{R}\left(\frac{1}{T_b} - \frac{1}{T_{l0}}\right)\right] \qquad (4.39)$$

where p_0 and T_b are atmospheric pressure and boiling point, and R is the specific gas constant defined by $R = R_u / M_m$, where R_u is the universal gas constant (8.314 J/(mol.K)) and M_m is the molar mass. Therefore, if p_{vap} is known, T_{l0} can be calculated.

In addition to Eq.(4.39), the melt surface temperature may also be determined from [76]:

$$T_{l0} = I_{abs}\sqrt{\frac{4t}{\pi \rho_l c_{eff} k_l}} \qquad (4.40)$$

where c_{eff} is the effective heat capacity and is defined as

$$c_{eff} = c_{ps} + \frac{L_m}{T_m}$$ (4.41)

where c_{ps}, L_m and T_m are specific heat of solid, latent heat of melting, and melting temperature of the material.

However, it is worth mentioning that only the latent heat of melting is included in the melt surface temperature estimated by Eq.(4.40) (included in c_{eff}, see Eq.(4.41)) and the latent heat of vaporisation is not accounted for. Therefore, some errors can be expected from using Eq.(4.40) to estimate the melt surface temperature.

Although Eqs.(4.33)-(4.38) are the most basic equations for this type of problem, solving these non-linear differential equations simultaneously is complex. Therefore, in order to simplify the equations, researchers have made further assumptions in their models. These assumptions are, for example:

1) linear temperature distribution in the liquid layer [89, 166]:

$$\frac{\partial T_l(z,t)}{\partial z} = \frac{T_m - T_{l0}}{z_m(t) - z_v(t)} \quad ,$$ (4.42)

2) linear temperature distribution in the solid, starting from the solid-liquid interface to the thermal diffusion depth [76]:

$$\frac{\partial T_s(z,t)}{\partial z} = \frac{T_0 - T_m}{\sqrt{2\alpha_s t}} \quad , \text{ and}$$ (4.43)

3) constant and equal moving speeds for the solid-liquid and liquid-vapour interface [183]:

$$\frac{dz_m(t)}{dt} = \frac{dz_v(t)}{dt} = \text{constant.}$$ (4.44)

By using the assumption as in Eq.(4.43) with the same thermal properties for solid and liquid, Dowden [183] has developed the model in dimensionless form. The dimensionless interface velocity (U') and dimensionless melt depth (a') were given by:

$$U' = \frac{I'}{1+c+d+T_0'}$$ (4.45)

$$a' = \frac{Ua}{\alpha}$$ (4.46)

where

$$U' = \frac{U}{\sqrt{L_v}} \quad , \quad T_0' = \frac{T_m - T_0}{k} \quad , \quad I' = \frac{I}{\rho L_m \sqrt{L_v}} \quad , \quad c = \frac{T_v - T_m}{\rho \alpha L_m} k \quad , \quad d = \frac{L_v}{L_m} \quad ,$$

$$U = \frac{dz_m(t)}{dt} = \frac{dz_v(t)}{dt} , \quad \text{and} \quad T_v = \text{vaporisation temperature.}$$

In recent years, the effect of interface curvature has often been included in the model developed by implementing $z_v(r,t)$ and $z_m(r,t)$ instead of $z_v(t)$ and $z_m(t)$ [166, 179, 184].

However, for laser drilling of a vertical hole, as most of the laser energy is transferred to the workpiece in z direction, heat conduction in the z direction is dominant compared to the heat conducted in the radial direction r [171]. Hence, the one-dimensional heat conduction equations in solid and liquid are commonly accepted for this type of problems [166, 184].

Following the above description, the liquid-vapour and solid-liquid interfaces are formed respectively at

$$z = z_v(r,t)$$ (4.47)

$$z = z_m(r,t)$$ (4.48)

The interface equations are now given by

$$I_{abs} + k_l \frac{\partial T_l(z,t)}{\partial z} \left[1 + \left(\frac{\partial z_v(r,t)}{\partial r} \right)^2 \right] = \rho_l L_v \frac{\partial z_v(r,t)}{\partial t} \quad ; \quad \text{at} \quad z = z_v(r,t)$$ (4.49)

$$\rho_s L_m \frac{\partial z_m(r,t)}{\partial t} = k_s \frac{\partial T_s(z,t)}{\partial z} \left[1 + \left(\frac{\partial z_m(r,t)}{\partial r} \right)^2 \right] - k_l \frac{\partial T_l(z,t)}{\partial z} \left[1 + \left(\frac{\partial z_m(r,t)}{\partial r} \right)^2 \right] ;$$

$$\text{at} \quad z = z_m(r,t)$$ (4.50)

Most of the models previously developed required additional auxiliary equations to enable the equations solving. These auxiliary equations are generally established from the conservation of mass and momentum. Of particular interest is the mass balance which will be included in the currently developed model presented in Chapter 5. If the melt ejection is taken into consideration, the mass balance can be written as [52, 69, 121]:

$$\dot{m}_s = \dot{m}_m + \dot{m}_v \tag{4.51}$$

where $\dot{m}_s$, $\dot{m}_m$, and $\dot{m}_v$ are solid melting rate, molten liquid ejection rate, and vaporisation rate, respectively.

(a)   (b)

(c)
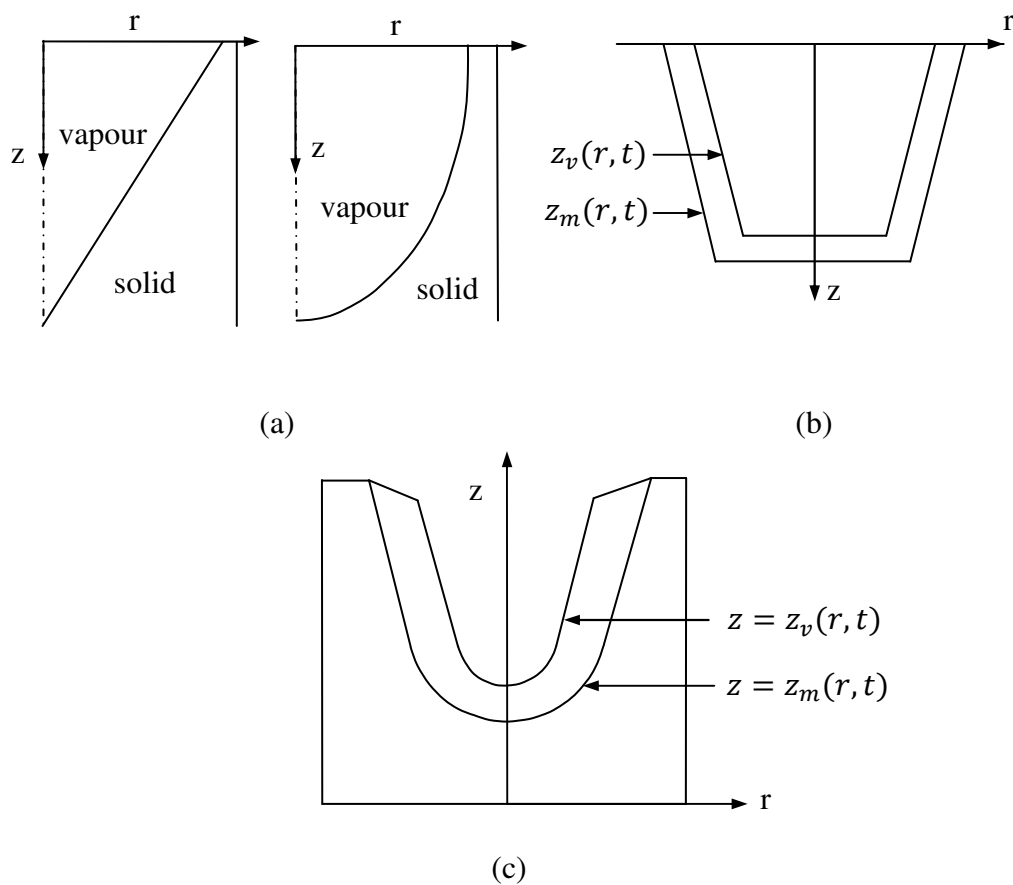
Figure 4.11 Hole profiles used in laser drilling models

(a) conical and parabolic profiles [191],

(b) conical with cut-off bottom [140],

(c) conical and parabolic combined profile [179].

In order to reduce a variable in the previously defined equations, specified profiles were assigned to $z_m(r,t)$ and $z_v(r,t)$. For example, Collins and Gremaud [191]

used conical and parabolic profiles (Figure 4.11 (a)), Cheng et al. [140] used a conical profile with cut-off bottom (Figure 4.11 (b)), and Kar and Mazumder [179] employed a combined profile consisting of a parabolic profile at the hole bottom and a conical profile for the cavity side (Figure 4.11 (c)). By using this technique, mathematical complexity of the problem is greatly reduced.

In addition to the basic laser induced mechanisms i.e. heating, melting, and vaporisation, modelling of laser drilling has been continuously improved by incorporating other related mechanisms into the models. These consist of heat convection and radiation at the surface, multiple reflection along the hole wall, absorption of laser energy in the vapour and/or plasma, recoil pressure, assist gas pressure, and oxidation energy etc. A summary of thermal models of laser drilling developed previously are listed as in Table 4.1.

Table 4.1 Summary of thermal models of laser drilling process.

Reference	Phase change	Method	Prediction
Ready [192]	Vaporisation.	1-D analytical transient heat conduction analytical model for semi-infinite material.	Hole depth.
Wagner [193]	Melting.	1-D finite difference model with bulk absorption mechanism.	Hole depth, hole shape.
Allmen [53]	Melting & vaporisation.	1-D steady state heat transfer analysis. Material removal is calculated on volume basis.	Drilling velocity.
Chan and Mazumder [68]	Melting & vaporisation.	1-D steady state model with the discontinuity across the Knudsen layer. Stefan conditions are applied at the two interfaces.	Liquid and vapour removal rates, and melt thickness.

Reference	Phase change	Method	Prediction
Smurov et al. [170]	Melting & vaporisation.	1-D transient model of the moving interface subjected to pulsed heating. A set of PDEs were solved numerically.	Melt thickness, melt front velocity, and melt surface temperature.
Kar et al. [89]	Melting & vaporisation.	2-D transient model including the assist gas and multiple reflection effects. Liquid flow is accounted in the model.	Hole depth, recast layer thickness.
Ganesh et al.[50]	Melting & vaporisation	2-D transient numerical model. Velocity of the vapour leaving the surface was assumed to be sonic velocity.	Hole profile.
Xie and Kar [169]	Melting	1-D transient model in a semi-infinite slab. A set of PDEs was solved by assuming temperature profiles in the melt and solid layers.	Melt depth.
Zhang and Faghri [166]	Melting & vaporisation	2-D transient heat conduction model in the liquid layer and 1-D transient heat conduction in the solid. An implicit finite difference method was employed to solve the PDEs.	Locations of the solid-liquid and liquid-vapour interfaces.
Cheng et al. [140]	Melting & vaporisation	1-D transient model in a semi-infinite material to study the effects of laser pulse shaping.	Hole depth, hole taper, and recast layer thickness.
Shen and Zhang [167]	Solid heating (no phase change)	1-D transient heat conduction in solid with the temperature-dependent absorptivity.	Surface temperature evolution.

Reference	Phase change	Method	Prediction
Shen et al. [163]	Melting	1-D transient heat conduction with moving solid-liquid interface	Temperature profile in solid and melt depth.
Ruf et al. [194]	Vaporisation	3-D transient heat conduction in an infinite medium. The local laser beam absorption on the inclined hole wall was considered.	Hole depth, drilling velocity.
Pandey et al. [41]	Melting & vaporisation	2-D transient finite element model for percussion laser drilling. Variation of the absorptivity with drilling depth is taken into account.	Temperature and stress distributions
Ng et al. [121]	Melting & vaporisation	1-D transient analytical model for single pulse drilling based on mass, energy and fluid flow equations. Effects of O_2 assist gas are included.	Melt ejection, vaporization and overall drilling velocities.
Zhang et al. [171]	Sublimation	1-D transient model for laser drilling of a multilayer polymer-copper workpiece.	Hole profiles, drilling depth.
Salonitis et al. [136]	Melting	1-D transient analytical model of percussion laser drilling based on heat conduction and energy balance equations.	Temperature evolutions and hole depth.
Mazhukin et al.[143]	Melting & vaporisation	1-D steady-state model to investigate effects of the temporal pulse shape on laser drilling.	Interface velocity, hole depth.

CHAPTER 5
MATHEMATICAL FORMULATION

5.1 INTRODUCTION

Literature review shows that most laser percussion drilling models previously developed are typically based on heat conduction, melting, and vaporisation equations with a set of defined assumptions. However, most reported investigations either ignore the effects of the additional heat generated from exothermic reaction or disregard the solidification during the pulse off which in fact have great influence on the drilling mechanisms. This indicates that the accuracy of the available models can be considerably improved by reducing a number of assumptions and coupling more related phenomena into the newly developed model. In addition, the previous modelling of laser drilling is mainly focused on single pulse process.

In this chapter, a mathematical model of laser percussion drilling is developed. The model is divided into two steps: pulse on and pulse off durations. The governing equations are set up from the heat conduction, boundary and initial equations, and mass balance. The model accounts for the recoil pressure, additional heat generated due to oxidation of metal with assist gas (O_2), and assist gas pressure. The developed model enables the prediction of the hole depth, hole taper and recast layer thickness.

5.2 MODELLING OF PULSE ON HEATING PROCESS

5.2.1 Governing equations

A schematic diagram of the model currently developed is illustrated in Figure 5.1. A laser beam with intensity I_0 irradiates the substrate surface which is initially at temperature T_0. The solid substrate is then heated, melted and vaporised. Once the vapour is formed, it exerts recoil pressure on the molten liquid as it leaves the cavity, and pushes the melt away radially. The material removal therefore consists of two mechanisms; vaporisation and melt ejection. Oxygen assist gas also plays some role in the process. The oxidation reaction between oxygen and metal provides the exothermic energy to the laser beam-material interaction. The assist gas also enhances the melt ejection mechanism by adding more pressure to the recoil

pressure. Moreover, the assist gas also promotes heat convection rate at the surface of the liquid layer.
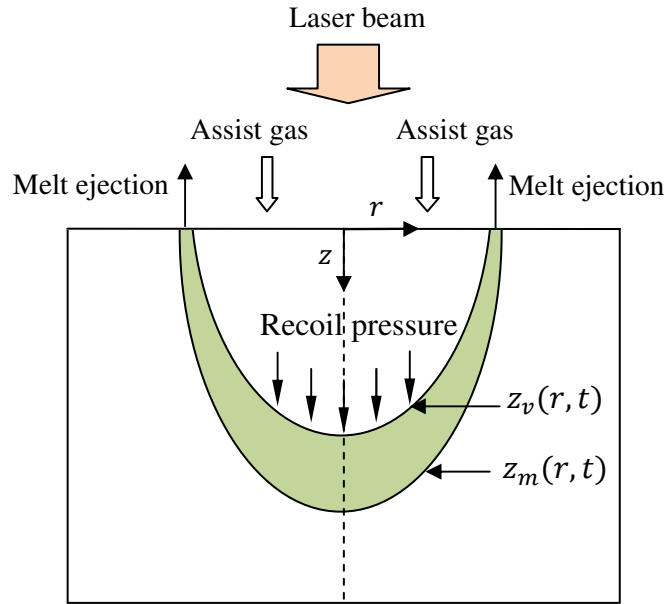
Figure 5.1 Schematic diagram of the model.

The following assumptions are made for the model:

1. The absorbed laser intensity distribution over the workpiece surface is assumed to be uniform. This assumption is reasonable because the laser beam considered is produced by the Nd:YAG laser and is delivered through a fibre with an approximately top hat profile [52].

2. Plasma generation is neglected in the model. It is valid to assume so because, unlike the CO_2 laser, in case of Nd:YAG laser operating at 1.06 μm, plasma may not be formed during the drilling process [52, 90, 195]. Only solid, molten liquid, and vapour are accounted for.

3. No interaction between laser beam and the vapour. It is considered here that the vapour is optically thin, hence no laser power is absorbed. Moreover, assist gas employed also help to remove the vapour from the cavity.

4. No laser power is absorbed by the ejected melt.

5. The generation of shock waves is ignored.

6. The changes in surface absorptivity, melting point, and boiling point due to oxide layer formed are neglected. The competing effects between the possible change in

the absorptivity and the difference in the melting and boiling points of the oxide and parent material are assumed to cancel each other.

7. Not all of the metal oxidises with O_2 assist gas. The oxidation efficiency is introduced in the model.

8. The discontinuity between the vapour directly above the liquid surface and the liquid is negligible. That is, the vapour and liquid at the surface are in thermodynamic equilibrium and there are no temperature and pressure discontinuities across the Knudsen layer.

Energy balance

Once the vaporisation has started, the liquid-vapour and solid-liquid interfaces are formed, respectively, at

$$z = z_v(r,t) \tag{5.1}$$

$$z = z_m(r,t) \tag{5.2}$$

where $z_v(r,t)$ and $z_m(r,t)$ are the depth of vaporisation and melting fronts, r and t are radial distance and time. Figure 5.2 illustrates the variables defined in the model.
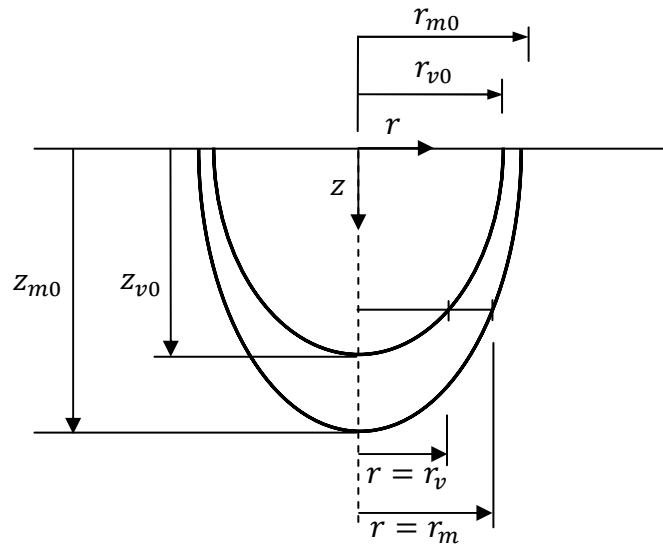
Figure 5.2 Schematic diagram of the variables defined in the model.

At the liquid-vapour interface, the Stefan equation can be written as:

$$\rho_l L_v \frac{\partial z_v}{\partial t} - k_l \frac{\partial T_l}{\partial z} \left[1 + \left(\frac{\partial z_v}{\partial r} \right)^2 \right] = I_{abs} + \rho_l H_{ox} \eta_{ox} \frac{\partial z_m}{\partial t} - h_g (T_{l0} - T_g) \qquad (5.3)$$

where ρ_l, k_l, and L_v are liquid density, liquid thermal conductivity, and latent heat of vaporisation, I_{abs}, H_{ox}, η_{ox}, and h_g are absorbed laser intensity, enthalpy of oxidation, oxidation efficiency, and heat transfer coefficient of assist gas, T_l, T_g and T_{l0} are melt temperature, assist gas temperature, and melt surface temperature, respectively. The oxidation efficiency η_{ox} defines the percentage of the melt that actually oxidises with the O_2 assist gas. It was determined experimentally by Ng et al.[121] and the value of $\eta_{ox} = 0.26$ is used in the present model.

The heat transfer coefficient h_g, is required for calculating the convection heat loss in Eq.(5.3). In case of forced convection, h_g can be determined from [52, 192]:

$$h_g = \frac{k_g}{2r_{v0}} \left(C_c \, \text{Re}^{n_c} \, \text{Pr}^{1/3} \right) \qquad (5.4)$$

where r_{v0} is the radius of the liquid-vapour interface (vapour front radius) at the hole entrance (as shown in Figure 5.2), k_g, Re, and Pr are the thermal conductivity, Reynolds number, and Prandtl number of the assist gas, respectively, C_c and n_c are the constants for forced convection perpendicular to the liquid surface, and are taken to be 0.228 and 0.731 [193], respectively. The Reynolds number, Re, is expressed as:

$$\text{Re} = \frac{\rho_g v_g \, 2r_{v0}}{\mu_g} \qquad (5.5)$$

where ρ_g, v_g, and μ_g are the density, flow velocity, and dynamic viscosity of the assist gas, respectively.

The Stefan equation for the solid-liquid interface can be written as:

$$\rho_s L_m \frac{\partial z_m}{\partial t} = \left(k_s \frac{\partial T_s}{\partial z} - k_l \frac{\partial T_l}{\partial z} \right) \left[1 + \left(\frac{\partial z_m}{\partial r} \right)^2 \right] \qquad (5.6)$$

where ρ_s, k_s and T_s are density of solid, thermal conductivity of solid, and temperature profile in the solid, respectively.

At the symmetry axis, $\dfrac{\partial z_m}{\partial r} = 0$ and $\dfrac{\partial z_v}{\partial r} = 0$, and hence the Stefan equations at the two interfaces can be rewritten as:

$$\rho_l L_v \frac{\partial z_v}{\partial t} - k_l \frac{\partial T_l}{\partial z} = I_{abs} + \rho_l H_{ox}\eta_{ox} \frac{\partial z_m}{\partial t} - h_g(T_{l0} - T_g) \tag{5.7}$$

$$\rho_s L_m \frac{\partial z_m}{\partial t} = \left(k_s \frac{\partial T_s}{\partial z} - k_l \frac{\partial T_l}{\partial z} \right) \tag{5.8}$$

By considering at the actual drilled hole geometry, $z_m(r,t)$ and $z_v(r,t)$ may be assumed to have parabolic profiles, i.e.

$$z_m(r,t) = z_{m0}(t) - \frac{r^2}{r_{m0}^2} z_{m0}(t) \tag{5.9}$$

$$z_v(r,t) = z_{v0}(t) - \frac{r^2}{r_{v0}^2} z_{v0}(t) \tag{5.10}$$

where $z_{m0}(t)$ and $z_{v0}(t)$ are the melt depth and vaporisation depth at $r = 0$, and r_{m0} is the radius of the solid-liquid interface (melt front radius) at the hole entrance, respectively.

By substituting Eqs.(5.9) and (5.10) into Eqs.(5.7) and (5.8), and further assuming the linear temperature profiles in the thin layers of liquid and solid [76], Stefan conditions at the two interfaces are expressed as:

$$\rho_l L_v \frac{dz_{v0}(t)}{dt} - k_l \frac{T_m - T_{l0}}{z_{m0}(t) - z_{v0}(t)} = I_{abs} + \rho_l H_{ox}\eta_{ox} \frac{dz_{m0}(t)}{dt} - h_g(T_{l0} - T_g)$$

$$\tag{5.11}$$

$$\rho_s L_m \frac{dz_{m0}(t)}{dt} = k_s \frac{T_0 - T_m}{2\sqrt{\alpha_s t}} - k_l \frac{T_m - T_{l0}}{z_{m0}(t) - z_{v0}(t)} \tag{5.12}$$

where α_s is the thermal diffusivity of solid.

Combining Eqs.(5.11) and (5.12) gives

$$\rho_s L_m \frac{dz_{m0}(t)}{dt} + \rho_l L_v \frac{dz_{v0}(t)}{dt} = k_s \frac{T_0 - T_m}{2\sqrt{\alpha_s t}} + I_{abs} + \rho_l H_{ox} \eta_{ox} \frac{dz_{m0}(t)}{dt} - h_g(T_{l0} - T_g)$$

(5.13)

which can also be written as

$$z'_{v0}(t) = \frac{1}{\rho_l L_v}[I_{abs} + h_g(T_g - T_{l0}) + \frac{k_s(T_0 - T_m)}{2\sqrt{\alpha_s t}} + \rho_l H_{ox} \eta_{ox} z'_{m0}(t) + \rho_s L_m z'_{m0}(t)]$$

(5.14)

where $z'_{v0}(t) = \dfrac{dz_{v0}(t)}{dt}$ and $z'_{m0}(t) = \dfrac{dz_{m0}(t)}{dt}$.

Mass balance

In laser drilling, a hole is formed by material removal from the cavity in the form of melt ejection and vaporisation. That is, it can be written that the mass of the solid melt at the solid-liquid interface is equal to the total mass removed due to melt ejection and vaporisation, i.e.

$$\dot{m}_s = \dot{m}_m + \dot{m}_v$$

$$S_{sl}\rho_s \frac{\partial z_m}{\partial t} = S_m \rho_l V_m + S_{lv} \rho_l \frac{\partial z_v}{\partial t}$$

(5.15)

where S_{sl}, S_{lv}, S_m, and V_m are the solid-liquid interface area, liquid-vapour interface area, melt ejection area, and the melt ejection velocity, respectively.

The area S_m can be approximated by:

$$S_m = \pi(r_{m0}^2 - r_{v0}^2)$$

(5.16)

For parabolic hole profile, the surface area S_{sl} and S_{lv} are estimated by:

$$S_{sl} = \frac{\pi r_{m0}}{6z_{m0}^2(t)}[(r_{m0}^2 + 4z_{m0}^2(t))^{3/2} - r_{m0}^3]$$

(5.17)

$$S_{lv} = \frac{\pi r_{v0}}{6z_{v0}^2(t)}[(r_{v0}^2 + 4z_{v0}^2(t))^{3/2} - r_{v0}^3]$$

(5.18)

By substituting Eqs.(5.16) - (5.18) into the Eq.(5.15), the mass balance becomes:

92

$$\frac{\pi r_{m0}}{6z_{m0}^2(t)}[(r_{m0}^2 + 4z_{m0}^2(t))^{3/2} - r_{m0}^3]\rho_s\left(z_{m0}'(t) - \frac{r^2 z_{m0}'(t)}{r_{m0}^2}\right)$$

$$= \pi(r_{m0}^2 - r_{v0}^2)\rho_l V_m + \frac{\pi r_{v0}}{6z_{v0}^2(t)}[(r_{v0}^2 + 4z_{v0}^2(t))^{3/2} - r_{v0}^3]\rho_l\left(z_{v0}'(t) - \frac{r^2 z_{v0}'(t)}{r_{v0}^2}\right)$$

$$(5.19)$$

As $r \to 0$, the mass equation becomes:

$$\frac{\pi r_{m0}}{6z_{m0}^2(t)}[(r_{m0}^2 + 4z_{m0}^2(t))^{3/2} - r_{m0}^3]\rho_s z_{m0}'(t)$$

$$= \pi(r_{m0}^2 - r_{v0}^2)\rho_l V_m + \frac{\pi r_{v0}}{6z_{v0}^2(t)}[(r_{v0}^2 + 4z_{v0}^2(t))^{3/2} - r_{v0}^3]\rho_l z_{v0}'(t) \qquad (5.20)$$

In order to get a solution of the problem, the energy equation (5.14) and the mass equation (5.20) must be solved simultaneously. However, because Eq.(5.20) is quite complex, solving the system of equations analytically would be a time consuming process. It was found that even Mathematica 7 was unable to solve this set of equations. Therefore, for the sake of simplicity, the paraboloid surface area is approximated here by the conical surface area, which can be formulated in a much simpler form. Collins [191] has also developed a model using both conical and parabolic profiles. The results confirm that there is no significant difference in the hole depth prediction.

To apply a conical surface area instead of a poraboloid, a surface area correction factor is needed. Consider conical and paraboloid holes with radius a at height h, the corresponding surface area can be estimated from:

$$S_c = \pi a \sqrt{a^2 + h^2} \qquad (5.21)$$

$$S_p = \frac{\pi a}{6h^2}[(a^2 + 4h^2)^{3/2} - a^3] \qquad (5.22)$$

where S_c and S_p are the conical surface area and the paraboloid surface area, respectively.
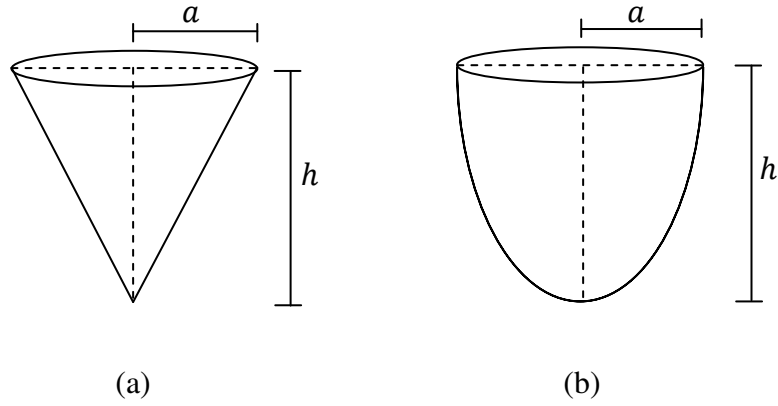
Figure 5.3 Schematic diagram of the hole profiles: (a) conical and (b) paraboloid.

The deviation percentage in the surface area of the paraboloid and the conical profiles is given by:

$$deviation \ (\%) = \frac{S_p - S_c}{S_p} \times 100 \tag{5.23}$$

For an assumed range of hole diameter a from 20 μm to 1 mm and hole depth h from 1 μm to 5 mm, the deviation of the surface area is plotted as shown in Figure 5.4. In Figure 5.5, deviations of the surface area for three values of the hole diameter i.e. 150, 240 and 350 μm, are plotted. It can be seen from these two figures that the difference in the surface area of the two profiles is smaller for the shallow hole and tends to approach a constant value; around 25%, as the hole gets deeper. Therefore, in order to use the conical surface area instead of the paraboloid surface area in the mass equation, a surface area correction factor; defined here as sc, is estimated to be between 1.20-1.24. In this present model, $sc = 1.23$ is selected.

The mass balance can now be expressed in term of the conical surface area as:

$$sc \, \pi r_{m0} \sqrt{r_{m0}^2 + z_{m0}^2(t)} \, \rho_s \frac{\partial z_m}{\partial t} = \pi(r_{m0}^2 - r_{v0}^2)\rho_l V_m + sc \, \pi r_{v0} \sqrt{r_{v0}^2 + z_{v0}^2(t)} \, \rho_l \frac{\partial z_v}{\partial t}$$

i.e.

94
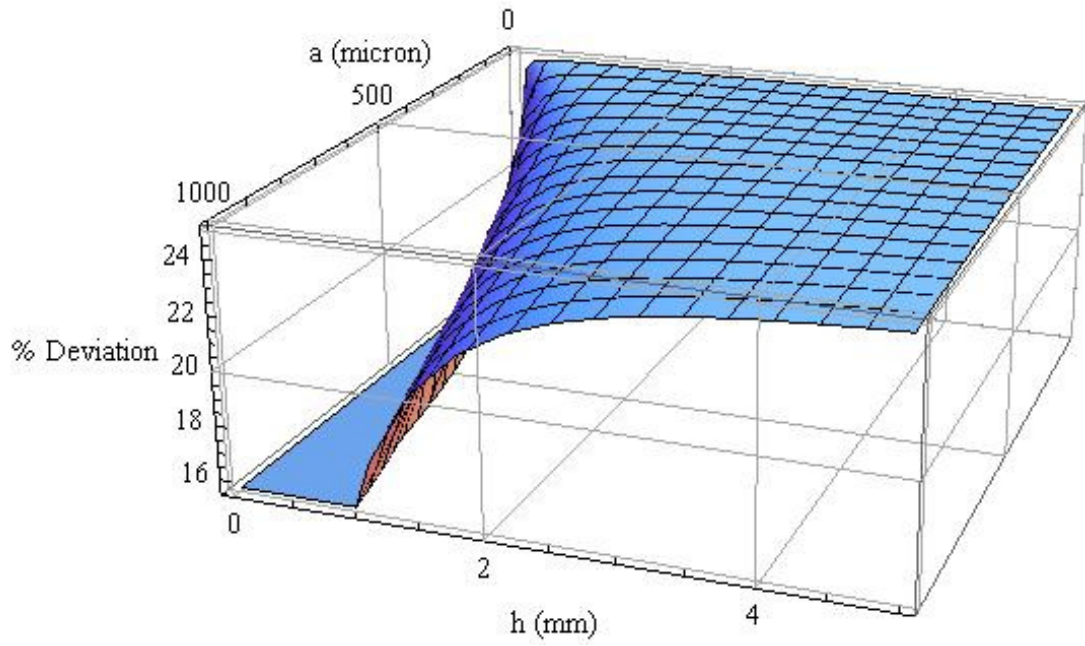
Figure 5.4 Surface area deviation (see Eq.(5.23)) at various hole radius, a, and depth, h.
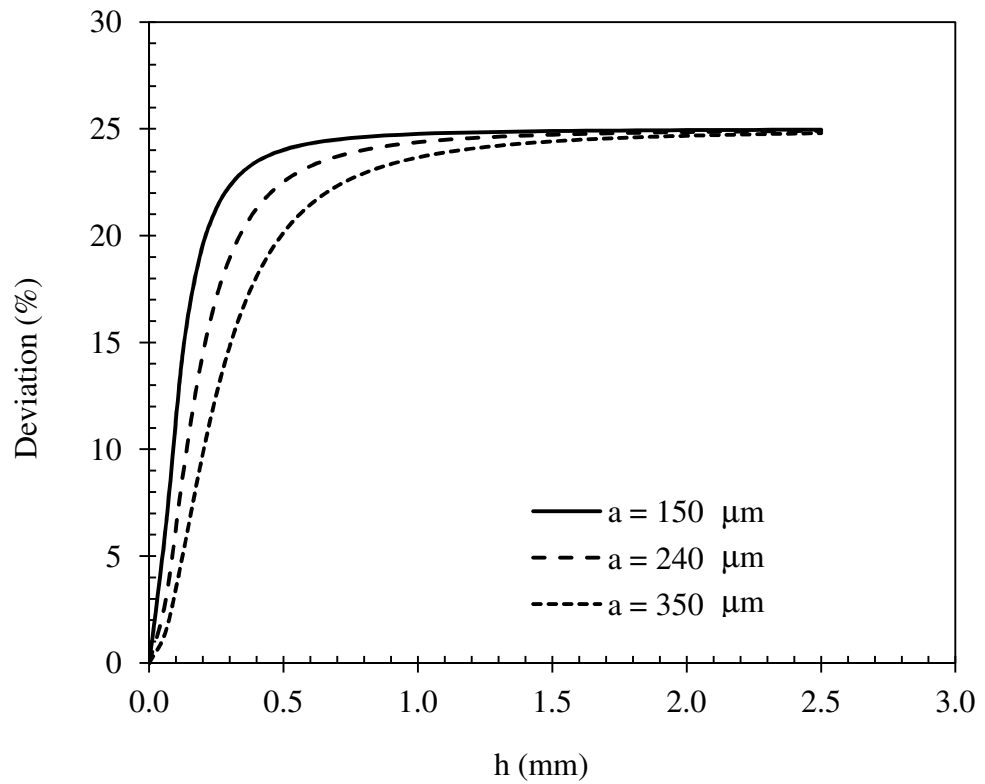
Figure 5.5 Deviation percentage at a = 150, 240, and 350 μm.

$$sc\,r_{m0}\sqrt{r_{m0}^2 + z_{m0}^2(t)}\,\rho_s\left(z_{m0}'(t) - \frac{r^2 z_{m0}'(t)}{r_{m0}^2}\right) = (r_{m0}^2 - r_{v0}^2)\rho_l V_m$$

$$+ sc\,r_{v0}\sqrt{r_{v0}^2 + z_{v0}^2(t)}\,\rho_l\left(z_{v0}'(t) - \frac{r^2 z_{v0}'(t)}{r_{v0}^2}\right)$$

(5.24)

As $r \to 0$, the mass equation becomes:

$$sc\,r_{m0}\rho_s z_{m0}'(t)\sqrt{r_{m0}^2 + t^2(z_{m0}'(t))^2} = (r_{m0}^2 - r_{v0}^2)\rho_l V_m +$$

$$sc\,r_{v0}\rho_l z_{v0}'(t)\sqrt{r_{v0}^2 + t^2(z_{v0}'(t))^2}$$

(5.25)

which may be rearranged as:

$$z_{v0}'(t) = \frac{1}{\sqrt{2}}\sqrt{\frac{-r_{v0}^4 sc^2 \rho_l^2 + \sqrt{r_{v0}^2 sc^2 \rho_l^2 (a_1 + a_2 + a_3)}}{r_{v0}^2 sc^2 t^2 \rho_l^2}}$$

(5.26)

where $a_1 = (r_{v0}^6 sc^2 + 4r_{m0}^4 t^2 V_m^2 - 8r_{m0}^2 r_{v0}^2 t^2 V_m^2 + 4r_{v0}^4 t^2 V_m^2)\rho_l^2$,

$$a_2 = 4r_{m0}^4 sc^2 t^2 \rho_s^2 (z_{m0}'(t))^2 + 4r_{m0}^2 sc^2 t^4 \rho_s^2 (z_{m0}'(t))^4,$$

$$a_3 = 8r_{m0}(-r_{m0}^2 + r_{v0}^2)sct^2 V_m \rho_l \rho_s z_{m0}'(t)\sqrt{r_{m0}^2 + t^2(z_{m0}'(t))^2}$$

By equating Eq.(5.14) to Eq.(5.26), $z_{m0}'(t)$ can now be determined from:

$$\frac{1}{\rho_l L_v}[I_{abs} + h_g(T_g - T_{l0}) + \frac{k_s(T_0 - T_m)}{2\sqrt{\alpha_s t}} + \rho_l H_{ox}\eta_{ox}z_{m0}'(t) + \rho_s L_m z_{m0}'(t)] =$$

$$\frac{1}{\sqrt{2}}\sqrt{\frac{-r_{v0}^4 sc^2 \rho_l^2 + \sqrt{r_{v0}^2 sc^2 \rho_l^2 (a_1 + a_2 + a_3)}}{r_{v0}^2 sc^2 t^2 \rho_l^2}}$$

(5.27)

A higher order polynomial form of Eq.(5.27) is obtained using Mathematica 7 software as:

$$b_0 + b_1(z_{m0}'(t)) + b_2(z_{m0}'(t))^2 + b_3(z_{m0}'(t))^3$$

$$+ b_4(z_{m0}'(t))^4 + b_5(z_{m0}'(t))^5 + b_6(z_{m0}'(t))^6 + b_7(z_{m0}'(t))^7 + b_8(z_{m0}'(t))^8 = 0$$

(5.28)

where

$$b_0 = L_v^8 r_{v0}^{12} sc^4 \rho_l^8 + 8 L_v^6 r_{v0}^{10} sc^4 t^2 \rho_l^6 c_1^2 + 24 L_v^4 r_{v0}^8 sc^4 t^4 \rho_l^4 c_1^4$$
$$+ 32 L_v^2 r_{v0}^6 sc^4 t^6 \rho_l^2 c_1^6 + 16 r_{v0}^4 sc^4 t^8 c_1^8 - 2 L_v^8 r_{v0}^6 sc^4 \rho_l^8 c_2$$
$$- 8 L_v^6 r_{v0}^4 sc^4 t^2 \rho_l^6 c1^2 c2 - 8 L_v^4 r_{v0}^2 t^4 \rho_l^4 c_1^4 c_2 + L_v^8 \rho_l^8 c_2^2$$

$$b_1 = 16 H_{ox} L_v^6 r_{v0}^{10} sc^4 t^2 \eta_{ox} \rho_l^7 c_1 - 16 L_m L_v^6 r_{v0}^{10} sc^4 t^2 \rho_l^6 \rho_s c_1$$
$$+ 96 H_{ox} L_v^4 r_{v0}^8 sc^4 t^4 \eta_{ox} \rho_l^5 c_1 - 96 L_m L_v^4 r_{v0}^8 sc^4 t^4 \rho_l^4 \rho_s c_1^3$$
$$+ 192 H_{ox} L_v^2 r_{v0}^6 sc^4 t^6 \eta_{ox} \rho_l^3 c_1^5 - 192 L_m L_v^2 r_{v0}^6 sc^4 t^6 \rho_l^2 \rho_s c_1^3$$
$$+ 128 H_{ox} r_{v0}^4 sc^4 t^8 \eta_{ox} \rho_l c_1^7 - 128 L_m r_{v0}^4 sc^4 t^8 \rho_s c_1^7$$
$$- 16 H_{ox} L_v^6 r_{v0}^4 sc^2 t^2 \eta_{ox} \rho_l^7 c_1 c_2 + 16 L_m L_v^6 r_{v0}^4 sc^2 t^2 \rho_l^6 \rho_s c_1 c_2$$
$$- 32 H_{ox} L_v^4 r_{v0}^2 sc^2 t^4 \eta_{ox} \rho_l^5 c_1^3 c_2 + 32 L_m L_v^4 r_{v0}^2 sc^2 t^4 \rho_l^4 \rho_s c_1^3 c_2$$

$$b_2 = 8 H_{ox} L_v^6 r_{v0}^{10} sc^4 t^2 \eta_{ox}^2 \rho_l^8 - 16 H_{ox} L_m L_v^6 r_{v0}^{10} sc^4 t^2 \eta_{ox} \rho_l^7 \rho_s$$
$$- 8 L_v^8 r_{m0}^4 r_{v0}^6 sc^4 t^2 \rho_l^6 \rho_s^2 + 8 L_m^2 L_v^6 r_{v0}^{10} sc^4 t^2 \rho_l^6 \rho_s^2$$
$$- 64 L_v^8 r_{m0}^8 sc^2 t^4 V_m^2 \rho_l^6 \rho_s^2 + 128 L_v^8 r_{m0}^6 r_{v0}^2 sc^2 t^4 V_m^2 \rho_l^6 \rho_s^2$$
$$- 64 L_v^8 r_b^4 r_{v0}^4 sc^2 t^4 V_m^2 \rho_l^6 \rho_s^2 + 144 H_{ox}^2 L_v^4 r_{v0}^8 sc^4 t^4 \eta_{ox}^2 \rho_l^6 c_1^2$$
$$- 288 H_{ox} L_m L_v^4 r_{v0}^8 sc^4 t^4 \eta_{ox} \rho_l^5 \rho_s c_1^2 - 32 L_v^6 r_{m0}^4 r_{v0}^4 sc^4 t^4 \rho_l^4 \rho_s^2 c_1^2$$
$$+ 144 L_m^2 L_v^4 r_{v0}^8 sc^4 t^4 \rho_l^4 \rho_s^2 c_1^2 + 480 H_{ox}^2 L_v^2 r_{v0}^6 sc^4 t^6 \eta_{ox}^2 \rho_l^4 c_1^4$$
$$- 960 H_{ox} L_m L_v^2 r_{v0}^6 sc^4 t^6 \eta_{ox} \rho_l^3 \rho_s c_1^4 - 32 L_v^4 r_{m0}^4 r_{v0}^2 sc^4 t^6 \rho_l^2 \rho_s^2 c_1^4$$
$$+ 480 L_m^2 L_v^2 r_{v0}^6 sc^4 t^6 \rho_l^2 \rho_s^2 c_1^4 + 448 H_{ox}^2 r_{v0}^4 t^8 \eta_{ox}^2 \rho_l^2 c_1^6$$
$$- 896 H_{ox} L_m r_{v0}^4 sc^4 t^8 \eta_{ox} \rho_l \rho_s c_1^6 + 448 L_m^2 r_{v0}^4 sc^4 t^8 \rho_s^2 c_1^6$$
$$- 8 H_{ox}^2 L_v^6 r_{v0}^4 sc^2 t^2 \eta_{ox}^2 \rho_l^8 c_2 + 16 H_{ox} L_m L_v^6 r_{v0}^4 sc^2 t^2 \eta_{ox} \rho_l^7 \rho_s c_2$$
$$+ 8 L_v^8 r_{v0}^4 sc^2 t^2 \rho_l^6 \rho_s^2 c_2 - 8 L_m^2 L_v^6 r_{v0}^4 sc^2 t^2 \rho_l^6 \rho_s^2 c_2$$
$$- 48 H_{ox}^2 L_v^4 r_{v0}^2 sc^2 t^4 \eta_{ox}^2 \rho_l^6 c_1^2 c_2 + 96 H_{ox} L_m L_v^4 r_{v0}^2 sc^2 t^4 \eta_{ox} \rho_l^5 \rho_s c_1^2 c_2$$
$$- 48 L_m^2 L_v^4 r_{v0}^2 sc^2 t^4 \rho_l^4 \rho_s^2 c_1^2 c_2$$

$$b_3 = 96H_{ox}{}^3L_v{}^4r_{v0}{}^8sc^4t^4\eta_{ox}{}^3\rho_l{}^7c_1 - 288H_{ox}{}^2L_mL_v{}^4r_{v0}{}^8sc^4t^4\eta_{ox}{}^2\rho_l{}^6\rho_sc_1$$

$$- 64H_{ox}L_v{}^6r_{m0}{}^4r_{v0}{}^4sc^4t^4\eta_{ox}\rho_l{}^5\rho_s{}^2c_1 + 288H_{ox}L_m{}^2L_v{}^4r_{v0}{}^8sc^4t^4\eta_{ox}{}^2\rho_l{}^5\rho_s{}^2c_1$$

$$+ 64L_mL_v{}^6r_{m0}{}^4r_{v0}{}^4sc^4t^4\rho_l{}^4\rho_s{}^3c_1 - 96L_m{}^3L_v{}^4r_{v0}{}^8sc^4t^4\rho_l{}^4\rho_s{}^3c_1$$

$$+ 640H_{ox}{}^3L_v{}^2r_{v0}{}^6sc^4t^6\eta_{ox}{}^3\rho_l{}^5c_1{}^3 - 1920H_{ox}{}^2L_mL_v{}^2r_{v0}{}^6sc^4t^6\eta_{ox}{}^2\rho_l{}^4\rho_sc_1{}^3$$

$$- 128H_{ox}L_v{}^4r_b{}^4r_{v0}{}^2sc^4t^6\eta_{ox}\rho_l{}^3\rho_s{}^2c_1{}^3 + 1920H_{ox}L_m{}^2L_v{}^2r_{v0}{}^6sc^4t^6\eta_{ox}\rho_l{}^3\rho_s{}^2c_1{}^3$$

$$+ 128L_mL_v{}^4r_{m0}{}^4r_{v0}{}^2sc^4t^6\rho_l{}^2\rho_s{}^3c_1{}^3 - 640L_m{}^3L_v{}^2r_{v0}{}^6sc^4t^6\rho_l{}^2\rho_s{}^3c_1{}^3$$

$$+ 896H_{ox}{}^3r_{v0}{}^4sc^4t^8\eta_{ox}{}^3\rho_l{}^3c_1{}^5 - 2688H_{ox}{}^2L_mr_{v0}{}^4sc^4t^8\eta_{ox}{}^2\rho_l{}^2\rho_sc_1{}^5$$

$$+ 2688H_{ox}L_m{}^2r_{v0}{}^4sc^4t^8\eta_{ox}\rho_l\rho_s{}^2c_1{}^5 - 896L_m{}^3r_{v0}{}^4sc^4t^8\rho_s{}^3c_1{}^5$$

$$- 32H_{ox}{}^3L_v{}^4r_{v0}{}^2sc^2t^4\eta_{ox}{}^3\rho_l{}^7c_1c_2 + 96H_{ox}{}^2L_mL_v{}^4r_{v0}{}^2sc^2t^4\eta_{ox}{}^2\rho_l{}^6\rho_sc_1c_2$$

$$- 96H_{ox}L_m{}^2L_v{}^4r_{v0}{}^2sc^2t^4\eta_{ox}\rho_l{}^5\rho_s{}^2c_1c_2 + 32L_m{}^3L_v{}^4r_{v0}{}^2sc^2t^4\rho_l{}^4\rho_s{}^3c_1c_2$$

$$b_4 = 24H_{ox}{}^4L_v{}^4r_{v0}{}^8sc^4t^4\eta_{ox}{}^4\rho_l{}^8 - 96H_{ox}{}^3L_mL_v{}^4r_{v0}{}^8sc^4t^4\eta_{ox}{}^3\rho_l{}^7\rho_s$$

$$- 8L_v{}^8r_{m0}{}^2r_{v0}{}^6sc^4t^4\rho_l{}^6\rho_s{}^2 - 64L_v{}^8r_{m0}{}^6sc^2t^6V_m{}^2\rho_l{}^6\rho_s{}^2$$

$$+ 128L_v{}^8r_{m0}{}^4r_{v0}{}^2sc^2t^6V_m{}^2\rho_l{}^6\rho_s{}^2 - 64L_v{}^8r_{m0}{}^2r_{v0}{}^4sc^2t^6V_m{}^2\rho_l{}^6\rho_s{}^2$$

$$- 32H_{ox}{}^2L_v{}^6r_{m0}{}^4r_{v0}{}^4sc^4t^4\eta_{ox}{}^2\rho_l{}^6\rho_s{}^2 + 144H_{ox}{}^2L_m{}^2L_v{}^4r_{v0}{}^8sc^4t^4\eta_{ox}{}^2\rho_l{}^6\rho_s{}^2$$

$$+ 64H_{ox}L_mL_v{}^6r_{m0}{}^4r_{v0}{}^4sc^4t^4\eta_{ox}\rho_l{}^5\rho_s{}^3 - 96H_{ox}L_m{}^3L_v{}^4r_{v0}{}^8sc^4t^4\eta_{ox}\rho_l{}^5\rho_s{}^3$$

$$+ 16L_v{}^8r_{m0}{}^8sc^4t^4\rho_l{}^4\rho_s{}^4 - 32L_m{}^2L_v{}^6r_{m0}{}^4r_{v0}{}^4sc^4t^4\rho_l{}^4\rho_s{}^4$$

$$+ 24L_m{}^4L_v{}^4r_{v0}{}^8sc^4t^4\rho_l{}^4\rho_s{}^4 + 480H_{ox}{}^4L_v{}^6r_{v0}{}^6sc^4t^6\eta_{ox}{}^4\rho_l{}^6c_1{}^2$$

$$- 1920H_{ox}{}^3L_mL_v{}^2r_{v0}{}^6sc^4t^6\eta_{ox}{}^3\rho_l{}^5\rho_sc_1{}^2 - 32L_v{}^6r_{m0}{}^2r_{v0}{}^4sc^4t^6\rho_l{}^4\rho_s{}^2c_1{}^2$$

$$- 192H_{ox}{}^2L_v{}^4r_{m0}{}^4r_{v0}{}^2sc^4t^6\eta_{ox}{}^2\rho_l{}^4\rho_s{}^2c_1{}^2$$

$$+ 2880H_{ox}{}^2L_m{}^2L_v{}^2r_{v0}{}^6sc^4t^6\eta_{ox}{}^2\rho_l{}^4\rho_s{}^2c_1{}^2$$

$$+ 384H_{ox}L_mL_v{}^4r_{m0}{}^4r_{v0}{}^2sc^4t^6\eta_{ox}\rho_l{}^3\rho_s{}^2c_1{}^2 - 1920H_{ox}L_m{}^3L_v{}^2r_{v0}{}^6sc^4t^6\eta_{ox}\rho_l{}^3\rho_s{}^3c_1{}^2$$

$$- 192L_m{}^2L_v{}^4r_{m0}{}^4r_{v0}{}^2sc^4t^6\rho_l{}^2\rho_s{}^4c_1{}^2 + 480L_m{}^4L_v{}^2r_{v0}{}^6sc^4t^6\rho_l{}^2\rho_s{}^4c_1{}^2$$

$$+ 1120H_{ox}{}^4r_{v0}{}^4sc^4t^8\eta_{ox}{}^4\rho_l{}^4c_1{}^4 - 4480H_{ox}{}^3L_mr_{v0}{}^4sc^2t^8\eta_{ox}{}^3\rho_l{}^3\rho_sc_1{}^4$$

$$- 32L_v{}^4r_b{}^2r_{v0}{}^2sc^4t^8\rho_l{}^2\rho_s{}^2c_1{}^4 + 6720H_{ox}{}^2L_m{}^2r_{v0}{}^4sc^4t^8\eta_{ox}{}^2\rho_l{}^2\rho_s{}^2c_1{}^4$$

$$- 4480H_{ox}L_m{}^3r_{v0}{}^4sc^4t^8\eta_{ox}\rho_l\rho_s{}^3c_1{}^4 + 1120L_m{}^4r_{v0}{}^4sc^4t^8\rho_s{}^4c_1{}^4$$

$$- 8H_{ox}{}^4L_v{}^2r_{v0}{}^2sc^2t^4\eta_{ox}{}^4\rho_l{}^8c_2 + 32H_{ox}{}^3L_mL_v{}^4r_{v0}{}^2sc^2t^4\eta_{ox}{}^3\rho_l{}^7\rho_sc_2$$

$$+ 8L_v{}^8r_{m0}{}^2sc^2t^4\rho_l{}^6\rho_s{}^2c_2 - 48H_{ox}{}^2L_m{}^2L_v{}^4r_{v0}{}^2sc^2t^4\eta_{ox}{}^2\rho_l{}^6\rho_s{}^2c_2$$

$$+ 32H_{ox}L_m{}^3L_v{}^4r_{v0}{}^2sc^2t^4\eta_{ox}\rho_l{}^5\rho_s{}^3c_2 - 8L_m{}^4L_v{}^4r_{v0}{}^2sc^2t^4\rho_l{}^4\rho_s{}^4c_2$$

$$b_5 = 192 H_{ox}{}^5 L_v{}^2 r_{v0}{}^6 sc^4 t^6 \eta_{ox}{}^5 \rho_l{}^7 c_1 - 960 H_{ox}{}^4 L_m L_v{}^2 r_{v0}{}^6 sc^4 t^6 \eta_{ox}{}^4 \rho_l{}^6 \rho_s c_1$$

$$- 64 H_{ox} L_v{}^6 r_{m0}{}^2 r_{v0}{}^4 sc^4 t^6 \eta_{ox} \rho_l{}^5 \rho_s{}^2 c_1 - 128 H_{ox}{}^3 L_v{}^4 r_{m0}{}^4 r_{v0}{}^2 sc^4 t^6 \eta_{ox}{}^3 \rho_l{}^5 \rho_s{}^2 c_1$$

$$+ 1920 H_{ox}{}^3 L_m{}^2 L_v{}^2 r_{v0}{}^6 sc^4 t^6 \eta_{ox}{}^3 \rho_l{}^5 \rho_s{}^2 c_1 + 64 L_m L_v{}^6 r_{m0}{}^2 r_{v0}{}^4 sc^4 t^6 \eta_{ox} \rho_l{}^4 \rho_s{}^3 c_1$$

$$+ 384 H_{ox}{}^2 L_m L_v{}^4 r_{m0}{}^4 r_{v0}{}^2 sc^4 t^6 \eta_{ox}{}^2 \rho_l{}^4 \rho_s{}^3 c_1$$

$$- 1920 H_{ox}{}^2 L_m{}^3 L_v{}^2 r_{v0}{}^6 sc^4 t^6 \eta_{ox}{}^2 \rho_l{}^4 \rho_s{}^3 c_1$$

$$- 3844 H_{ox} L_m{}^2 L_v{}^4 r_{m0}{}^4 r_{v0}{}^2 sc^4 t^6 \eta_{ox} \rho_l{}^3 \rho_s{}^4 c_1 + 960 H_{ox} L_m{}^4 L_v{}^2 r_{v0}{}^6 sc^4 t^6 \eta_{ox} \rho_l{}^3 \rho_s{}^4 c_1$$

$$+ 128 L_m{}^3 L_v{}^4 r_{m0}{}^4 r_{v0}{}^2 sc^4 t^6 \rho_l{}^2 \rho_s{}^5 c_1 - 192 L_m{}^5 L_v{}^2 r_{v0}{}^6 sc^4 t^6 \rho_l{}^2 \rho_s{}^5 c_1$$

$$+ 896 H_{ox}{}^5 r_{v0}{}^4 sc^4 t^8 \eta_{ox}{}^5 \rho_l{}^5 c_1{}^3 - 4480 H_{ox}{}^4 L_m r_{v0}{}^4 sc^4 t^8 \eta_{ox}{}^4 \rho_l{}^4 \rho_s c_1{}^3$$

$$- 128 H_{ox} L_v{}^4 r_{m0}{}^2 r_{v0}{}^2 sc^4 t^8 \eta_{ox} \rho_l{}^3 \rho_s{}^2 c_1{}^3 + 8960 H_{ox}{}^3 L_m{}^2 r_{v0}{}^4 sc^4 t^8 \eta_{ox}{}^3 \rho_l{}^3 \rho_s{}^2 c_1{}^3$$

$$+ 128 L_m L_v{}^4 r_{m0}{}^2 r_{v0}{}^2 sc^4 t^8 \rho_l{}^2 \rho_s{}^3 c_1{}^3 - 8960 H_{ox}{}^2 L_m{}^3 r_{v0}{}^4 sc^4 t^8 \eta_{ox}{}^2 \rho_l{}^2 \rho_s{}^3 c_1{}^3$$

$$+ 4480 H_{ox} L_m{}^4 r_{v0}{}^4 sc^4 t^8 \eta_{ox} \rho_l \rho_s{}^4 c_1{}^3 - 896 L_m{}^5 r_{v0}{}^4 sc^4 t^8 \rho_s{}^5 c_1{}^3$$

$$b_6 = 32 H_{ox}{}^6 L_v{}^2 r_{v0}{}^6 sc^4 t^6 \eta_{ox}{}^6 \rho_l{}^8 - 192 H_{ox}{}^5 L_m L_v{}^2 r_{v0}{}^6 sc^4 t^6 \eta_{ox}{}^5 \rho_l{}^7 \rho_s$$

$$- 32 H_{ox}{}^2 L_v{}^6 r_{m0}{}^2 r_{v0}{}^4 sc^4 t^6 \eta_{ox}{}^2 \rho_l{}^6 \rho_s{}^2 - 32 H_{ox}{}^4 L_v{}^4 r_{m0}{}^4 r_{v0}{}^2 sc^4 t^6 \eta_{ox}{}^2 \rho_l{}^6 \rho_s{}^2$$

$$+ 480 H_{ox}{}^4 L_m{}^2 L_v{}^2 r_{v0}{}^6 sc^4 t^6 \eta_{ox}{}^4 \rho_l{}^6 \rho_s{}^2 + 64 H_{ox} L_m L_v{}^6 r_{m0}{}^2 r_{v0}{}^4 sc^4 t^6 \eta_{ox} \rho_l{}^6 \rho_s{}^3$$

$$+ 128 H_{ox}{}^3 L_m L_v{}^4 r_{m0}{}^4 r_{v0}{}^2 sc^4 t^6 \eta_{ox}{}^3 \rho_l{}^5 \rho_s{}^3 - 64 H_{ox}{}^3 L_m{}^3 L_v{}^2 r_{v0}{}^6 sc^4 t^6 \eta_{ox}{}^3 \rho_l{}^5 \rho_s{}^3$$

$$+ 32 L_v{}^8 r_{m0}{}^6 sc^4 t^6 \rho_l{}^4 \rho_s{}^4 - 32 L_m{}^2 L_v{}^6 r_{m0}{}^2 r_{v0}{}^4 sc^4 t^6 \rho_l{}^4 \rho_s{}^4$$

$$- 192 H_{ox}{}^2 L_m{}^2 L_v{}^4 r_{m0}{}^4 r_{v0}{}^2 sc^4 t^6 \eta_{ox}{}^2 \rho_l{}^4 \rho_s{}^4$$

$$+ 480 H_{ox}{}^2 L_m{}^4 L_v{}^2 r_{v0}{}^6 sc^4 t^6 \eta_{ox}{}^2 \rho_l{}^4 \rho_s{}^4 + 128 H_{ox} L_m{}^3 L_v{}^4 r_{m0}{}^4 r_{v0}{}^2 sc^4 t^6 \eta_{ox} \rho_l{}^3 \rho_s{}^5$$

$$- 192 H_{ox} L_m{}^5 L_v{}^2 r_{v0}{}^6 sc^4 t^6 \eta_{ox} \rho_l{}^3 \rho_s{}^5 - 32 L_m{}^4 L_v{}^4 r_{m0}{}^4 r_{v0}{}^2 sc^4 t^6 \rho_l{}^2 \rho_s{}^6$$

$$+ 448 H_{ox}{}^6 r_{v0}{}^4 sc^4 t^8 \eta_{ox}{}^6 \rho_l{}^6 c_1{}^2 - 2688 H_{ox}{}^5 L_m r_{v0}{}^4 sc^4 t^8 \eta_{ox}{}^5 \rho_l{}^5 \rho_s c_1{}^2$$

$$- 192 H_{ox}{}^2 L_v{}^4 r_{m0}{}^2 r_{v0}{}^2 sc^4 t^8 \eta_{ox}{}^2 \rho_l{}^4 \rho_s{}^2 c_1{}^2 + 6720 H_{ox}{}^4 L_m{}^2 r_{v0}{}^4 sc^4 t^8 \eta_{ox}{}^4 \rho_l{}^4 \rho_s{}^2 c_1{}^2$$

$$+ 384 H_{ox} L_m L_v{}^4 r_{m0}{}^2 r_{v0}{}^2 sc^4 t^8 \eta_{ox} \rho_l{}^3 \rho_s{}^5 c_1{}^2 - 8960 H_{ox}{}^3 L_m{}^3 r_{v0}{}^4 sc^4 t^8 \eta_{ox}{}^3 \rho_l{}^3 \rho_s{}^3 c_1{}^2$$

$$- 192 L_m{}^2 L_v{}^4 r_{m0}{}^2 r_{v0}{}^2 sc^4 t^8 \rho_l{}^2 \rho_s{}^4 c_1{}^2 + 6720 H_{ox}{}^2 L_m{}^4 r_{v0}{}^2 sc^4 t^8 \eta_{ox}{}^2 \rho_l{}^2 \rho_s{}^4 c_1{}^2$$

$$- 2688 H_{ox} L_m{}^5 r_{v0}{}^4 sc^4 t^8 \eta_{ox} \rho_l \rho_s{}^5 c_1{}^2 + 448 L_m{}^6 r_{v0}{}^4 sc^4 t^8 \rho_s{}^6 c_1{}^2$$

$$b_7 = 128 H_{ox}{}^7 r_{v0}{}^4 sc^4 t^8 \eta_{ox}{}^7 \rho_l{}^7 c_1 - 896 H_{ox}{}^6 L_m r_{v0}{}^4 sc^4 t^8 \eta_{ox}{}^6 \rho_l{}^6 \rho_s c_1$$

$$- 128 H_{ox}{}^3 L_v{}^4 r_{m0}{}^2 r_{v0}{}^2 sc^4 t^8 \eta_{ox}{}^3 \rho_l{}^5 \rho_s{}^2 c_1 + 2688 H_{ox}{}^5 L_m{}^2 r_{v0}{}^4 sc^4 t^8 \eta_{ox}{}^5 \rho_l{}^5 \rho_s{}^2 c_1$$

$$+ 384 H_{ox}{}^2 L_m L_v{}^4 r_{m0}{}^2 r_{v0}{}^2 sc_4 t^8 \eta_{ox}{}^2 \rho_l{}^4 \rho_s{}^3 c_1 - 4480 H_{ox}{}^4 L_m{}^3 r_{v0}{}^4 sc^4 t^8 \eta_{ox}{}^4 \rho_l{}^4 \rho_s{}^3 c_1$$

$$- 384 H_{ox} L_m{}^2 L_v{}^4 r_{m0}{}^2 r_{v0}{}^2 sc^4 t^8 \eta_{ox} \rho_l{}^3 \rho_s{}^4 c_1 + 4480 H_{ox}{}^3 L_m{}^4 r_{v0}{}^4 sc^4 t^8 \eta_{ox}{}^3 \rho_l{}^3 \rho_s{}^4 c$$

$$_1 + 4480 H_{ox}{}^3 L_m{}^4 r_{v0}{}^4 sc^4 t^8 \eta_{ox}{}^3 \rho_l{}^3 \rho_s{}^4 c_1 + 128 L_m{}^3 L_v{}^4 r_{m0}{}^2 r_{v0}{}^2 sc^4 t^8 \rho_l{}^2 \rho_s{}^5 c_1$$

$$- 128 L_m{}^7 r_{v0}{}^4 sc^4 t^8 \rho_s{}^7 c_1$$

$$
\begin{aligned}
b_8 = {} & 16 H_{ox}{}^8 r_{v0}{}^4 sc^4 t^8 \eta_{ox}{}^8 \rho_l{}^8 - 128 H_{ox}{}^7 L_m r_{v0}{}^4 sc^4 t^8 \eta_{ox}{}^7 \rho_l{}^7 \rho_s \\
& - 32 H_{ox}{}^4 L_v{}^4 r_{m0}{}^2 r_{v0}{}^2 sc^4 t^8 \eta_{ox}{}^4 \rho_l{}^6 \rho_s{}^2 + 448 H_{ox}{}^6 L_m{}^2 r_{v0}{}^4 sc^4 t^8 \eta_{ox}{}^6 \rho_l{}^6 \rho_s{}^2 \\
& + 128 H_{ox}{}^3 L_m L_v{}^4 r_{m0}{}^2 r_{v0}{}^2 sc^4 t^8 \eta_{ox}{}^3 \rho_l{}^5 \rho_s{}^3 - 896 H_{ox}{}^5 L_m{}^3 r_{v0}{}^4 sc^4 t^8 \eta_{ox}{}^5 \rho_l{}^5 \rho_s{}^3 \\
& + 16 L_v{}^8 r_{m0}{}^4 sc^4 t^8 \rho_l{}^4 \rho_s{}^4 - 192 H_{ox}{}^2 L_m{}^2 L_v{}^4 r_{m0}{}^2 r_{v0}{}^2 sc^4 t^8 \eta_{ox}{}^2 \rho_l{}^4 \rho_s{}^4 \\
& + 1120 H_{ox}{}^4 L_m{}^4 r_{v0}{}^4 sc^4 t^8 \eta_{ox}{}^4 \rho_l{}^4 \rho_s{}^4 + 128 H_{ox} L_m{}^3 L_v{}^4 r_{m0}{}^2 r_{v0}{}^2 sc^4 t^8 \eta_{ox} \rho_l{}^3 \rho_s{}^5 \\
& - 896 H_{ox}{}^3 L_m{}^5 r_{v0}{}^4 sc^4 t^8 \eta_{ox}{}^3 \rho_l{}^3 \rho_s{}^5 - 32 L_m{}^4 L_v{}^4 r_{m0}{}^2 r_{v0}{}^2 sc^4 t^8 \rho_l{}^2 \rho_s{}^6 \\
& + 448 H_{ox}{}^2 L_m{}^6 r_{v0}{}^4 sc^4 t^8 \eta_{ox}{}^2 \rho_l{}^2 \rho_s{}^6 - 128 H_{ox} L_m{}^7 r_{v0}{}^4 sc^4 t^8 \eta_{ox} \rho_l \rho_s{}^7 \\
& + 16 L_m{}^8 r_{v0}{}^4 sc^4 t^8 \rho_s{}^8
\end{aligned}
$$

$$
c_1 = I_{abs} + h_g (T_g - T_{l0}) + \frac{k_s (T_0 - T_m)}{2\sqrt{\alpha_s t}}
$$

$$
c_2 = \frac{a_1}{\rho_l{}^2}
$$

As Eq.(5.28) is of order eight, its solution produces eight roots. A numerical solution gives these with four as imaginary numbers, two as negative numbers, and one feasible option from the remaining two roots.

The positions of the solid-liquid and liquid-vapour interfaces at $r = 0$ can be estimated from

$$
z_{m0}(t) = \int_0^t z'_{m0}(t)dt \tag{5.29}
$$

$$
z_{v0}(t) = \int_0^t z'_{v0}(t)dt \tag{5.30}
$$

Finally, the solid-liquid and liquid-vapour profiles are obtained from Eqs.(5.9) and (5.10).

5.2.2 Melt surface temperature (T_{l0})

To calculate the melt surface temperature, T_{l0}, some researchers employed the following equation in their models [76, 184]:

$$
T_{l0} = I_{abs} \sqrt{\frac{4t}{\pi \rho_l c_{eff} k_l}} \tag{5.31}
$$

where c_{eff} is the effective heat capacity and is defined as

$$c_{eff} = c_{ps} + \frac{L_m}{T_m} \qquad (5.32)$$

where c_{ps}, L_m and T_m are specific heat of solid, latent heat of melting and melting temperature of the material.

Calculation shows that Eq.(5.31) predicts quite high melt surface temperature (for example, T_{l0} = 19,960 K for mild steel, t =1.5 ms and P_{peak} = 3 kW) which is not likely to be practical. Although experimental data to confirm the melt surface temperature inside a laser drilled hole is not available at present, it can be expected that, for mild steel workpiece, the reasonable melt surface temperature should range between 3,100 K (boiling point of mild steel) and 5,000 K, approximately. At temperature higher than 5,000 K, ionisation should be expected. The laser energy would be consumed in the ionisation rather than transferring the kinetic energy to the atoms, making any further increase of the melt surface temperature be difficult [121].

Therefore, in this present model, a range of the melt surface temperatures is assumed from a value starting from slightly above the vaporisation point. A suitable value of the melt surface temperature is later determined by comparing the predicted results with those obtained from the experiments. It is worth mentioning here that, in practice, variation of the melt surface temperature with the laser intensity should be expected. Assuming a constant temperature over the range of the laser intensity would cause some errors in the model.

5.2.3 Melt front radius at the hole entrance (r_{m0})

In previously developed laser drilling models, it is often assumed that the hole entrance diameter would not exceed the beam spot diameter [52, 89, 179, 191]. In fact, especially in case of metals, the hole entrance diameter is usually larger than the theoretical beam spot diameter due to radial heat diffusion. Hence, to improve from the previous models, the hole entrance diameter is estimated from the spatial temperature distribution due to an instantaneous point source, which is written as[165]:

$$T_r(r,t) = \frac{P_P}{2\pi\, \alpha_l \rho c_l t} \exp\left(\frac{-r^2}{4\alpha_l t}\right) \tag{5.33}$$

where T_r and P_P are temperature distribution in the radial direction and laser peak power.

The melt front radius at the hole entrance (r_{m0}) is hence approximate by a radial distance at which $T_r = T_m$.

5.2.4 Melt ejection velocity (V_m)

Melt ejection velocity is another variable required in the model. It can be determined from the Bernoulli's equation:

$$p_{vap} + p_{eff} = \frac{\rho_l V_m^2}{2} + \rho_l g\, z_{m0}(t) + \frac{\sigma}{r_{v0}} \tag{5.34}$$

where p_{vap}, p_{eff}, g and σ are vapour pressure (recoil pressure), effective assist gas pressure, gravitational acceleration and surface tension, respectively. The hydrostatic and surface tension terms on the right-hand side are negligible compared to other terms. Therefore, the expression for melt ejection velocity can be written as

$$V_m = \sqrt{\frac{2\,(p_{vap} + p_{eff})}{2\,\rho_l}} \tag{5.35}$$

It can be seen from Eq.(5.35) that in order to calculate the melt ejection velocity, values of the vapour pressure, p_{vap}, and the effective gas pressure, p_{eff}, are essential.

5.2.5 Vapour pressure (p_{vap})

Vapour pressure exerted on the melt surface can be estimated from the Clausius-Clapeyron equation [189, 190]:

$$p_{vap} = p_0 \exp\left[\frac{L_v}{R}\left(\frac{1}{T_b} - \frac{1}{T_{l0}}\right)\right] \tag{5.36}$$

where p_0 and T_b are atmospheric pressure and boiling temperature, R is the specific gas constant and is calculated from:

$$R = \frac{R_u}{M_m} \qquad (5.37)$$

For low carbon mild steel, $M_m = 0.05575$ kg/mol (mild steel contains approximately 99% iron [123]), hence

$$R = \frac{8.314}{0.05575} = 149.13 \qquad \text{J/kg.K.}$$

5.2.6 Effective assist gas pressure (p_{eff})

In addition to supplying exothermic energy to the process, the process gas also assists the melt ejection mechanism. By adding the assist gas pressure to the recoil pressure exerted on the molten liquid surface, more liquid can be removed and thus producing a higher penetration rate.

For isentropic gas flow, total pressure, which consists of static and dynamic pressure terms, is constant along the gas stream. However, in case of laser drilling, where the hole bottom is perpendicular to the gas axis, and if a uniform gas pressure profile is assumed within the laser beam, the dynamic gas pressure may be negligible. Due to adiabatic expansion of the assist gas at the nozzle exit, the gas is accelerated up to the local speed of sound leading to the critical state [52, 121]. The critical assist gas pressure at the nozzle exit, p_c, can be defined as

$$p_c = \left(\frac{2}{\gamma + 1} \right)^{\frac{\gamma}{\gamma - 1}} p_g \qquad (5.38)$$

where p_g is the pressure inside the nozzle, γ is the specific heat ratio which is taken to be 1.4 for oxygen assist gas.

At the hole entrance, assist gas pressure is reduced from p_c to the effective assist gas pressure, p_{eff}, due to pressure loss between the gas nozzle exit and the hole entrance.

$$p_{eff} = p_c \frac{A_{eff}}{A_{eff} + A_{rl}} \qquad (5.39)$$

where A_{eff} is the effective area of gas entering the hole, A_{rl} is the cylindrical area of radial loss of assist gas pressure defined by the nozzle exit diameter, d_n, and nozzle-workpiece distance, z_n:

$$A_{eff} = \pi r_{v0}^2 \qquad (5.40)$$

$$A_{rl} = \pi d_n z_n \qquad (5.41)$$

5.2.7 Exothermic reaction

When oxygen is used as an assist gas in laser beam-metals processing, it can oxidise with the metals and releases additional energy, called exothermic energy, to the process. The oxide phases and the amount of exothermic energy released depend on the chemical reaction between the elements within the metals and oxygen. In general, the chemical reaction between a metal, M, and oxygen gas, O_2, to form an oxide M_aO_b, can be written as:

$$aM + \frac{b}{2}O_2 \rightarrow M_aO_b + exothermic\ energy \qquad (5.42)$$
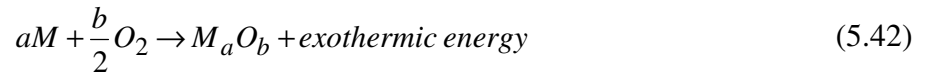
where a and b in this case are appropriate stoichiometric coefficients.

In laser processing, exothermic reaction between a mild steel plate (mild steel contains approximately 99% iron [123]) and oxygen assist gas produces iron oxide (FeO) [52, 123]. The oxidation reaction is expressed as:

$$Fe + \frac{1}{2}O_2 \rightarrow FeO \qquad ;\ H_{ox} = \text{-}242.758\ \text{kJ/mol}\ [196] \qquad (5.43)$$
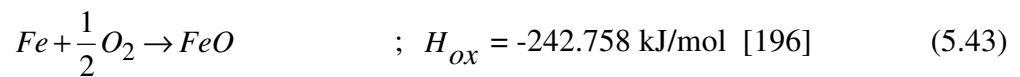
where H_{ox} is the enthalpy of oxidation.

The rate of oxidation reaction is determined by the propagation rate of the solid-liquid interface as it controls the availability of the parent material for the reaction [121]. Therefore, the exothermic energy may be expressed as :

$$exothermic\ energy = \rho_l H_{ox} \eta_{ox} \frac{\partial z_m}{\partial t} \qquad (5.44)$$

where η_{ox} is the oxidation efficiency.

5.3 SOLIDIFICATION DURING PULSE OFF

In laser percussion drilling, each laser pulse is separated by a pulse off time interval. During the pulse off duration, the molten liquid layer is cooled down and solidification of the molten liquid layer occurs. To model the freezing problem, Dowden [183] exploited the Neumann's solution (given by F.Neumann in his lectures in the 1860's, see Dowden [183], p.146), in which the error function is used for solving the one-dimensional transient heat conduction problem. By assuming that the solidification takes place mainly in vertical direction, the schematic diagram of the pulse off model is shown in Figure 5.6.
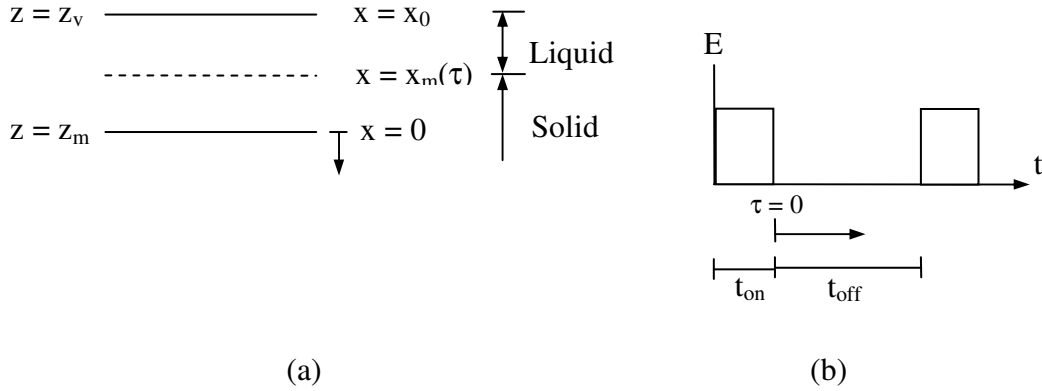
Figure 5.6 (a) Schematic diagram of the solidification model,

(b) time scale of the solidification model.

At the end of the pulse on period $(\tau = 0)$, the solid-liquid interface is at $x = 0$ and the liquid at $x < 0$. During the pulse off duration (from $\tau = 0$ to $\tau = t_{off} = \dfrac{1}{f} - t_{on}$, where f is the frequency) thin layer of the liquid is solidified and the solid-liquid interface is moved to $x = x_m(\tau)$. The initial and boundary conditions for this case are:

$$T_l(x_m(\tau),\tau) = T_m \tag{5.45}$$

$$T_l(x_0,\tau) = T_{l0,off}(\tau) \tag{5.46}$$

$$T_l(x_m(\tau),\tau) = T_s(x_m(\tau),\tau) = T_m \tag{5.47}$$

$$k_s \frac{\partial T_s(x,\tau)}{\partial x} - k_l \frac{\partial T_l(x,\tau)}{\partial x} = \rho_s L_m \frac{dx_m(\tau)}{d\tau} \tag{5.48}$$

$$T_s(\infty,\tau) = T_0 \tag{5.49}$$

and
$$x_m(0) = 0 \tag{5.50}$$

where $T_{l0,off}(\tau)$, x_0 and $x_m(\tau)$ are melt surface temperature during pulse off, liquid-vapour interface location, and solid-liquid interface location, respectively.

Temperature drop of the melt surface subjected to heat convection cooling may be estimated from [173]:

$$T_{l0,off}(\tau) = T_{l0} + (T_g - T_{l0})\left\{1 - \left[\exp\frac{h_g^2\alpha_l\tau}{k_l^2}\right]\left[1 - erf\left(\frac{h_g\sqrt{\alpha_l\tau}}{k_l}\right)\right]\right\} \tag{5.51}$$

The temperature profiles in solid and liquid that satisfy the boundary conditions may be assumed in the forms:

$$T_l(x,\tau) = T_{l0,off}(\tau) - B_1\,erf\left(\frac{x-x_0}{2\sqrt{\alpha_l\tau}}\right) \tag{5.52}$$

$$T_s(x,\tau) = T_0 + B_2\,erfc\left(\frac{x}{2\sqrt{\alpha_s\tau}}\right) \tag{5.53}$$

To seek solutions in these forms, $x_m(\tau)$ must be proportional to $\sqrt{\tau}$ [183] i.e.

$$x_m(\tau) = \xi\sqrt{4\tau\sqrt{\alpha_l\alpha_s}} \tag{5.54}$$

where ξ is a constant.

At $x = x_m(\tau)$, B_1 and B_2 in Eqs.(5.52) and (5.53) become:

$$B_1 = \frac{T_{l0,off}(\tau) - T_m}{erf\left[\dfrac{-x0 + 2\sqrt{\tau\sqrt{\alpha_l\alpha_s}}\,\xi}{2\sqrt{\alpha_l\tau}}\right]} \tag{5.55}$$

$$B_2 = \frac{T_m - T_0}{erfc\left[\left(\dfrac{\alpha_l}{\alpha_s}\right)^{1/4}\xi\right]} \tag{5.56}$$

Finally, ξ can be determined by solving the interface condition in Eq.(5.48). Substituting ξ into Eq.(5.54), location of the solidification front $x_m(\tau)$ is obtained.

106

In summary, each cycle of the multiple pulsed drilling passes through one step of drilling during the pulse heating (where the pulse width defines the interaction time), and one step of solidification during the pulse off (where the pulse frequency defines the pulse off duration). The calculation is then repeated one pulse at a time until the given constraints i.e. material thickness, number of pulses etc. are met.

Figure 5.7 illustrates the flow chart for calculation procedures of the model.
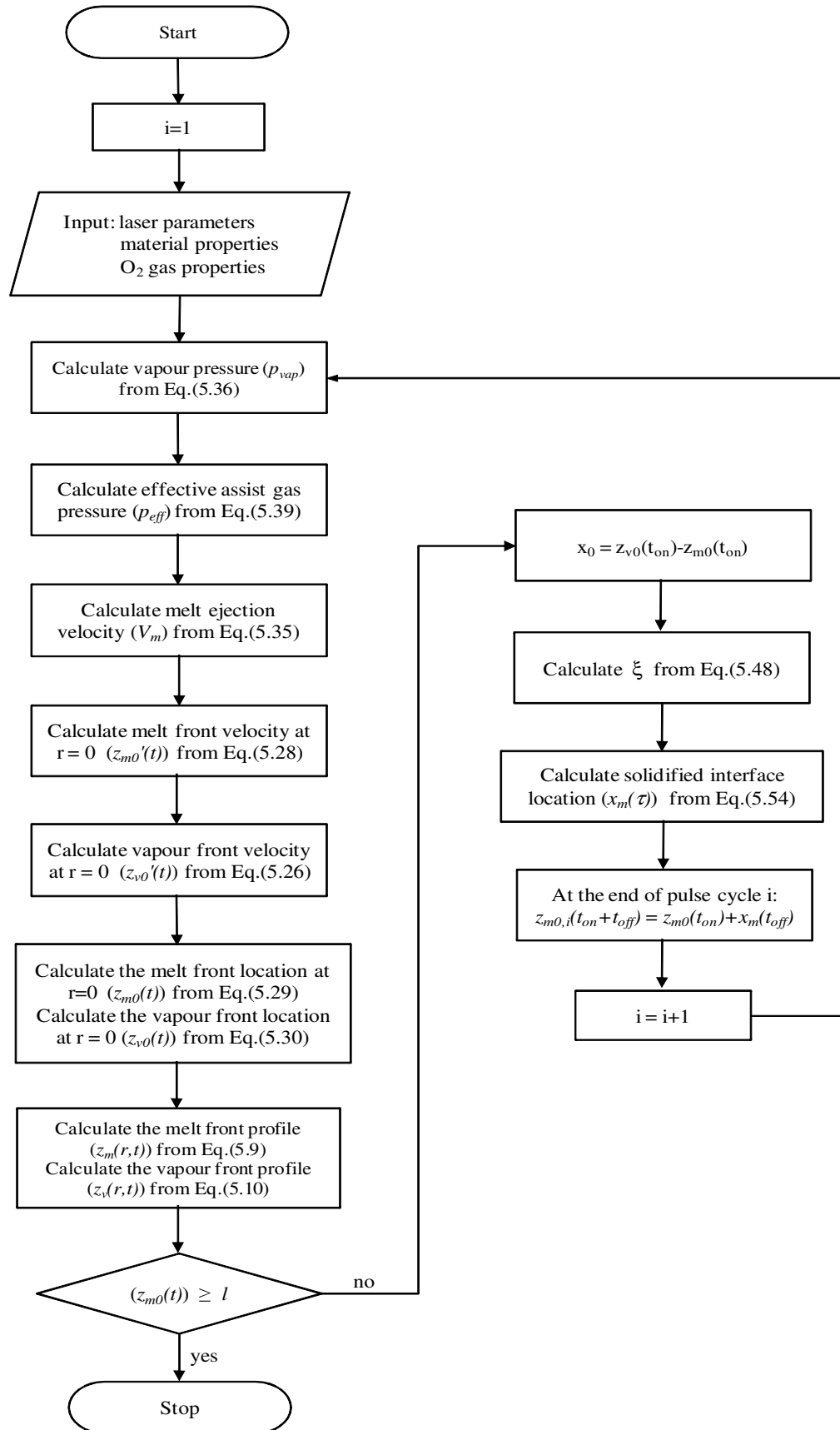
Figure 5.7 Calculation procedures of the model.

5.4 PHYSICAL PROPERTIES

The thermophysical properties of the low carbon steel and assist gas are given in Tables 5.1 and 5.2.

Table 5.1 Thermophysical properties of low carbon steel [69].

Material properties	
Density of solid, ρ_s (kg m^{-3})	7800
Density of liquid, ρ_l (kg m^{-3})	6980
Specific heat of solid, c_{ps} (J kg^{-1} K^{-1})	628
Specific heat of liquid, c_{pl} (J kg^{-1} K^{-1})	748
Thermal diffusivity of solid, α_s (m^2 s^{-1})	0.014×10^{-3}
Thermal diffusivity of liquid, α_l (m^2 s^{-1})	0.007×10^{-3}
Latent heat of melting, L_m (J kg^{-1})	276×10^3
Latent heat of vaporisation, L_v (J kg^{-1})	6088×10^3
Initial temperature, T_0 (K)	300
Melting temperature, T_m (K)	1808
Boiling temperature, T_b (K)	3100
Molar mass, M_m (kg mol^{-1})	0.05575

Table 5.2 Thermophysical properties O_2 assist gas [197-199] and gas nozzle parameters.

O_2 properties	
Density of gas, ρ_g (kg m^{-3})	1.3007
Viscosity of gas, μ_g (N s m^{-2})	2.01×10^{-5}
Thermal conductivity, k_g (W m^{-1}K^{-1})	0.0259
Prandtl number, Pr	0.73
Assist gas nozzle exit diameter, d_n (m^2)	1.5×10^{-3}
Nozzle-workpiece distance, z_n (m)	5.8×10^{-3}

CHAPTER 6

EXPERIMENTAL PROCEDURES FOR MODEL VERIFICATION

6.1 INTRODUCTION

In order to verify the model developed in Chapter 5, a comparison with the experimental data is essential. This chapter details the experimental work performed using a GSI-JK300D pulsed Nd:YAG laser. Holes are vertically drilled in mild steel plates with 2.4 mm thickness. Hole dimensions are captured and analysed using Polyvar and Leica microscopy. Moreover, measurement of the beam diameter and recast layer thickness at the hole entrance have also been conducted to obtain the appropriate values of the laser beam diameter (r_b) and the radius of the liquid-vapour interface at the hole entrance (r_{v0}).

6.2 EXPERIMENTAL PROCEDURES

6.2.1 Experimental apparatus

In the current experiments, laser percussion drilling of 2.4 mm thick mild steel is performed using 300W GSI-JK300D pulsed Nd:YAG laser; emitting at 1.06 μm wavelength. The laser beam is delivered via an optical fibre, having 300 μm in diameter, before it is focused by the recollimating and focus lens, which are mounted in the laser processing head. Oxygen assist gas used throughout the experiment is supplied coaxially to the laser processing head before being projected onto the workpiece.

The workpiece used in the experiment is 70×100×2.4 mm^3 plate of mild steel. To eliminate the rust and dust particles which may deposit on the plate, a shot blasting machine is used to clean up both sides of the plate. The mild steel plate is then clamped at the focal distance. Positioning of the location to be drilled on the workpiece is controlled by the CNC machine mounted to the laser head unit. Figure 6.1 shows the schematic diagram of the experimental apparatus.

For a set of operating parameters, holes are drilled using a one-step increase of pulse, i.e. the first hole is drilled using one pulse, the second and third holes are

subsequently drilled with two and three pulses, respectively. This process is repeated until a breakthrough is achieved. Number of pulses required to initiate breakthrough is then recorded.
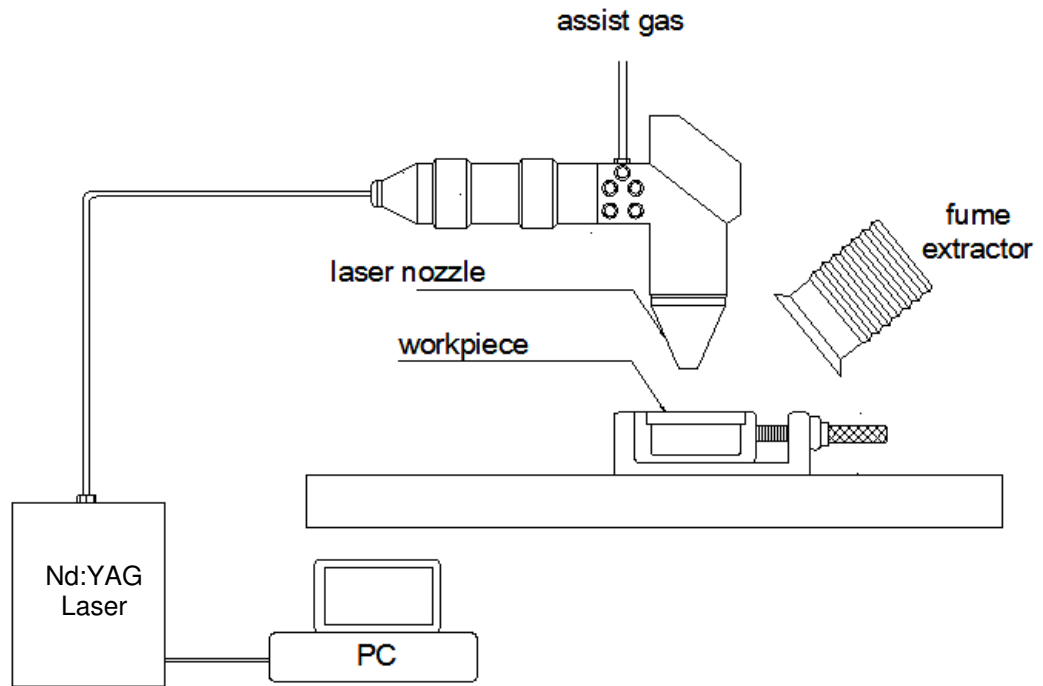
Figure 6.1 Schematic diagram of the experimental apparatus.

6.2.2 Sample preparation

Following the drilling experiments, the plate is cut into pieces ($7 \times 10 \times 2.4$ mm^3 approximately) each containing a single hole. Each of these plates is then mounted in a clear resin and ground using 320, 600 and 1200 grit SiC papers, in that order, until the hole centre is reached. To analyse the microstructures, these samples are subsequently etched with Nital etchant, which is a solution of 1 ml nitric acid and 9 ml methanol or ethanol [200].
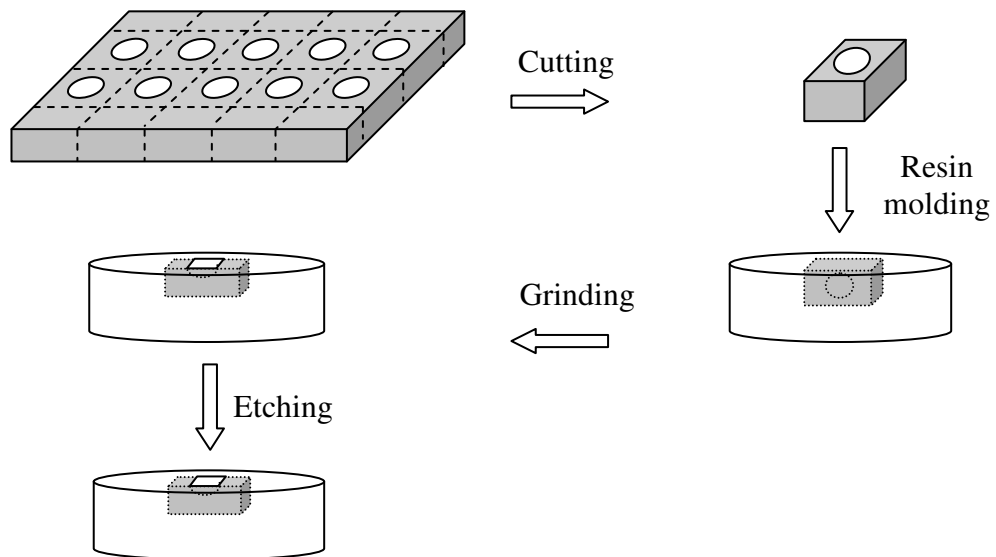
Figure 6.2 Sample preparation procedures.

6.2.3 Hole dimension measurement

In laser percussion drilling, the main concerns are minimum number of pulses required to generate a through hole, maximum hole depth achieved with a particular number of pulses, hole taper, and recast layer thickness. To obtain the breakthrough pulse, holes are drilled using a same set of operating parameters whilst the number of pulses employed is varied. Starting by drilling with one pulse, the subsequent holes are drilled with two, three, four pulses and so on until the breakthrough is achieved.

In order to measure the hole diameter, hole depth, and recast layer thickness, Polyvar and Leica microscopy is used for capturing and analysing the images. To ensure that the hole centre is reached after polishing, hole diameters at the entrance and exit sides are measured before mounting the sample to the clear resin.

6.2.4 Process parameters

Range of the various process parameters employed in this study are listed as in Table 6.1.

Table 6.1 Process parameters.

Pulse peak power (kW)	3, 4, 5
Pulse width (ms)	0.5, 1,1.5, 1.8, 2
Pulse frequency (Hz)	50, 100
Gas pressure (bar)	3, 4, 5

6.3 BEAM SPOT DIAMETER MEASUREMENT

According to the mathematical formulation in Chapter 5, diameter of the melt front at the hole entrance $(2r_{m0})$ is needed as an input to the model. Previous models often assumed that this diameter would not exceed the beam spot diameter $(2r_b)$ [52, 89, 179, 191]. However, in practice, if material is metals or alloys, which is the material of interest in this study, the hole entrance diameter is usually much larger than the beam spot diameter due to the lateral heat effects. Therefore, if the diameter of the melt front at the hole entrance is approximate by the beam spot diameter $(2r_{m0} = 2r_b)$, some errors can be expected in the model.

To confirm that the entrance diameter of a laser drilled hole is usually larger than the beam spot diameter, hole diameter measurements have been performed on a mild steel plate and Kapton tape, which is a temperature resistant material and does not carbonise at elevated temperature. The laser system used in these experiments has theoretical beam spot diameter of 240 µm. To locate the focal plane of the laser beam, laser spot size is measured at various locations along the laser beam axis. A low energy ($\approx$0.4 J) single pulse is used.

The impingement of the laser beam on the Kapton tape shows a distinct surface ablation with little lateral heat effects as shown in Figure 6.3. It is found that the hole diameter produced on Kapton tape is approximately the same as the theoretical beam spot diameter, i.e. 240 µm. This reveals that for a heat resistant material, the hole diameter may be estimated by the beam spot diameter. The focal plane position is found to locate at 5.8 mm. Figure 6.4 shows the hole diameter measured on the mild steel plate using the same parameters setting as that in Figure 6.3. The hole diameter in this case is 292 µm which is larger than the beam spot diameter. The results presented in Figures 6.3 and 6.4 confirm that laser drilling of metals produces hole with larger entrance diameter than the beam spot diameter.

Therefore, instead of using $2r_{m0} = 2r_b$ in the model, Eq.(5.33), which is the spatial temperature distribution due to an instantaneous point source, is employed for estimating the melt front diameter at the hole entrance $(2r_{m0})$. It is hence

approximate by a radial distance at which the local temperature is equal to the melting point of the material i.e. $T_r(r_{m0}, t_{on}) = T_m$.
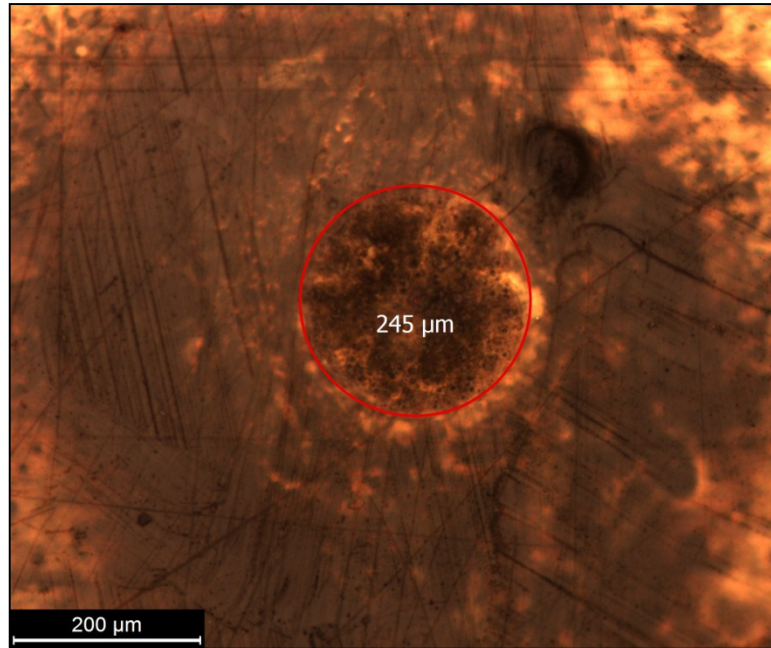
Figure 6.3 Measured beam spot diameter: Kapton tape
(E = 0.4 J, 5.8mm focal plan position).
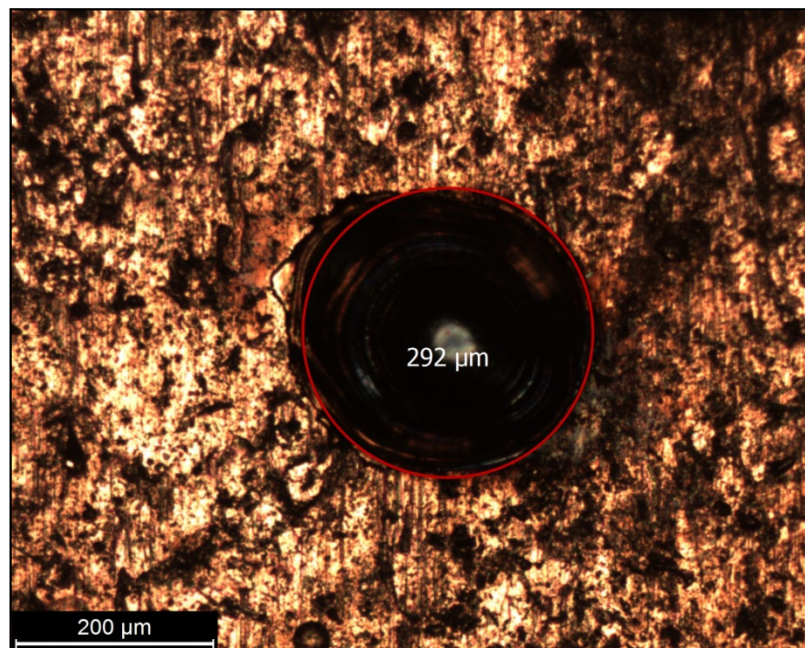
Figure 6.4 Measured hole diameter: mild steel.
(E = 0.4 J, 5.8mm focal plan position)

6.4 MEASUREMENT OF THE RECAST LAYER AT HOLE ENTRANCE

Another input for the model, which needs to be experimentally estimated, is the radius of the liquid-vapour interface at the hole entrance (r_{v0}). During the laser irradiation period, a thin layer of liquid is formed and pushed up along the hole wall with one side adjacent to the solid substrate and another side exposed to the vapour accumulated in the hole. At the end of the laser pulse-material interaction, solidification takes place resulting in the formation of the recast layer along the hole wall. Defining the actual location of the moving liquid-vapour interface during the interaction period is a difficult task. Therefore, to obtain a preliminary approximation, the radius of the liquid-vapour interface is taken to be the difference between the hole entrance radius (r_{m0}) and the recast layer thickness near the hole entrance i.e. $r_{v0} = r_{m0} - \delta_0$, where δ_0 is the recast layer thickness near the hole entrance.

To eliminate effects of other process variables on the recast layer thickness, samples are selected randomly. Measurements show that its values roughly lie in the range between 7-12 µm for most of the samples. Therefore, it is approximately taken here as $\delta_0 = 10$ µm . Therefore, as a preliminary approximation, radius of the liquid-vapour interface, or the vapour front radius, at the hole entrance is defined by: $r_{v0} = r_{m0} - 10$ µm.

Figure 6.5 Measurement of the recast layer thickness near the hole entrance.

Sameple#1: Pp = 3 kW, t_{on} = 1.5 ms, f = 50 Hz, p_g = 3 bar, pulse# 1.

Sameple#2: = 3 kW, t_{on} = 1.0 ms, f = 50 Hz, p_g = 3 bar, pulse# 1.

Sameple#3: Pp = 4 kW, t_{on} = 1.0 ms, f = 50 Hz, p_g = 5 bar, pulse# 14.

Sameple#4: Pp = 4 kW, t_{on} = 1.0 ms, f = 50 Hz, p_g = 4 bar, pulse# 11.
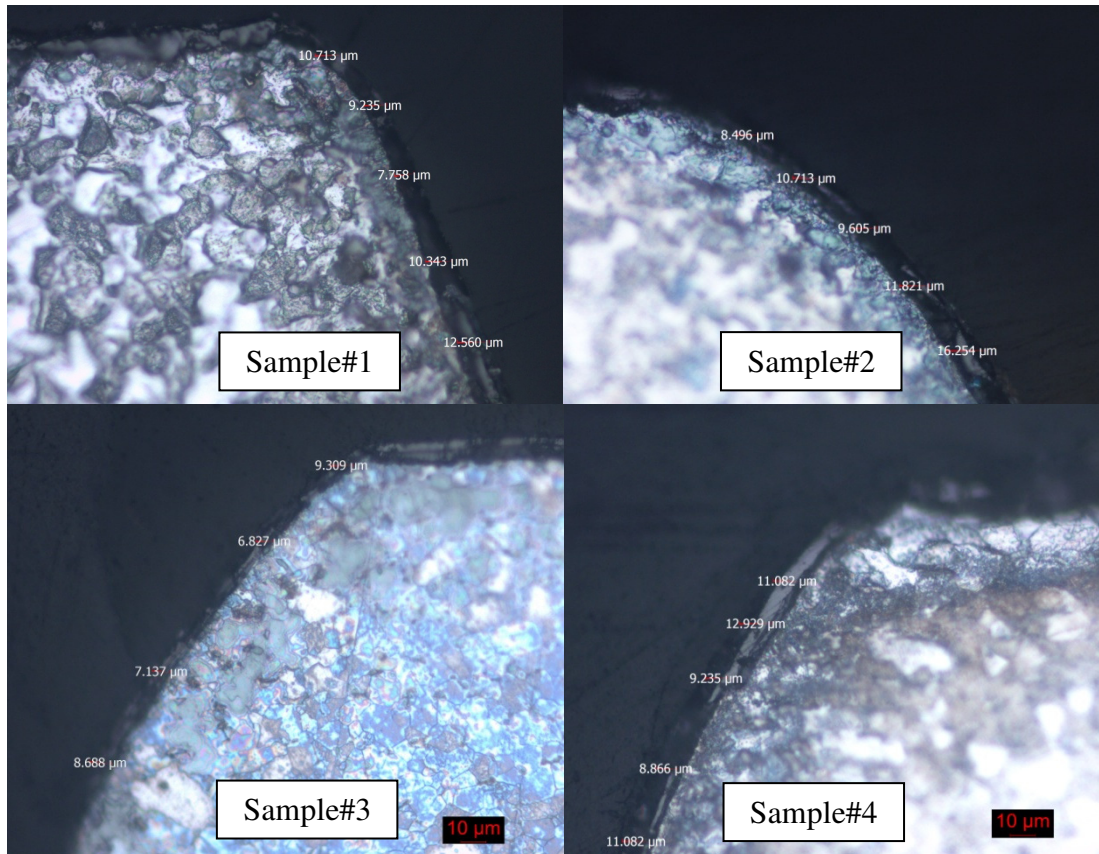
CHAPTER 7

RESULTS AND DISCUSSION

7.1 INTRODUCTION

In this chapter, results calculated from the model developed in Chapter 5 are presented and discussed with particular attention being paid to the hole depth, hole profile, hole taper, and recast layer thickness, which are the main concerns in laser percussion drilling. Contents of this chapter are divided into three main sections. The first section presents the model validation by comparing the calculated results to those obtained experimentally. In the second section, the characteristics of the hole profiles, hole taper, and recast layer thickness are discussed. Finally, parameters affecting the laser drilled hole quality are investigated.

7.2 VALIDATION OF THE MODEL

In order to validate the model, comparisons with the experimental data are being made. First of all, to ensure that an appropriate value of the melt front radius at the hole entrance (r_{m0}) is applied, comparison between the calculated hole depth and the measured hole depth is presented. In Figure 7.1, three plots of the hole depth are presented which include:

(1) measured hole depth,

(2) predicted hole depth using $r_{m0} = r_b = 120$ μm (beam spot diameter) in the model, and

(3) predicted hole depth using r_{m0} which is calculated from Eq.(5.33) as

$r_{m0} = 257$ μm.

It can be seen from Figure 7.1 that substituting $r_{m0} = 257$ μm in the model gives good prediction of the hole depth whereas using $r_{m0} = r_b = 120$ μm overpredicts the hole depth.

Table 7.1 lists the measured hole entrance diameter corresponding to the operating conditions provided in Figure 7.1. It is obvious that, due to heat diffusion in the radial direction, the actual hole entrance diameter is typically much larger than the

beam spot diameter and using Eq.(5.33) to estimate r_{m0} proves to give a better prediction. It is thereby used throughout used throughout the present modelling work.
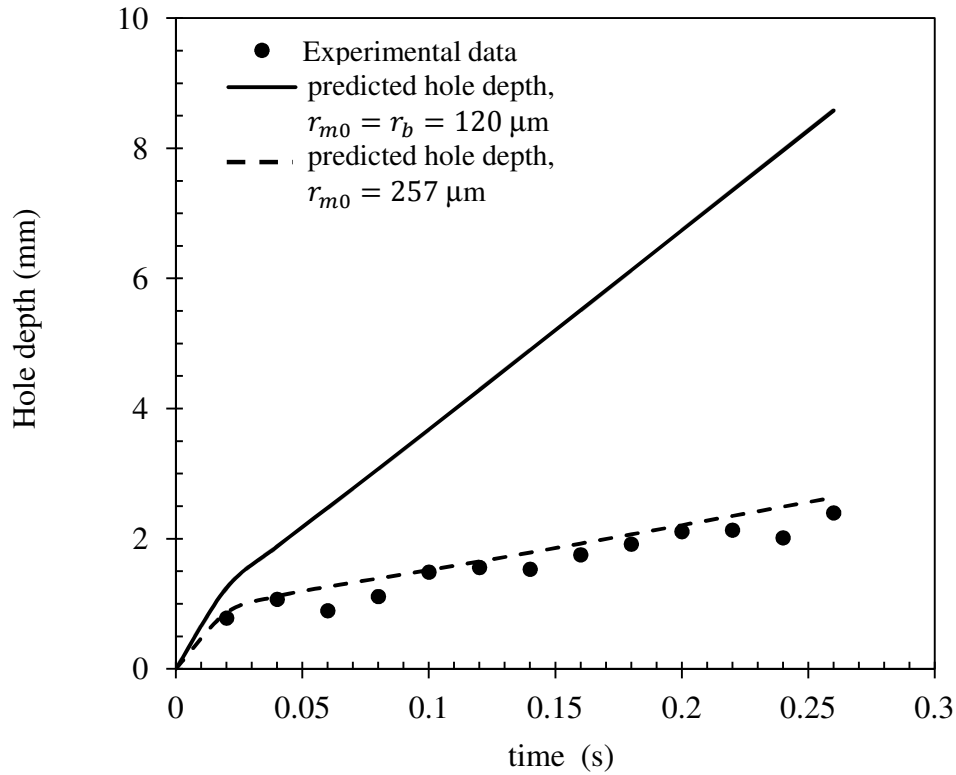
Figure 7.1 Comparison of the measured hole depth to the predicted hole depth obtained using $r_{m0} = r_b = 120\ \mu m$ and $r_{m0} = 257\ \mu m$. Mild steel, thickness = 2.4 mm, pulses width = 1.5 ms, frequency = 50 Hz, peak power = 3 kW, O_2 gas pressure = 3 bar

Table 7.1 Measured hole entrance diameter.
Material: mild steel , peak power: 3 kW, pulse frequency: 50 Hz,
pulse width: 1.5 ms, gas pressure: 3 bar.

Pulse#	Entrance diameter (μm)	Pulse#	Entrance diameter (μm)
1	667	8	576
2	549	9	646
3	606	10	585
4	663	11	563
5	625	12	655
6	613	13	571
7	634		

Theoretically, the measured hole diameter should increase as the pulse number increases, however reduction in the hole diameter can be occasionally observed as shown in Table 7.1. This could possibly due to several reasons such as the repeatability of the laser machine and the variation in the local surface roughness of the mild steel plate; which affect the laser beam absorptivity.

Another parameter which needs to be determined by comparing with the experimental data is the melt surface temperature r_{m0}. This is due to the lack of the measured data. In laser percussion drilling, interaction between each laser pulse and a material takes place at a short time interval (for example, 0.5-2 ms in the current experiment) and a small diameter hole (less than 1 mm in diameter) is produced. Under this circumstance, it is difficult to measure the surface temperature of the melt formed in the hole. Even infrared thermometer may not be possible to measure the melt surface temperature.

Figures 7.2-7.4 compare the predicted hole depth values with those obtained experimentally. Here, the melt surface temperature is assumed to be from slightly above the boiling point up to some point around 5,000 K. It is found that the melt surface temperature ranging between 3,900 and 4,300 K provides the reasonable predictions compared to the experimental data. Variation of the melt surface temperature within this range would cause a slight deviation in the predicted hole depth. To generalise the model for other ranges of operating parameters, $T_{l0} = 4,000$ K seems to be the best compromise option for mild steel. Therefore, this value is used throughout the modelling work presented here. It can be seen from Figures 7.2 and 7.3 that the current model gives good agreement compared to the experimental data whilst in Figure 7.4, the model gives good prediction of the hole depth for the first 4 pulses and slightly underpredicts the hole depth for the last two pulses.

Figure 7.2 Comparison between the predicted and measured hole depth,

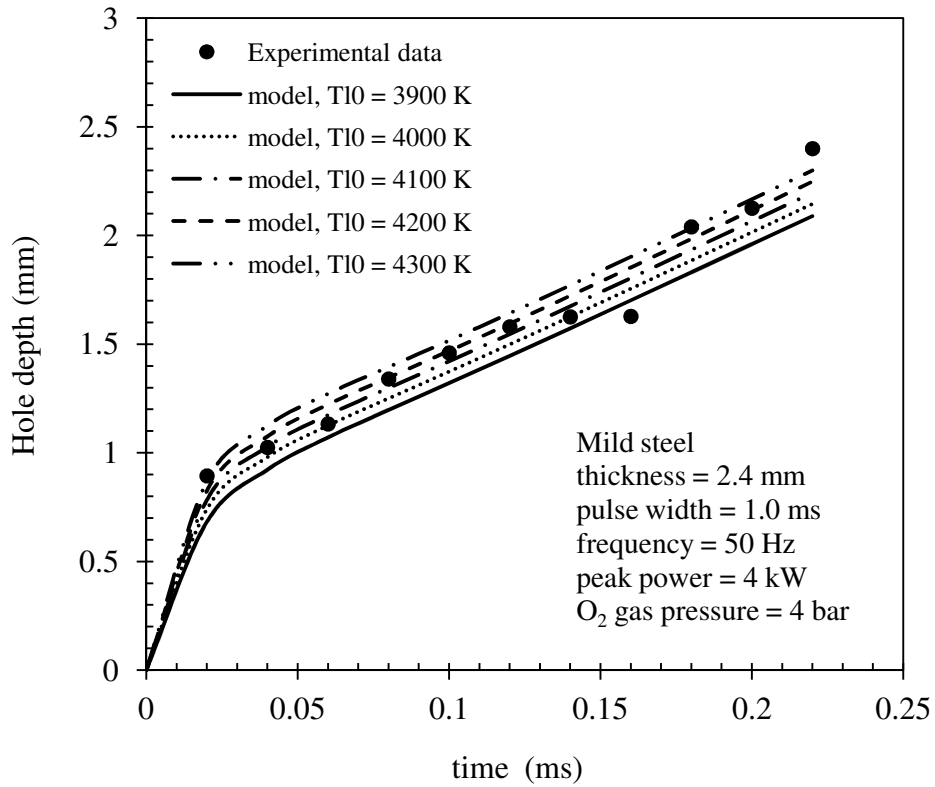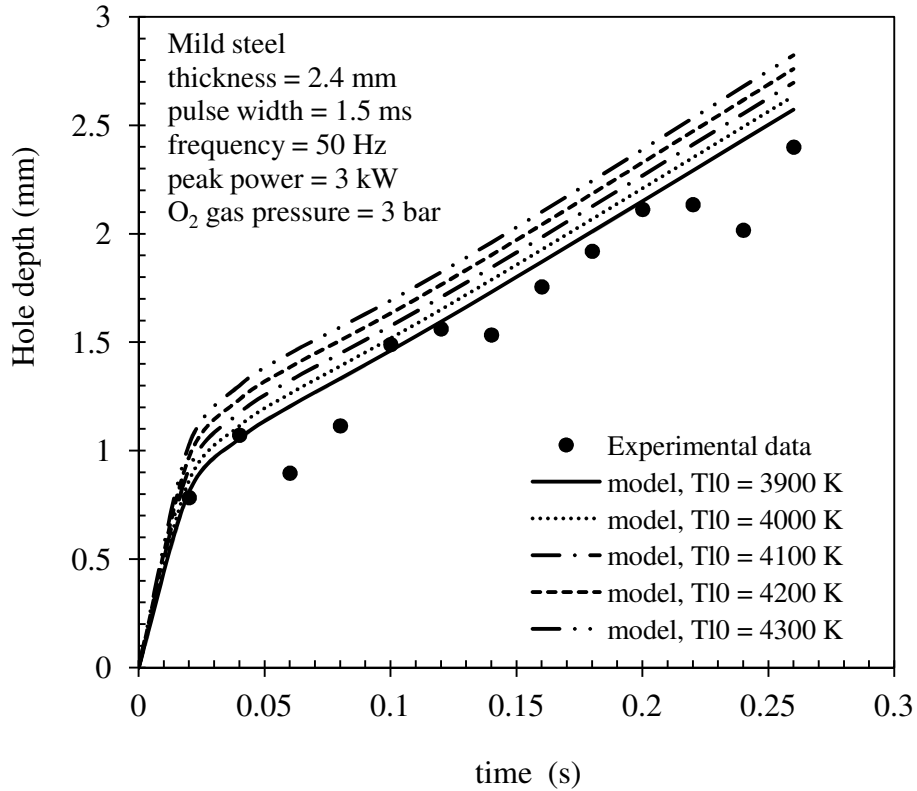t_{on} = 1 ms, T_{l0} from 3,900 – 4,300 K.

Figure 7.3 Comparison between the predicted and measured hole depth,

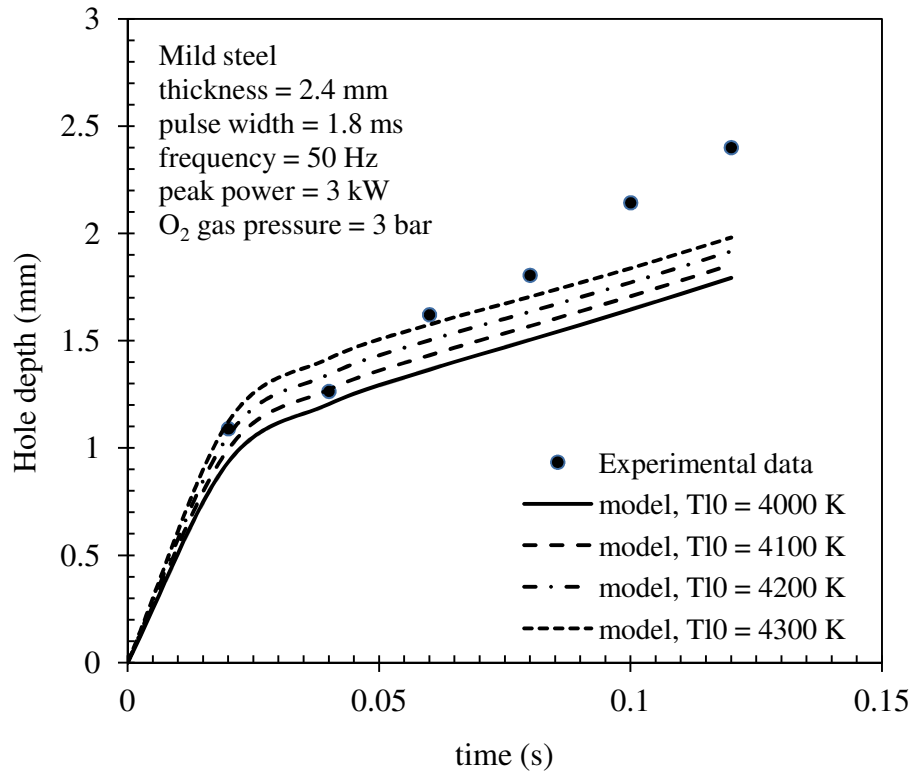t_{on} = 1.5 ms, T_{l0} from 3,900 – 4,300 K.

Figure 7.4 Comparison between the predicted and measured hole depth,

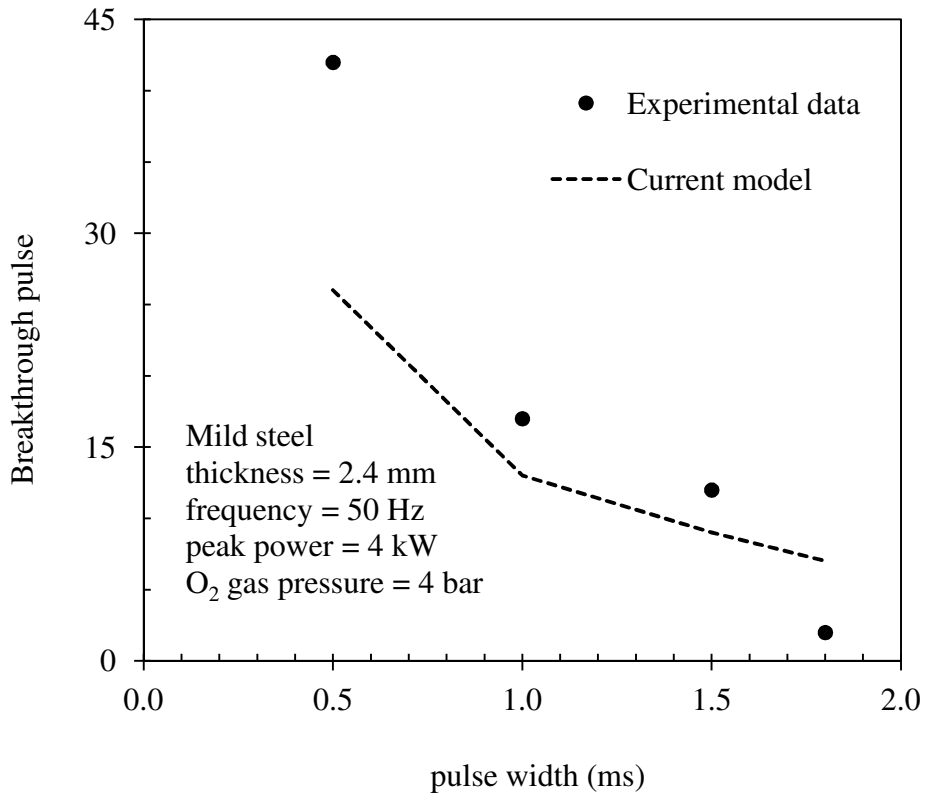t_{on} = 1.8 ms, T_{l0} from 4,000 – 4,300 K.

Figure 7.5 Effect of pulse width on breakthrough pulse.

Figure 7.5 compares the predicted breakthrough pulses to those required experimentally for 0.5, 1.0, 1.5, and 1.8 ms pulse widths. It is obvious that as the pulse width increases, less pulses are required to generate a through hole. This is due to the fact that, for a longer pulse width, higher laser energy per pulse irradiates the workpiece surface. This consequently leads to more heating, melting, and vaporisation of the material. In other words, longer pulse width gives deeper holes. Similar trends have also been reported in literature [15, 96, 115, 133].

It should be noted from Figure 7.5 that the current model gives a fair prediction for the cases of 1.0, 1.5, and 1.8 ms pulse width whilst the model underestimates the breakthrough pulse for 0.5 ms pulse width. This discrepancy could possibly be attributed to the difference in the actual melt surface temperature and the melt surface temperature assumed in the model. For actual laser drilling with a short laser-material interaction time, a lower melt surface temperature and hence a lower recoil pressure can be expected. However, because the current model assumes the same value of the melt surface temperature for all ranges of the pulse width, the same value of the recoil pressure is applied (see Eq.5.36). In this case, it could possibly be because the assumed melt surface temperature is higher than the actual melt surface temperature; hence, the higher predicted recoil pressure and the higher drilling rate.

In Figure 7.6, the predicted hole profile is plotted against that obtained experimentally. It can be seen that the model gives excellent prediction for the melt front; however, a discrepancy between the predicted and experimentally obtained vapour front can be observed. This could probably due to two main reasons. Firstly, there is multiple reflections of the laser beam inside the cavity during actual drilling whereas the current model ignores this effect. Modest [95] has revealed that multiple reflections inside the cavity raise the laser intensity in the cavity to some extent especially at the hole centre. With higher laser intensity in the cavity, more melt can be removed, which in turn results in smaller recast layer thickness. Secondly, it could possibly be due to the difference in the actual drilled hole geometry and the parabolic profile assumed in the model. From Figure 7.6, it is quite clear that the actual drilled hole profile is not a perfect parabola but an 'inlet cone' at the hole entrance. Because the current model assumes a hole to be parabolic with a fixed diameter, volume of

the material to be melted, vaporised, and removed is greater and hence at the end of the laser irradiation a thicker recast layer is predicted.

Radial distance (μm)
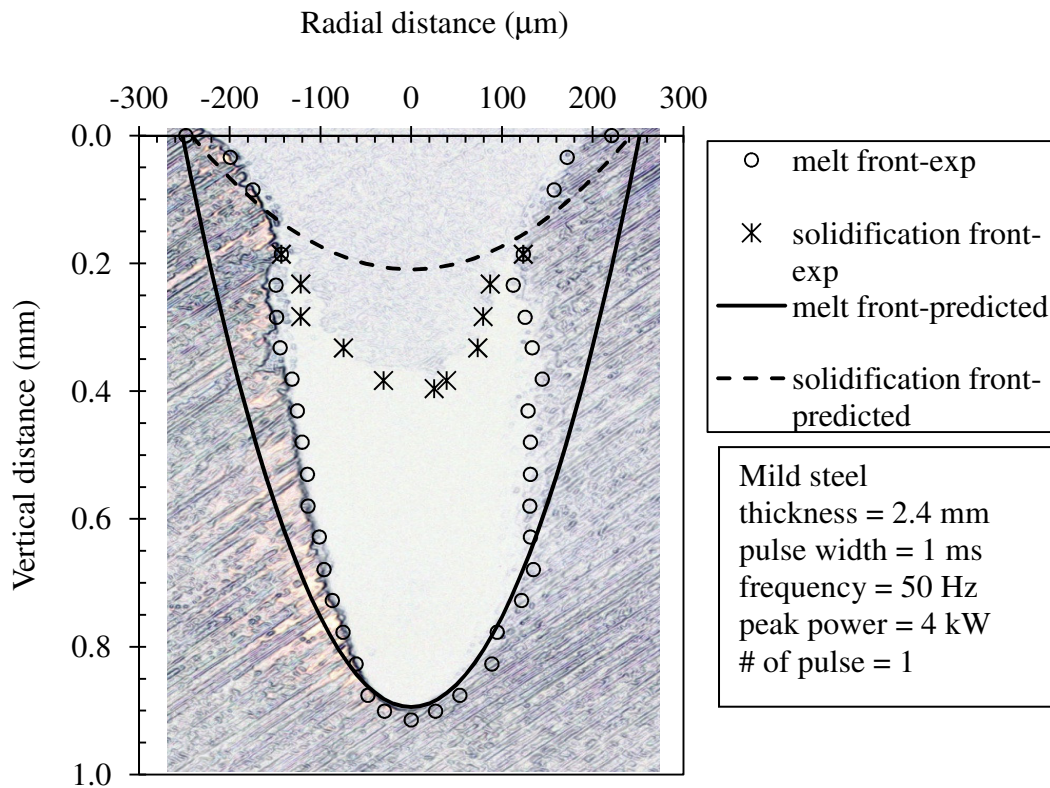
Figure 7.6 Comparison of the laser drilled hole profile.

Figure 7.7 compares the predicted hole profile to that obtained experimentally. In the current model, for the given workpiece thickness of 2.4 mm, a through hole is achieved when the predicted melt front (z_m, blue line in Figure 7.7) reaches the bottom of the workpiece, i.e. $z_m = 2.4$ mm. Although the vaporisation front (z_v, red line in Figure 7.7) has not reached the hole bottom, it can be imagined that once a through hole is produced, all the remaining liquid is flushed down the hole exit.

It can be seen from Figure 7.7 that, there is a slight discrepancy between the predicted and the actual drilled hole profiles. This discrepancy becomes larger as the drilling approaches the hole exit. This may suggest that the radial heat conduction becomes more important as the hole gets deeper. Hence, to improve the model accuracy, radial heat conduction should be included in the laser drilling model. It is

also worth noting here that the inlet cone is also observed at the entrance of the actual drilled hole.
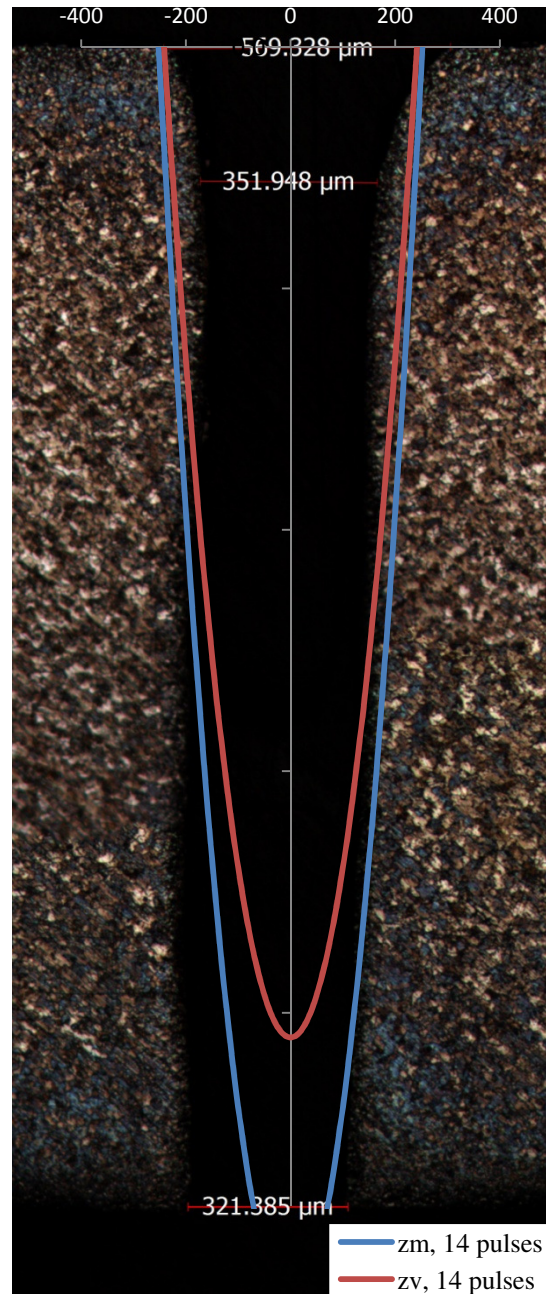
Figure 7.7 Comparison between the predicted and actual drilled hole profiles.
Mild steel, thickness = 2.4 mm, pulse width = 1ms,
frequency = 50 Hz, peak power = 4 kW, pulses # 14.
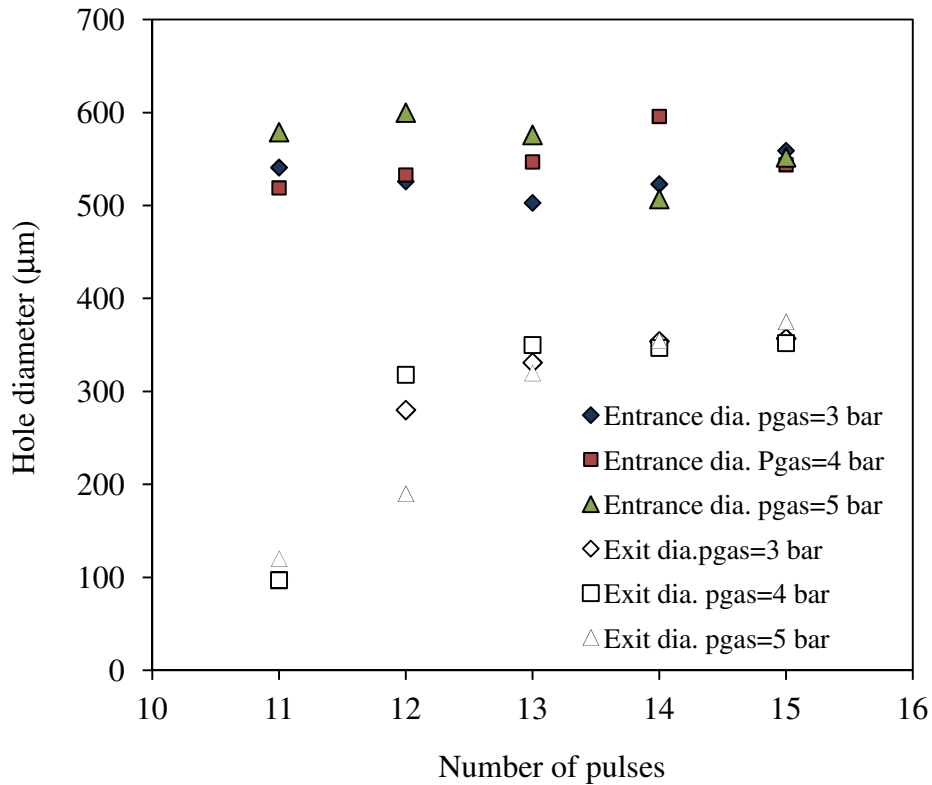
Figure 7.8 Measured hole diameter after drilling with 11-15 pulses.

Mild steel, thickness = 2.4 mm, pulse width = 1ms,

frequency = 50 Hz, peak power = 4 kW.

In the current model, for the sake of simplicity, and for a set of given operating parameters, the diameter of the hole entrance is assumed to be constant throughout the multiple pulses drilling. Although this may cause some errors in the model, experiments confirm that when holes are drilled with multiple pulses, the increasing number of pulses would have more influence on the hole exit diameter rather than the entrance diameter.

In Figure 7.8, the measured hole diameters at the entrance and exit sides are plotted for 3, 4, and 5 bar assist gas pressure. The corresponding breakthrough pulses for these conditions are 12, 11, and 11 pulses, respectively. It can be seen that as more laser pulses irradiate the workpiece surface, the exit hole diameter increases considerably whereas the entrance diameter changes slightly. This may imply that once a through hole has been achieved, subsequent laser pulses will enlarge the hole exit diameter making the hole wall more straight.

7.3 HOLE PROFILE, HOLE TAPER, AND RECAST LAYER THICKNESS

In laser percussion drilling, drilled hole geometry and hole quality are primary concerns. The results presented in this section are therefore focused on the predicted hole depth, hole profile, hole taper, and recast layer thickness.

Figures 7.9 and 7.10 show the evolution of melt depth as a function of time. These results indicate that the hole depth increases sharply during the interaction with the first laser pulse. In other words, maximum drilling speed per pulse is obtained with the first pulse. The subsequent laser pulses propagate into the workpiece at an approximately constant speed. Similar trend is observed from the experiments as shown previously in Figures 7.1-7.4. The recession of the drilling speed can be attributed to the fact that once the cavity is generated, vapour formed above the liquid surface may absorb and block part of laser energy resulting in beam scattering and causing less energy being delivered to the workpiece, hence lowering penetration rate.

Figure 7.11 illustrates the predicted profiles of solid-liquid and liquid-vapour interfaces after irradiating with 1, 2 and 3 pulses. The horizontal axis represents the radial distance from the hole symmetry line whereas the vertical axis represents the vertical distance from the workpiece surface. The hole profiles plotted in this figure are for the case of blind holes.

In Figure 7.12, the predicted hole profiles are plotted for 20 to 24 pulses. Figure 7.13 shows the predicted hole taper and exit diameter corresponding to the conditions in Figure 7.12. Here, the hole taper is calculated from the solidification front. It can be seen that the hole taper decreases as more pulses irradiate. This can be explained in the same manner as the experimental results reported previously in Figure 7.8. Once a through hole has been produced, subsequent laser pulses enlarge the hole wall, hence resulting in a smaller hole taper.
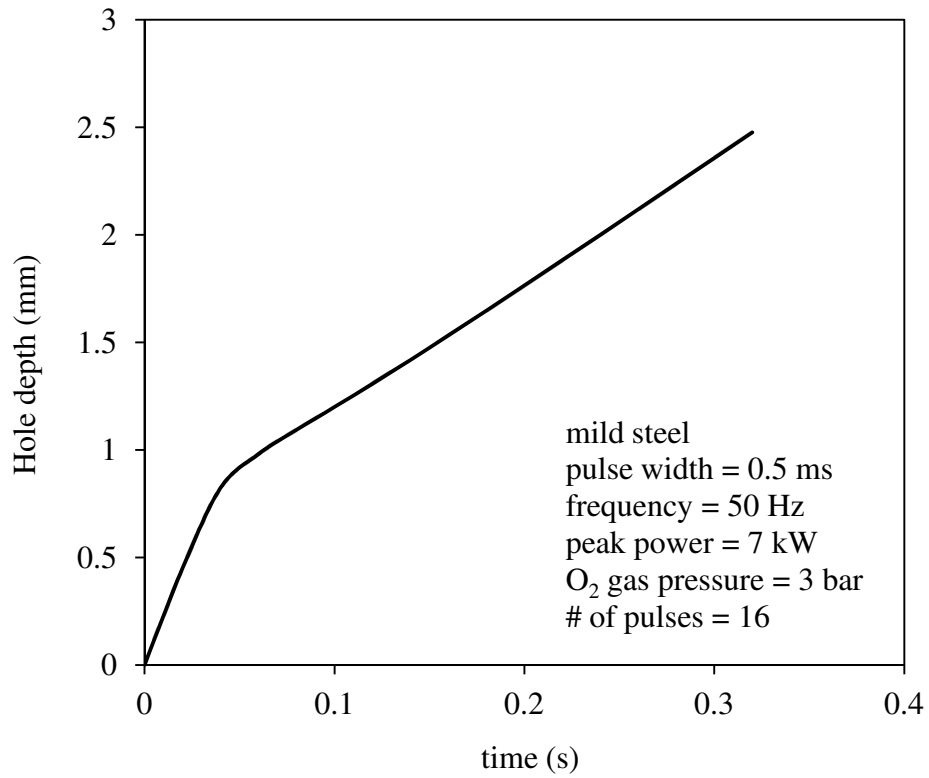
Figure 7.9 Predicted melt depth evolution as a function of time.
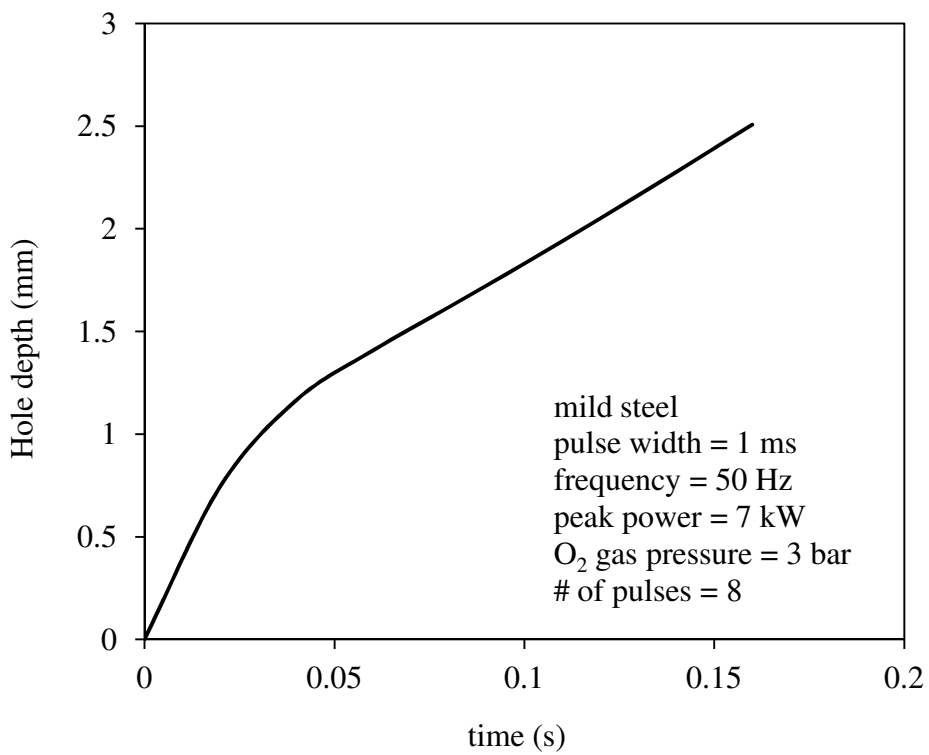
Figure 7.10 Predicted melt depth evolution as a function of time.
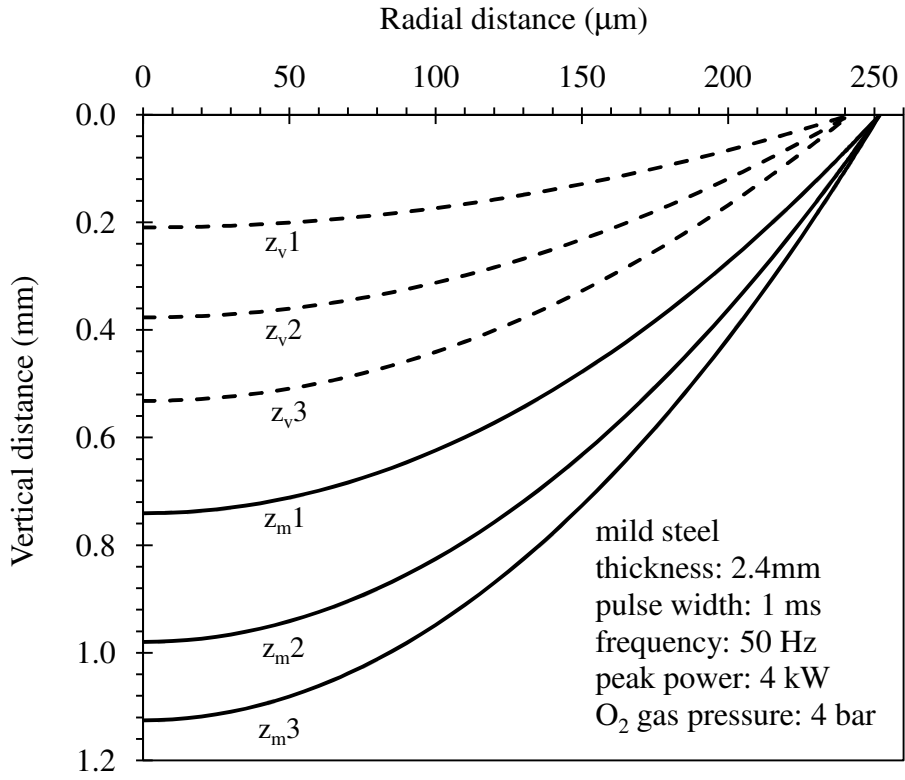
Figure 7.11 Predicted profiles of the solid-liquid and liquid-vapour interfaces after 1, 2 and 3 pulses (blind holes).
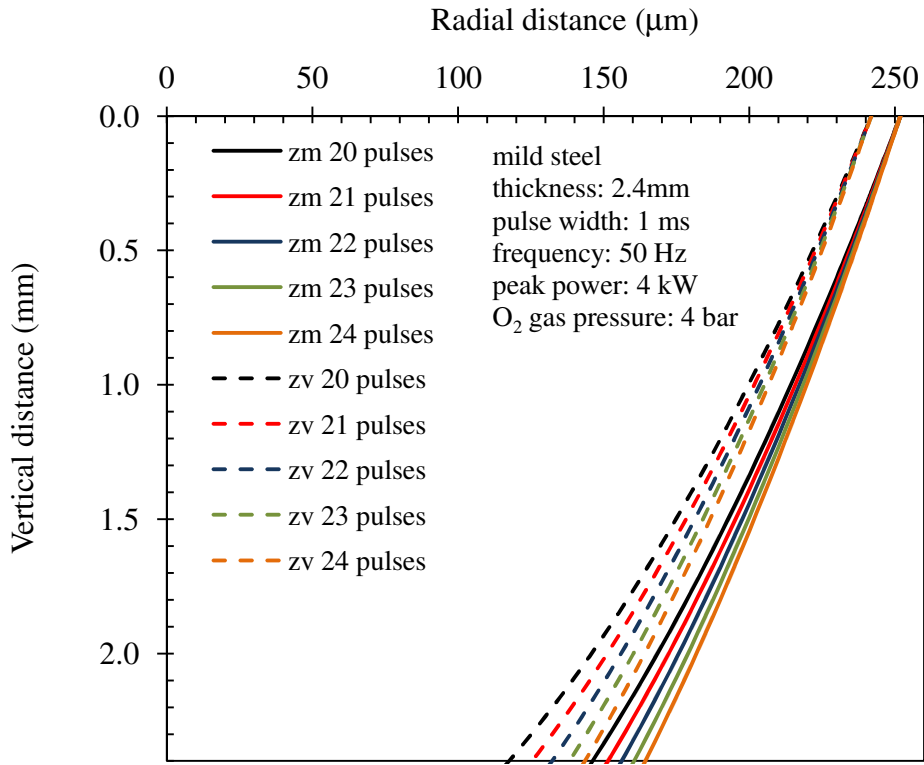
Figure 7.12 Predicted hole profiles after 20 to 24 pulses (through holes).
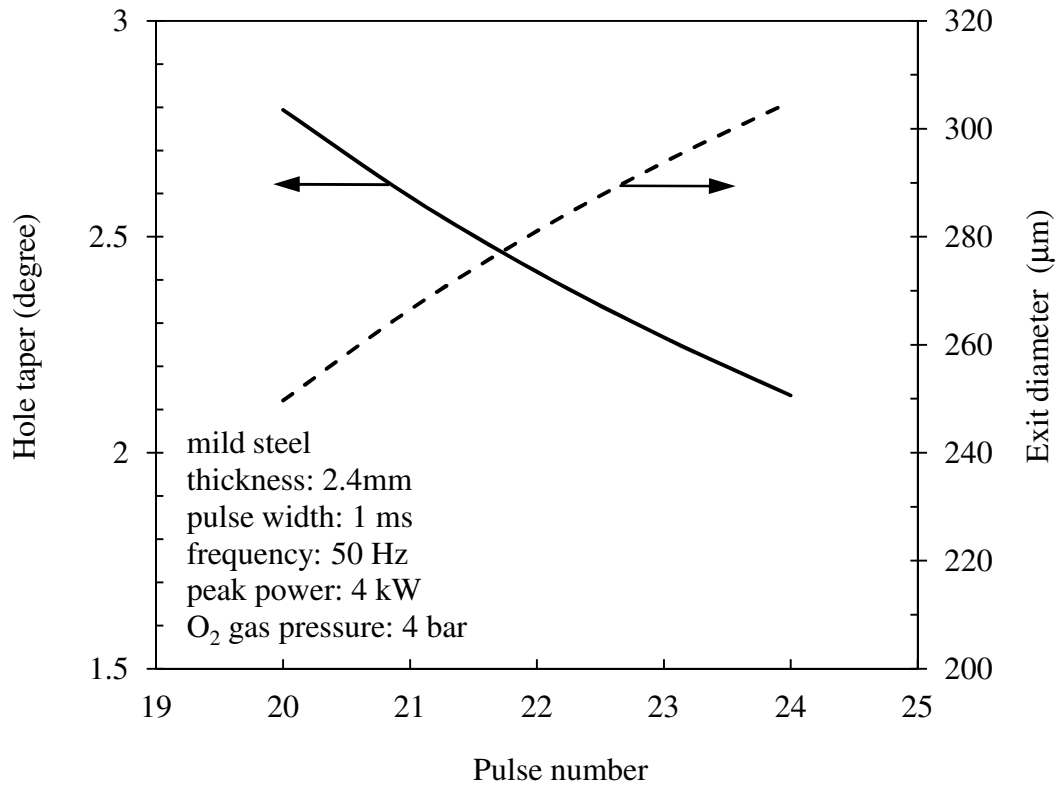
Figure 7.13 Predicted hole exit diameter and hole taper.

Due to a short time interval of the laser drilling process, the melt layer may not be completely expelled from the cavity. Once the irradiation is completed, the remaining liquid is solidified and forms the recast layer adhering to the hole wall. The presence of the recast layer is generally undesirable as it affects the hole geometrical and metallurgical qualities. An accurate prediction of the recast layer thickness is therefore crucial for laser percussion drilling applications.

Figures 7.14 and 7.15 show the predicted recast layer thickness of laser percussion drilled holes after irradiating with 12 and 17 pulses, respectively. It is found that the recast layer thickness is largest at the hole bottom and becomes smaller as it approaches the hole entrance. In case of drilling, melting proceeds mainly in z-direction. The liquid is therefore accumulated at the hole bottom before it is pushed up along the hole wall. During pulse off duration, the remaining liquid in the cavity is solidified, hence thicker recast layer at the hole bottom.
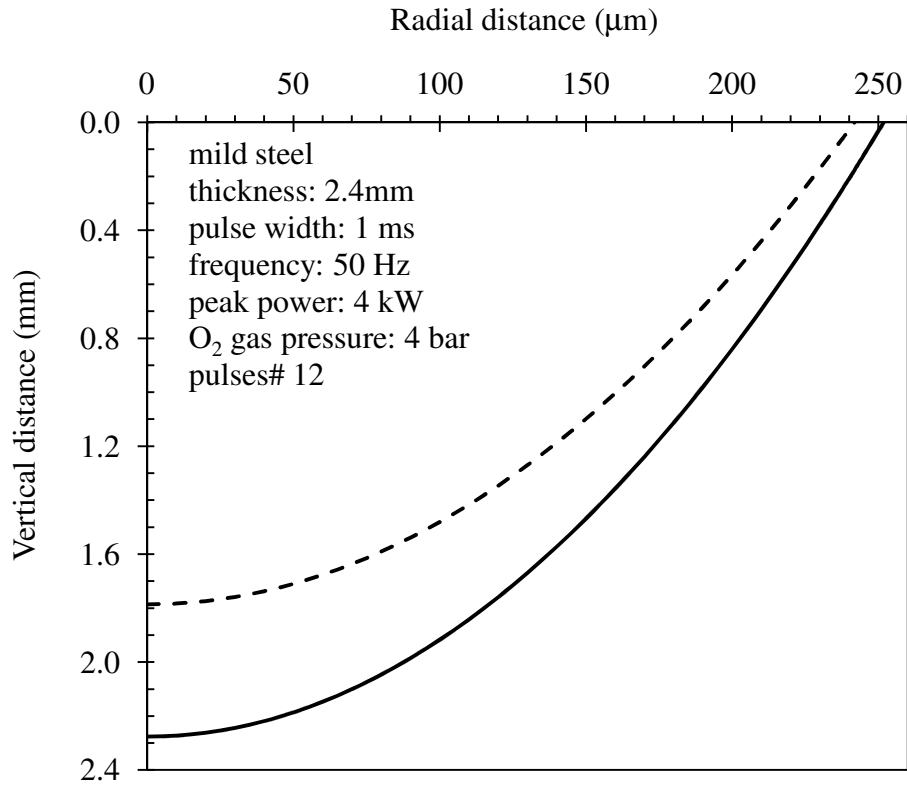
Figure 7.14 Predicted recast layer thickness after 12 pulses (blind hole).
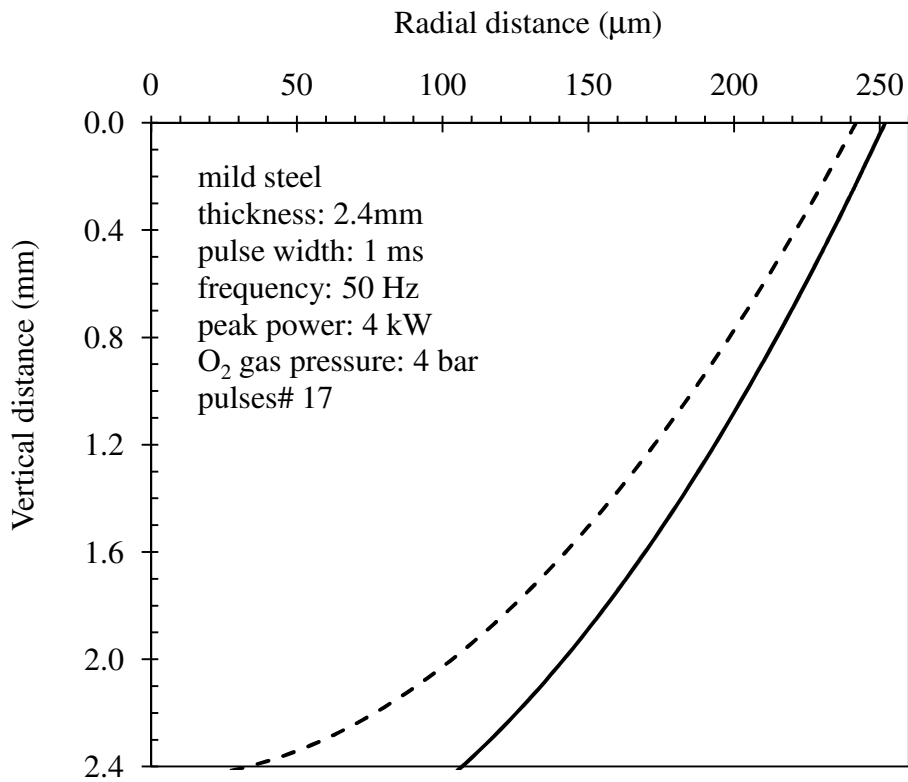
Figure 7.15 Predicted recast layer thickness after 17 pulses (through hole).
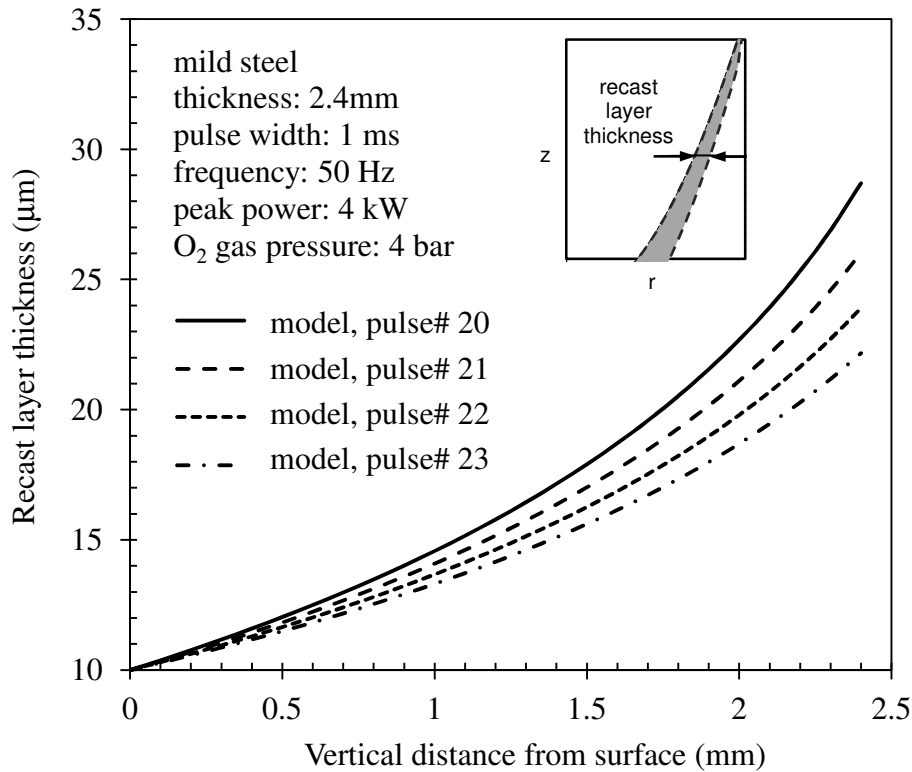
Figure 7.16 Variation of the predicted recast layer thickness for 20-23 laser pulses.

In case of a through hole as plotted in Figure 7.15, it can be expected that once the through hole has been achieved, the recast layer thickness would be significantly reduced. This is because the molten liquid accumulated at the hole bottom is flushed down the hole exit. Therefore, only wall recast layer is formed.

Number of pulses employed also influences the recast layer thickness. Figure 7.16 illustrates the variation of predicted wall recast layer thickness with vertical distance from the workpiece surface for 20-23 laser pulses. It is found that the recast layer thickness decreases as the number of pulses increases.

7.4 EFFECTS OF OPERATING PARAMETERS ON LASER DRILLED HOLE QUALITY

7.4.1 Peak power

Figure 7.17 shows predicted number of pulses required to initiate breakthrough at various values of peak power. It can be seen that as the peak power increases,

number of pulses required to generate a through hole is decreased. This is because at higher peak power, energy per pulse impinging onto the workpiece is higher; hence deeper hole depth per pulse.
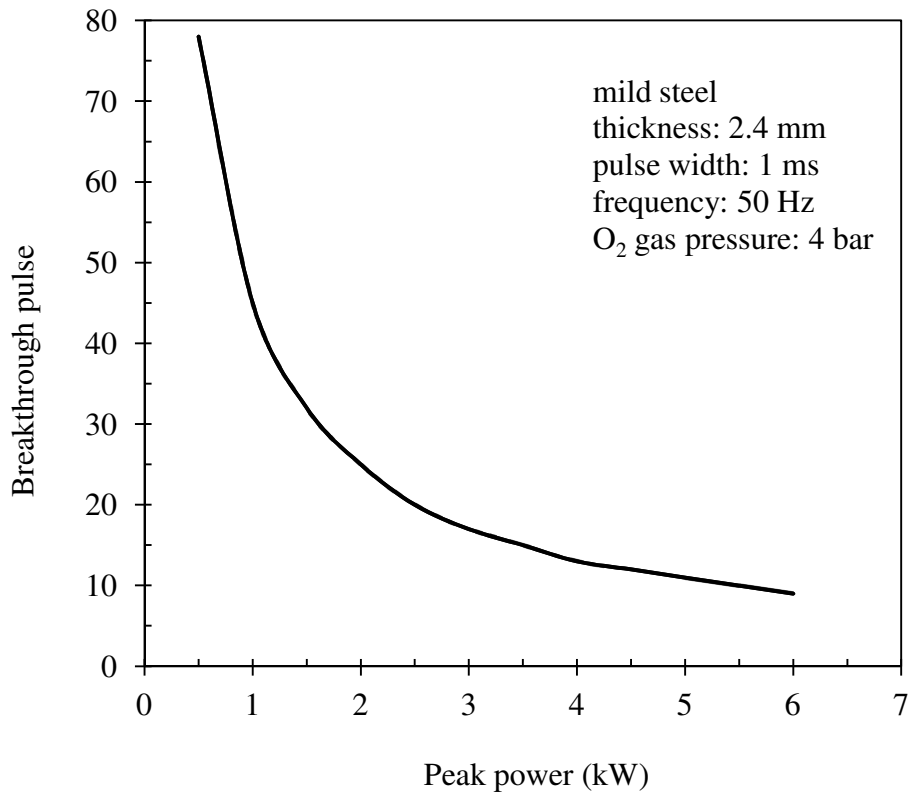
Figure 7.17 Number of pulses required to initiate breakthrough at various peak power values.

Effects of laser peak power on predicted hole exit diameter and hole taper are presented in Figure 7.18. These plots are obtained by using 30 laser pulses in the model. Figure 7.18 shows that as peak power increases, the exit diameter becomes larger, and the hole taper becomes smaller. In other words, the hole wall becomes more parallel as peak power increases. As discussed earlier, higher peak power requires less number of pulses to initiate breakthrough. Once breakthrough occurs, the subsequent laser pulses widen the hole diameter.
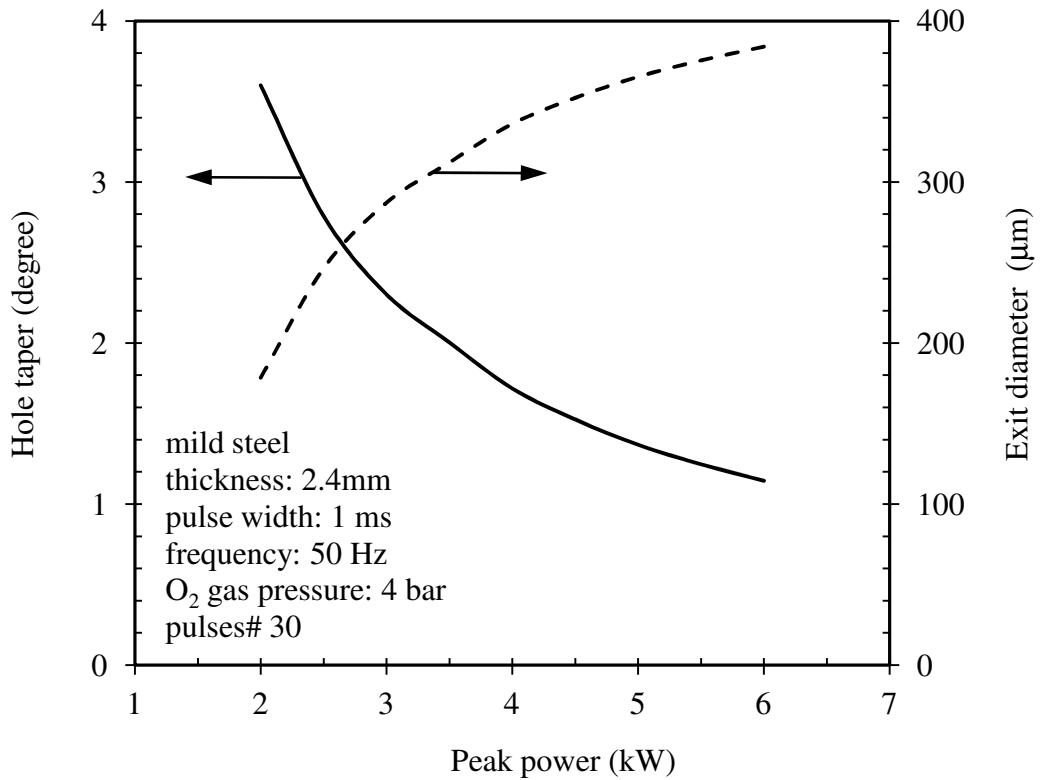
Figure 7.18 Effects of peak power on the predicted hole taper and exit diameter.
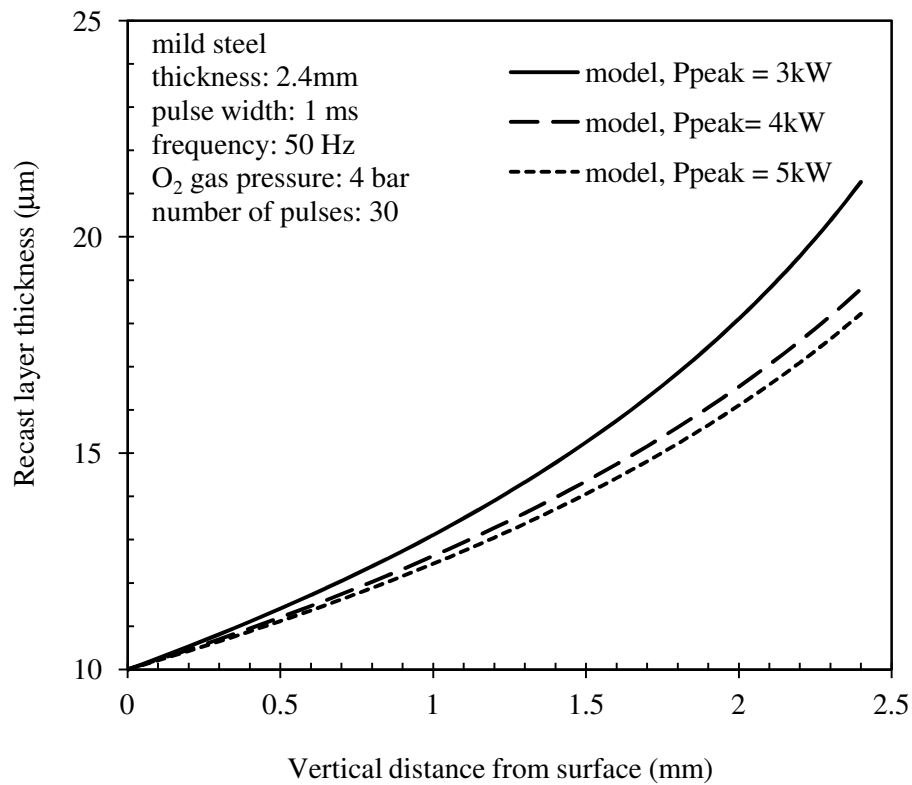
Figure 7.19 Effect of peak power on the predicted recast layer thickness.

In Figure 7.19, predicted recast layer thickness at various positions from the hole centre are plotted for 3, 4 and 5 kW peak power. It is obvious that as peak power increases, the recast layer thickness decreases. This is due to the fact that at high peak power, more vapour is formed in the cavity resulting in high recoil pressure at the liquid surface. The higher recoil pressure thereby expels more liquid from the cavity, hence smaller recast layer thickness.

7.4.2 Pulse width

Effect of pulse width on predicted hole depth is presented in Figure 7.20. It is obvious that by employing the same number of pulses, the longer pulse width produces a deeper hole. This is because, using the same pulse peak power, energy per pulse is larger for a longer pulse width. Hence, more laser energy is transferred to the substrate causing more melting and vaporisation, and thus enhances the drilling speed. Note that, by comparing the predicted hole depth in Figure 7.20 to that presented in Figure 7.9, although these are calculated using different input parameters, the number of pulses required to produce the same hole depth is not greatly different.
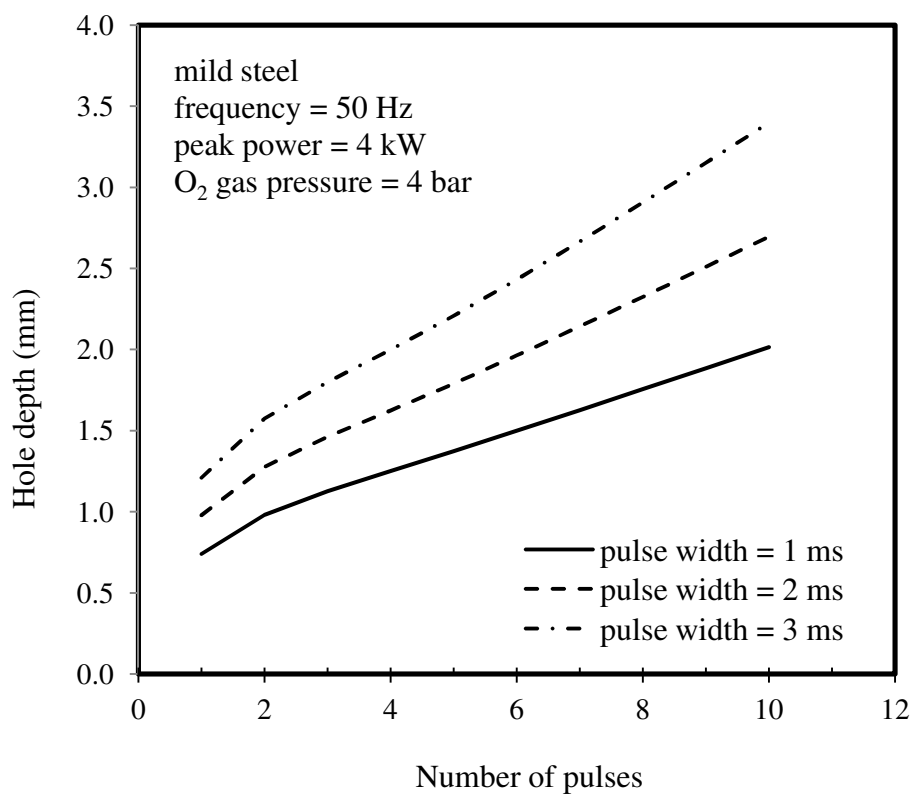
Figure 7.20 Predicted hole depth propagation for 1, 2 and 3 ms pulse widths.

Figure 7.21 Effects of pulse width on the predicted hole taper and exit diameter.
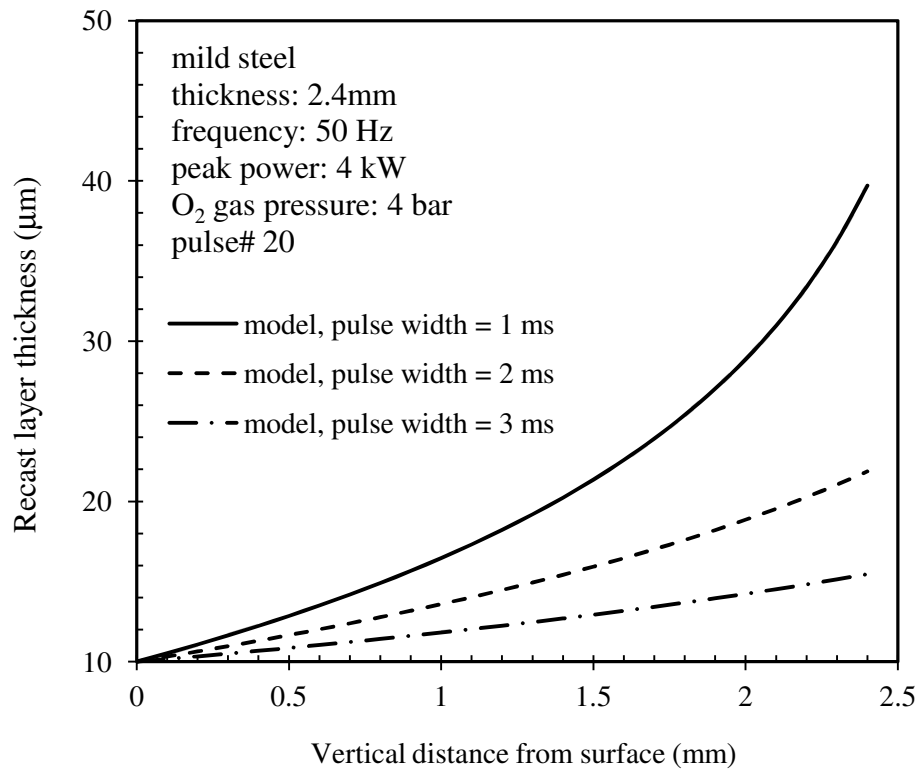
Figure 7.22 Effect of pulse width on the predicted recast layer thickness.

Effects of pulse width on predicted hole taper, exit diameter, and recast layer thickness are presented in Figures 7.21 and 7.22. It can be seen that as the pulse width increase, a smaller taper hole with thinner recast layer is produced. As explained earlier, for a particular number of pulses, a longer pulse width produces a deeper hole. Once a through hole is formed, the subsequent laser pulses thereby play the role of enlarging the hole exit diameter.

7.4.3 Pulse repetition frequency

The pulse frequency also plays its part in laser percussion drilling as it defines the pulse off duration between successive pulses. Figure 7.23 shows the effect of the laser pulse frequency on predicted hole depth. It can be seen that for a particular number of laser pulses, higher pulse frequency gives a deeper hole.

At high pulse frequency, due to very short pulse off duration, cooling during the pulse off time are smaller compared to the case of low pulse frequency. When a subsequent laser pulse hits the workpiece, less laser energy is required to raise the temperature of the existing liquid to the boiling point. The remaining energy is then spent on heating, melting, and vaporising new parent material. In other words, this leads to a higher penetration rate, thus producing a deeper hole.

The influence of pulse frequency on predicted hole taper and recast layer thickness are also presented in Figures 7.24 and 7.25, respectively. In Figure 7.25, it can be seen that the recast layer thickness increases with pulse frequency. This is due to the fact that, at high pulse frequency, the pulse off duration is too short to allow sufficient melt removal. The remaining liquid is therefore resolidified and adheres along the hole wall which contributes to a larger recast layer thickness. This is consistent with the experimental results reported by Leigh et al.[5].

It is worth mentioning that although pulse frequency influences the hole exit diameter, hole taper, and recast layer thickness, nevertheless changes in these hole quality characteristics are less pronounced compared to changes due to peak power and pulse width.
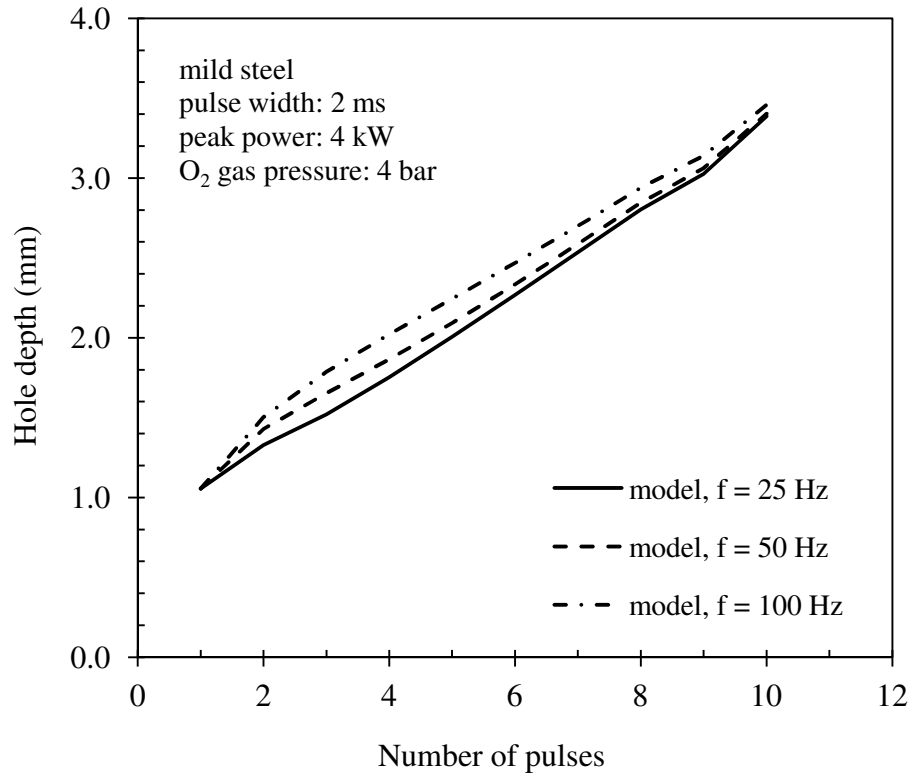
Figure 7.23 Effects of pulse frequency on the predicted hole depth.

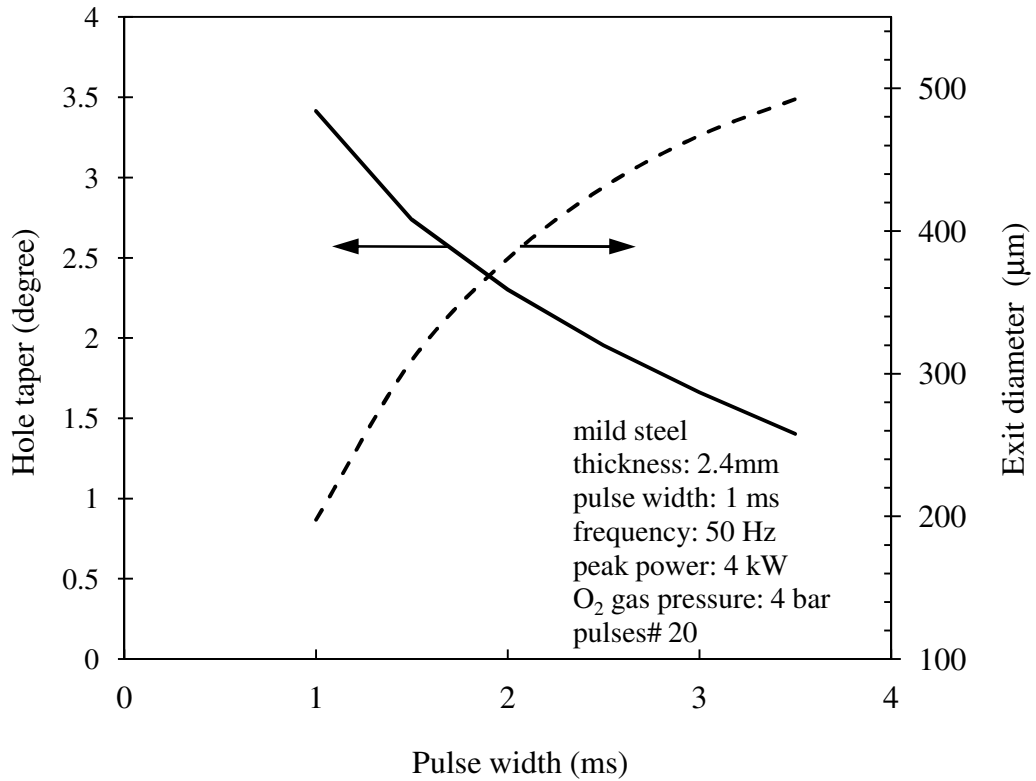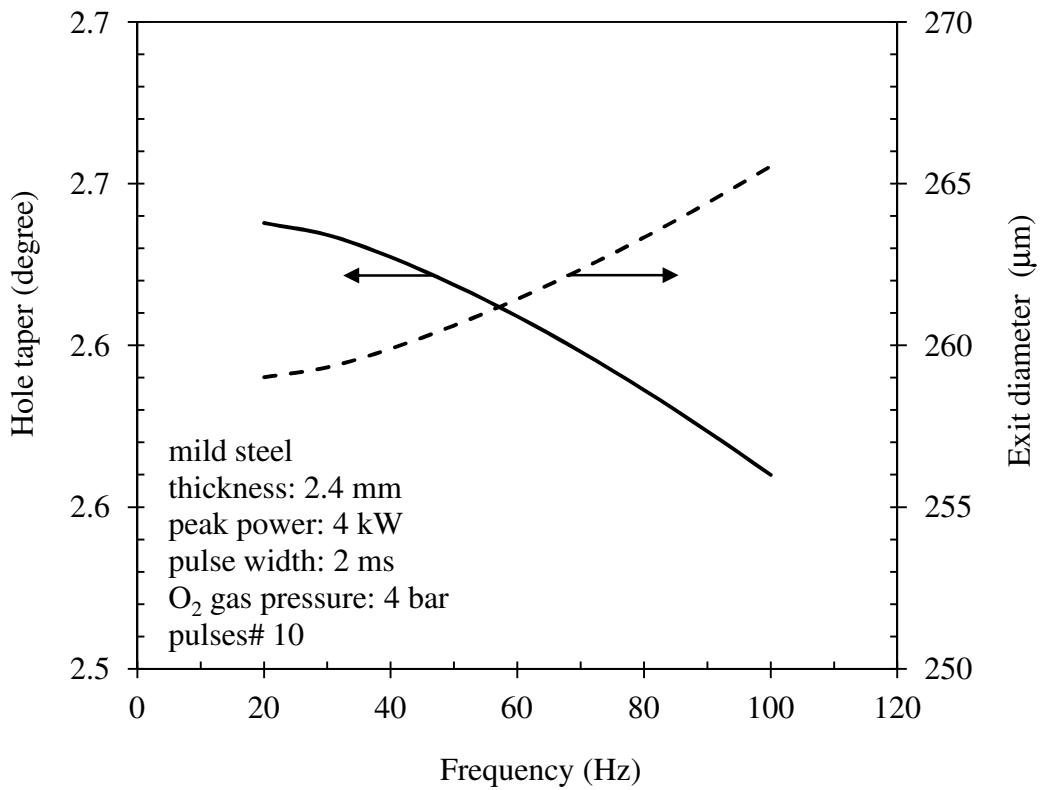Figure 7.24 Effects of pulse frequency on the predicted hole taper and exit diameter.
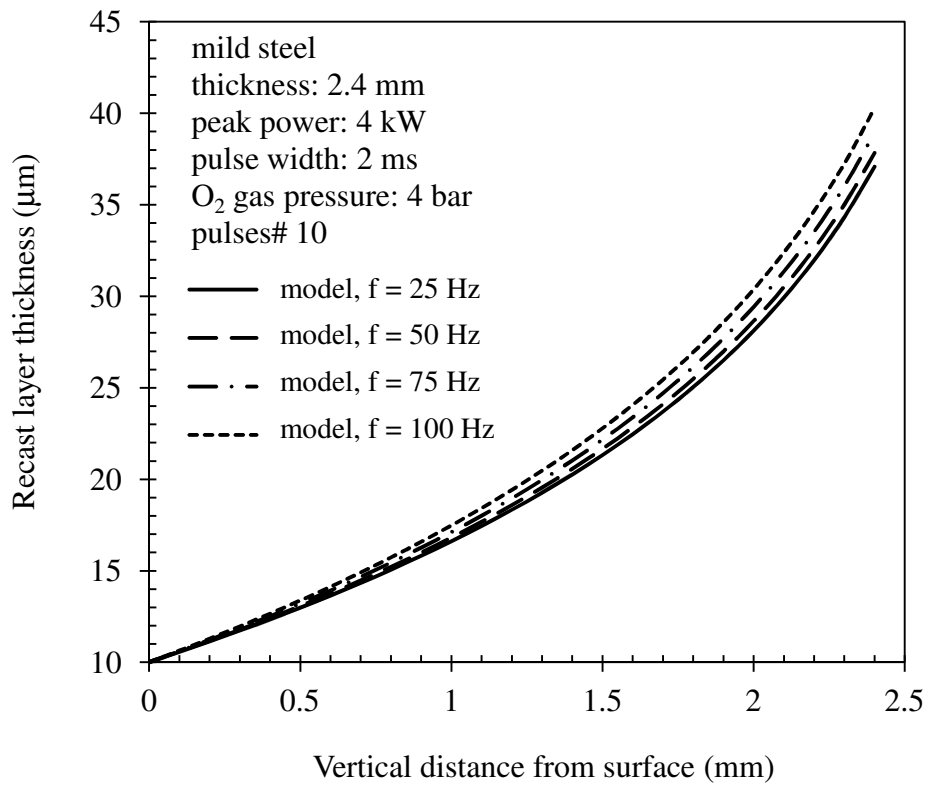
Figure 7.25 Effect of pulse frequency on the predicted recast layer thickness.

CHAPTER 8
CONCLUSION AND RECOMMENDATION FOR FUTURE WORK

8.1 CONCLUSION

In this research, a new mathematical model of multiple pulsed laser percussion drilling is developed. The new model accounts for the recoil pressure, exothermic reaction, melt ejection, O_2 assist gas effect, and solidification of the melt during laser pulse off period. These effects have been either ignored or not reported in previous studies. The governing equations are derived and solved by treating the laser drilling process as the Stefan problem at the solid-liquid and liquid-vapour interfaces. The Mathematica 7 Software is used to solve the resulting system of non-linear equations.

The newly developed model enables the prediction of the hole depth, number of pulses required to initiate breakthrough, hole profile, hole taper, and recast layer thickness. Comparisons with the experimental data show good agreement for the prediction of the hole depth, and not as good but acceptable predictions for the hole profile and recast layer thickness.

Effects of laser parameters, including number of pulses, peak power, pulse width, and pulse frequency, on laser percussion drilled hole quality are also investigated. The results show that:

- Number of pulses: once a through hole has been produced, further irradiation of laser pulse enlarges the exit hole diameter, making the hole taper and recast layer smaller.
- Peak power: the higher peak power gives a deeper hole, smaller hole taper, and thinner recast layer thickness.
- Pulse width: longer pulse width produces deeper hole, smaller hole taper, and thinner recast layer thickness.
- Pulse frequency: higher pulse frequency gives deeper hole, smaller hole taper, but thicker recast layer thickness.

In summary, the key contributions of this research work are:

1) Improvement is made in the models previously developed in literature by including more factors involved in multiple pulsed laser drilling. These are: recoil pressure, exothermic reaction, assist gas effects, and solidification.

2) The assumption of axi-symmetric parabolic profiles for representing the solid-liquid and liquid-vapour interfaces offers the benefit of dimension reduction in the analysis, whilst the hole geometry can still be adequately described. This remarkably reduces the complication of the full scale two-dimensional model in which a numerical approach is generally preferred.

3) For a particular application, where the desired hole geometry and material properties are specified, the developed model can be used to estimate the appropriate laser parameters for the process.

8.2 RECOMMENDATION FOR FUTURE WORK

In order to improve the accuracy of the laser drilling model developed and reported in this thesis, additional work is suggested. This may include both modelling and experimental work which is listed as follows:

Modelling work:

- Assumptions in the model can be reduced by incorporating more mechanisms involved in the actual laser drilling process into the model, such as multiple reflections of the laser beam along the hole wall, absorption of laser energy by the vapour and plasma, changes of the melting temperature and surface absorptivity due to oxide formed.

- Following the method of assuming an axi-symmetric parabolic profile presented in this thesis, development of a model using other hole profiles; which are similar to the actual hole geometry, would enhance the hole shape prediction. As the inlet cone was regularly observed in the experiments, a Gaussian hole profile should produce a good result.

- The melt surface temperature is assumed to be constant over the range of laser intensity in the current model. This produces some errors as can be expected. These errors would be reduced if the laser intensity dependent melt surface temperature is introduced in the model.

Experimental work:

- To fully assess the model accuracy, more experiments should be performed on a broader range of materials and operating parameters i.e. laser power, pulse width, pulse frequency, and gas pressure.

- Some of the inputs to the model are determined experimentally such as the recast layer thickness at the hole entrance and the degree of oxidation. To extend the developed model to include a wider range of operating conditions and materials, more experimental work would be required to more accurately define the inputs of the model.

APPENDIX A

SOURCE CODES FOR MATHEMATICA PROGRAMMING

This appendix provides the codes of the model developed in Mathematica 7 Software. Contents are divided into two sections; equation solving and calculation.

A.1 EQUATION SOLVING

ClearAll["Global`*"];

$zm[r\_, t\_] := zm0[t] - \frac{r^2 zm0[t]}{rb^2}$;

$zm[r\_, t\_] := zv0[t] - \frac{r^2 zv0[t]}{rv0^2}$;

(*Mass equation*)

$mass = \pi rbsc\rho s\sqrt{rb^2 + t^2 zm0'[t]^2} zm^{(0,1)}[r, t] =$
$$= \pi(rb^2 - rv0^2)Vm\rho l + \pi rv0sc\rho l\sqrt{rv0^2 + t^2 zv0'[t]^2} zv^{(0,1)}[r, t];$$

mass0 = mass/.$r \to 0$

$$\pi rbsc\rho szm0'[t]\sqrt{rb^2 + t^2 zm0'[t]^2} ==$$
$$\pi(rb^2 - rv0^2)Vm\rho l + \pi rv0sc\rho lzv0'[t]\sqrt{rv0^2 + t^2 zv0'[t]^2}$$

Solve[mass0, zv0'[t]]//Simplify

$$\{\{zv0'[t] \to -\frac{1}{\sqrt{2}}(\sqrt{(-1/(rv0^2 sc^2 t^2 \rho l^2)}) (rv0^4 sc^2 \rho l^2 + \sqrt{(rv0^2 sc^2 \rho l^2((rv0^6 sc^2}$$
$$+ 4rb^4 t^2 Vm^2 - 8rb^2 rv0^2 t^2 Vm^2 + 4rv0^4 t^2 Vm^2)\rho l^2$$
$$+ 4rb^4 sc^2 t^2 \rho s^2 zm0'[t]^2 + 4rb^2 sc^2 t^4 \rho s^2 zm0'[t]^4 + 8rb(-rb^2$$
$$+ rv0^2)sct^2 Vm\rho l\rho szm0'[t]\sqrt{rb^2 + t^2 zm0'[t]^2}))))\}, \{zv0'[t]$$
$$\to \frac{1}{\sqrt{2}}(\sqrt{(-1/(rv0^2 sc^2 t^2 \rho l^2)}) (rv0^4 sc^2 \rho l^2 + \sqrt{(rv0^2 sc^2 \rho l^2((rv0^6 sc^2}$$
$$+ 4rb^4 t^2 Vm^2 - 8rb^2 rv0^2 t^2 Vm^2 + 4rv0^4 t^2 Vm^2)\rho l^2$$
$$+ 4rb^4 sc^2 t^2 \rho s^2 zm0'[t]^2 + 4rb^2 sc^2 t^4 \rho s^2 zm0'[t]^4 + 8rb(-rb^2$$
$$+ rv0^2)sct^2 Vm\rho l\rho szm0'[t]\sqrt{rb^2 + t^2 zm0'[t]^2}))))\}, \{zv0'[t]$$
$$\to -\frac{1}{\sqrt{2}}(\sqrt{(1/(rv0^2 sc^2 t^2 \rho l^2)}) (-rv0^4 sc^2 \rho l^2 + \sqrt{(rv0^2 sc^2 \rho l^2((rv0^6 sc^2}$$
$$+ 4rb^4 t^2 Vm^2 - 8rb^2 rv0^2 t^2 Vm^2 + 4rv0^4 t^2 Vm^2)\rho l^2$$
$$+ 4rb^4 sc^2 t^2 \rho s^2 zm0'[t]^2 + 4rb^2 sc^2 t^4 \rho s^2 zm0'[t]^4 + 8rb(-rb^2$$
$$+ rv0^2)sct^2 Vm\rho l\rho szm0'[t]\sqrt{rb^2 + t^2 zm0'[t]^2}))))\}, \{zv0'[t]$$
$$\to \frac{1}{\sqrt{2}}(\sqrt{(1/(rv0^2 sc^2 t^2 \rho l^2)}) (-rv0^4 sc^2 \rho l^2 + \sqrt{(rv0^2 sc^2 \rho l^2((rv0^6 sc^2}$$
$$+ 4rb^4 t^2 Vm^2 - 8rb^2 rv0^2 t^2 Vm^2 + 4rv0^4 t^2 Vm^2)\rho l^2$$
$$+ 4rb^4 sc^2 t^2 \rho s^2 zm0'[t]^2 + 4rb^2 sc^2 t^4 \rho s^2 zm0'[t]^4 + 8rb(-rb^2$$
$$+ rv0^2)sct^2 Vm\rho l\rho szm0'[t]\sqrt{rb^2 + t^2 zm0'[t]^2})))))$$

$$zv0a'[t\_] := -\frac{1}{\sqrt{2}}(\sqrt{}(-1/(rv0^2 sc^2 t^2 \rho l^2))\,(rv0^4 sc^2 \rho l^2 + \sqrt{}(rv0^2 sc^2 \rho l^2((rv0^6 sc^2$$
$$+ 4rb^4 t^2 Vm^2 - 8rb^2 rv0^2 t^2 Vm^2 + 4rv0^4 t^2 Vm^2)\rho l^2$$
$$+ 4rb^4 sc^2 t^2 \rho s^2 zm0'[t]^2 + 4rb^2 sc^2 t^4 \rho s^2 zm0'[t]^4 + 8rb(-rb^2$$
$$+ rv0^2)sc t^2 Vm\rho l\rho s\, zm0'[t]\sqrt{rb^2 + t^2 zm0'[t]^2})))));$$

$$zv0b'[t\_] := \frac{1}{\sqrt{2}}(\sqrt{}(-1/(rv0^2 sc^2 t^2 \rho l^2))\,(rv0^4 sc^2 \rho l^2 + \sqrt{}(rv0^2 sc^2 \rho l^2((rv0^6 sc^2$$
$$+ 4rb^4 t^2 Vm^2 - 8rb^2 rv0^2 t^2 Vm^2 + 4rv0^4 t^2 Vm^2)\rho l^2$$
$$+ 4rb^4 sc^2 t^2 \rho s^2 zm0'[t]^2 + 4rb^2 sc^2 t^4 \rho s^2 zm0'[t]^4 + 8rb(-rb^2$$
$$+ rv0^2)sc t^2 Vm\rho l\rho s\, zm0'[t]\sqrt{rb^2 + t^2 zm0'[t]^2})))));$$

$$zv0c'[t\_] := -\frac{1}{\sqrt{2}}(\sqrt{}(1/(rv0^2 sc^2 t^2 \rho l^2))\,(-rv0^4 sc^2 \rho l^2 + \sqrt{}(rv0^2 sc^2 \rho l^2((rv0^6 sc^2$$
$$+ 4rb^4 t^2 Vm^2 - 8rb^2 rv0^2 t^2 Vm^2 + 4rv0^4 t^2 Vm^2)\rho l^2$$
$$+ 4rb^4 sc^2 t^2 \rho s^2 zm0'[t]^2 + 4rb^2 sc^2 t^4 \rho s^2 zm0'[t]^4 + 8rb(-rb^2$$
$$+ rv0^2)sc t^2 Vm\rho l\rho s\, zm0'[t]\sqrt{rb^2 + t^2 zm0'[t]^2})))));$$

$$zv0d'[t\_] := \frac{1}{\sqrt{2}}(\sqrt{}(1/(rv0^2 sc^2 t^2 \rho l^2))\,(-rv0^4 sc^2 \rho l^2 + \sqrt{}(rv0^2 sc^2 \rho l^2((rv0^6 sc^2$$
$$+ 4rb^4 t^2 Vm^2 - 8rb^2 rv0^2 t^2 Vm^2 + 4rv0^4 t^2 Vm^2)\rho l^2$$
$$+ 4rb^4 sc^2 t^2 \rho s^2 zm0'[t]^2 + 4rb^2 sc^2 t^4 \rho s^2 zm0'[t]^4 + 8rb(-rb^2$$
$$+ rv0^2)sc t^2 Vm\rho l\rho s\, zm0'[t]\sqrt{rb^2 + t^2 zm0'[t]^2})))));$$

$$(*a1[t\_] := Iabs + h(Tg - Tsat) + \frac{ks(T0 - Tm)}{2\sqrt{t\alpha s}}*)$$
$$(*a2[t\_] := (rv0^6 + 4rb^4 t^2 Vm^2 - 8rb^2 rv0^2 t^2 Vm^2 + 4rv0^4 t^2 Vm^2)*)$$
$$zv0'[t\_] := \frac{a1[t] + Hox\eta ox\rho l\, zm0'[t] - Lm\rho s\, zm0'[t]}{Lv\rho l};$$

CASE 1 : Solve zv0a'[t] and zv0'[t] from eqstefan.
$$zv0a'[t\_] := -\frac{1}{\sqrt{2}}(\sqrt{}(-\frac{1}{rv0^2 t^2 \rho l^2}(rv0^4 \rho l^2 + \sqrt{}(rv0^2 \rho l^2((a2[t])\rho l^2 + 4rb^4 t^2 \rho s^2 zm0'[t]^2$$
$$+ 4rb^2 t^4 \rho s^2 zm0'[t]^4 + 8rb(-rb^2$$
$$+ rv0^2)t^2 Vm\rho l\rho s\, zm0'[t]\sqrt{rb^2 + t^2 zm0'[t]^2})))));$$

Solve[zv0'[t] == zv0a'[t], zm0'[t]]//Simplify;

CASE 2 : Solve zv0b'[t] and zv0'[t] from eqstefan.
$$zv0b'[t\_] := \frac{1}{\sqrt{2}}(\sqrt{}(-\frac{1}{rv0^2 t^2 \rho l^2}(rv0^4 \rho l^2 + \sqrt{}(rv0^2 \rho l^2((a2[t])\rho l^2 + 4rb^4 t^2 \rho s^2 zm0'[t]^2$$
$$+ 4rb^2 t^4 \rho s^2 zm0'[t]^4 + 8rb(-rb^2$$
$$+ rv0^2)t^2 Vm\rho l\rho s\, zm0'[t]\sqrt{rb^2 + t^2 zm0'[t]^2})))));$$
Solve[zv0'[t] == zv0a'[t], zm0'[t]]//Simplify;

CASE 3 : Solve zv0c'[t] and zv0'[t] from eqstefan.

$$zv0c'[t\_] := -\frac{1}{\sqrt{2}}\left(\sqrt{\left(\frac{1}{rv0^2 t^2 \rho l^2}\left(-rv0^4 \rho l^2 + \sqrt{(rv0^2 \rho l^2((a2[t])\rho l^2 + 4rb^4 t^2 \rho s^2 zm0'[t]^2}\right.\right.\right.$$
$$+ 4rb^2 t^4 \rho s^2 zm0'[t]^4 + 8rb(-rb^2$$
$$\left.\left.\left.+ rv0^2)t^2 Vm\rho l\rho szm0'[t]\sqrt{rb^2 + t^2 zm0'[t]^2}\right)\right)\right)\right);$$

Solve[zv0'[t] == zv0c'[t], zm0'[t]]//Simplify;

CASE 4 : Solve zv0d'[t] and zv0'[t] from eqstefan.

$$zv0d'[t\_] := \frac{1}{\sqrt{2}}\left(\sqrt{(1/(rv0^2 sc^2 t^2 \rho l^2))(-rv0^4 sc^2 \rho l^2 + \sqrt{(rv0^2 sc^2 \rho l^2((a2[t])\rho l^2}}\right.$$
$$+ 4rb^4 sc^2 t^2 \rho s^2 zm0'[t]^2 + 4rb^2 sc^2 t^4 \rho s^2 zm0'[t]^4 + 8rb(-rb^2$$
$$\left.+ rv0^2)sct^2 Vm\rho l\rho szm0'[t]\sqrt{rb^2 + t^2 zm0'[t]^2})\right)\right);$$

zm = Solve[zv0'[t] == zv0d'[t], zm0'[t]]//Simplify ;
(*possible solutions are case4,   8 zm0'[t]are generated*)

(*Check for possible solutions*)
ClearAll["Global`*"];
Needs["PlotLegends`"]
zm0d1'[t_]:= $zm[[1]]$;
zm0d2'[t_]:= $zm[[2]]$;
zm0d3'[t_]:= $zm[[3]]$;
zm0d4'[t_]:= $zm[[4]]$;
zm0d5'[t_]:= $zm[[5]]$;
zm0d6'[t_]:= $zm[[6]]$;
zm0d7'[t_]:= $zm[[7]]$;
zm0d8'[t_]:= $zm[[8]]$;

ρs = 7800; (* kg/m^3 *)
ρl = 6980; (* kg/m^3 *)
ρv = 50;
cs = 628; (* J/kgK *)
cl = 748; (* J/kgK *)
αs = 0.014 * 10⁻³; (*thermal diffusivity , m^2/s *)
αl = 0.007 * 10⁻³; (*thermal diffusivity , m^2/s *)
ks = αs * ρs * cs; (*thermalconductivity , W/mK *)
kl = αl * ρl * cl; (*thermalconductivity , W/mK *)
Al = 1.05 * 0.22;
As = 0.22;
Lm = 276 * 10^3; (* J/kg *)
Lv = 6088 * 10^3; (* J/kg *)
Tm = 1808; (* K *)
Tb = 3100; (* K *)
T0 = 300;
Tg = 300;
R = 149.13; (* J/kg. K , Specific gas constant for steel*)
γ = 1.4; (*specific heat ratio*)
po = 101.325 * 10³; (*atmospheric pressure = 101.325 kPa*)
ma = 55.85(*atomic mass of Fe*);
kb = 5.67 * 10⁻⁸⁽* J/K, Stefan Boltzmann constant*);
I0 = Ppeak/(π * rb^2) ; (*I0 = 1.06952 * 10^10; (* W/m^2,
Iabs = AlI0;
dn = 1.5 * 10⁻³; (*nozzle exit diameter*)
zn = 5.8 * 10⁻³; (*nozzle − workpiece distance, = 5.8mm according to experiment*)

μg = 2.01 * 10^ − 5; (* $N.s$/m2 *)
kg = 0.0259; (* $W/m.K$ *)
Pr = 0.73;
vg = 377; (*gas flow velocity, m/s *)
ρg = 1.3007; (* m/s *)
Reynold = ρg * vg * 2 * rv0/μg;
Cc = 0.228;
nc = 0.73;
h1 = $\dfrac{kg}{2 * rv0}$ * Cc * (Reynold^nc) * (Pr^(1/3));
h = h1;
ceff = cs + $\dfrac{Lm}{Tm}$;
Aeff = Pi * rv0^2;
Arl = Pi * dn * zn;
pc = $(\dfrac{2}{\gamma + 1})^{\frac{\gamma}{\gamma-1}}$ * pi;
peff = pc * $\dfrac{Aeff}{Aeff + Arl}$;
pv = po * Exp[$\dfrac{Lv}{R}$ * ($\dfrac{1}{Tb}$ − $\dfrac{1}{Tsat}$)]
Vm = $\sqrt{\dfrac{2}{\rho l}}$ * (pv + peff);
ηox = 0.26; (*Forsteel*)
Hox = 4.354403587 * 10^6; (*Steel, J/kg, Hox = −242.758 kJ/mol, forsteel → 1mole
            = 55.75g*)
tv = 0.01923;
γ = 5/3 ; (*SeeRef#39, page3446*)
rv0 = rb − 10 * 10^{−6};
sc = 1.23;
zm0a[t_]: = NIntegrate[Vsl[t1], {t1, ti, t}];
zv0a[t_]: = NIntegrate[Vlv[t2], {t2, ti, t}];

Condition#1 :
ton = 0.0015;
Ppeak = 3000;
pi = 3 * 10^5;
Tsat = 3500; (*assumeTsat*)
f = 50;
toff = $\dfrac{1}{f}$ − ton;
ti = 3.210^{−6};
Plot[zm0d1′[t], {t, ti, ton}]
Plot[zm0d2′[t], {t, 0ti, ton}]
Plot[zm0d3′[t], {t, ti, ton}, AxesOrigin → {0,0}]
Plot[zm0d4′[t], {t, 13ti, ton}, AxesOrigin → {0,0}]
Plot[$t$zm0d4′[t], {t, 13ti, ton}, AxesOrigin−> {0,0}]
Plot[zm0d5′[t], {t, ti, ton}]
Plot[zm0d6′[t], {t, ti, ton}]
Plot[zm0d7′[t], {t, ti, ton}]
Plot[zm0d8′[t], {t, ti, ton}]
possible solution is zm0d4'[t]

A.2 CALCULATION

ClearAll["Global`*"];
Needs["PlotLegends`"];

sc = 1.23;

$a1[t\_] := Iabs + h(Tg - Tsat) + \dfrac{ks(T0 - Tm)}{2\sqrt{t\alpha s}}$

$a2[t\_] := (rv0^6 sc^2 + 4rb^4 t^2 Vm^2 - 8rb^2 rv0^2 t^2 Vm^2 + 4rv0^4 t^2 Vm^2)$

$Vsl04[t\_] := zm0d8'[t]$;

$Vlv0[t\_] := \dfrac{a1[t] + Hox\eta ox\rho lVsl04[t] - Lm\rho sVsl04[t]}{Lv\rho l}$;

$zm0a[t\_] := NIntegrate[Vsl04[t1], \{t1, ti, t\}];$

$zv0a[t\_] := NIntegrate[Vlv0[t2], \{t2, ti, t\}];$

During pulse off :

$Tw[t\_] := Tsat + (Tg - Tsat)(1 - Exp[\dfrac{h^2 \alpha lt}{kl^2}](1 - Erf[\dfrac{h\sqrt{\alpha lt}}{kl}]));$

$A[t\_] := \dfrac{-Tm + Tw[t]}{Erf[\dfrac{-x0 + 2\sqrt{t\sqrt{\alpha l\alpha s}}\xi}{2\sqrt{t\alpha l}}]}$;

$B[t\_] := \dfrac{-T0 + Tm}{Erfc[\dfrac{\sqrt{t\sqrt{\alpha l\alpha s}}\xi}{\sqrt{t\alpha s}}]}$;

$LHS[\xi\_, t\_] := \dfrac{\dfrac{e^{-\frac{\sqrt{\alpha l\alpha s}\xi^2}{\alpha s}}ks(T0 - Tm)}{\sqrt{t\alpha s}Erfc[\frac{\sqrt{t\sqrt{\alpha l\alpha s}}\xi}{\sqrt{t\alpha s}}]} + \dfrac{e^{-\frac{(-x0+2\sqrt{t\sqrt{\alpha l\alpha s}}\xi)^2}{4t\alpha l}}kl(-Tm + Tw[t])}{\sqrt{t\alpha l}Erf[\frac{-x0 + 2\sqrt{t\sqrt{\alpha l\alpha s}}\xi}{2\sqrt{t\alpha l}}]}}{\sqrt{\pi}}$;

$RHS[\xi\_, t\_] := \dfrac{Lm\sqrt{t\sqrt{\alpha l\alpha s}}\xi\rho s}{t}$;

$Tl[x\_, t\_] := Tw[t] - A[t]Erf[\dfrac{x - x0}{2\sqrt{\alpha lt}}];$

$Ts[x\_, t\_] := T0 + B[t]Erfc[\dfrac{x}{2\sqrt{\alpha st}}];$

$xm[t\_] := 2\sqrt{t\sqrt{\alpha l\alpha s}}\xi;$

$\rho s = 7800;$ (*kg/m3*)
$\rho l = 6980;$ (*kg/m3*)
$\rho v = 50;$
$cs = 628;$ (*J/kgK*)
$cl = 748;$ (*J/kgK*)
$\alpha s = 0.014 * 10^{-3};$ (*thermal diffusivity, m^2/s *)
$\alpha l = 0.007 * 10^{-3};$ (*thermal diffusivity, m^2/s *)

ks = αs * ρs * cs; (*thermal conductivity, W/mK*)
kl = αl * ρl * cl; (*thermal conductivity, W/mK*)
Al = 1.05 * 0.22;
As = 0.22;
Lm = 276 * 10^3; (*J/kg*)
Lv = 6088 * 10^3; (*J/kg*)
Tm = 1808; (*K*)
Tb = 3100; (*K*)
T0 = 300;
Tg = 300;
$R = 149.13$; (*$J/kg.K$, Specific gas constant for steel*)
$\gamma = 1.4$; (*specific heat ratio*)
po = $101.325 * 10^3$; (*atmospheric pressure = 101.325 kPa*)
ma = 55.85(*atomic mass of Fe*);
kb = $5.67 * 10^{-8}$(*J/K, Stefan Boltzmann constant*);
I0 = Ppeak/(π * rb^2); (*I0 = $1.06952 * 10^{10}$; (*$W/m2$,
Iabs = AlI0;
dn = $1.5 * 10^{-3}$; (*nozzle exit diameter*)
zn = $5.8 * 10^{-3}$; (*nozzle − workpiece distance,
               = 5.8mm according to our own experiment*)
μg = $2.01 * 10^{-5}$; (*$N.s/m2$*)
kg = 0.0259; (*$W/m.K$*)
Pr = 0.73;
vg = 377; (*gas flow velocity, m/s*)
ρg = 1.3007; (*m/s*)
Reynold = ρg * vg * 2 * rv0/μg;
Cc = 0.228;
nc = 0.73;
h1 = $\dfrac{\text{kg}}{2 * \text{rv0}}$ * Cc * (Reynold^nc) * (Pr^(1/3));
h = h1;
ceff = cs + $\dfrac{\text{Lm}}{\text{Tm}}$;
Aeff = Pi * rv0^2;
Arl = Pi * dn * zn;
pc = $(\dfrac{2}{\gamma + 1})^{\frac{\gamma}{\gamma-1}}$ * pi;
peff = pc * $\dfrac{\text{Aeff}}{\text{Aeff} + \text{Arl}}$;
pv = po * $\text{Exp}[\dfrac{\text{Lv}}{R} * (\dfrac{1}{\text{Tb}} - \dfrac{1}{\text{Tsat}})]$
Vm = $\sqrt{\dfrac{2}{\text{ρl}}}$ * (pv + peff);
ηox = 0.26; (*Forsteel*)
Hox = $4.354403587 * 10^6$; (*Steel, J/kg, Hox = −242.758 kJ/mol, forsteel → 1mole
               = 55.75g*)
tv = 0.01923;
$\gamma = 5/3$; (*SeeRef#39, page3446*)
rv0 = rb − $10 * 10^{-6}$;
sc = 1.23;
TT2[r_, t_] := $\dfrac{\text{Ppeak}}{2\text{Piαlρlclt}}$ $\text{Exp}[\dfrac{-r^2}{4αlt}]$;
(* The following codes give examples of the calculation for two conditions*)

Condition#1 :

Mild steel 2.4 mm thick
frequency = 50 Hz
pulse width = 1.5 ms
peak power = 3 kW
assist gas pressure = 3 bar
breakthough pulse: 13

Clear[ton, Ppeak, pi, Tsat, x0, ξ, xmi, tt, zm0ai2];

ton = 0.0015;
Ppeak = 3000;
pi = 3 * 10^5;
Tsat = 4000;
f = 50;
toff = $\frac{1}{f}$ − ton;
rb = 256.9610^{-6};

xmi = 0;
Data =
Grid[
Prepend[
Table[
{i
, tt = $N[i(1/f)]$
, zm0ai = zm0a[$i$ton] + xmi
, zv0ai = zv0a[$i$ton]
, x0 = zv0ai − zm0ai
, ξi = FindRoot[LHS[ξ, toff] == RHS[ξ, toff], {ξ, 0.1}]
; ξ = ξ/. ξi
, xm[toff]
, xmi = xmi + xm[toff]
; zm0ai2 = zm0ai + xm[toff]}
, {i, 1,13}]
, {"pulse number", "time (s)", "zm0ai (m)", "zv0ai (m)", "zv0ai
        − zm0ai (m)", "ξ", "xm(toff) (m)", "zm0ai2 (m)"}]
, Frame → All, Background → {None, {LightGray}}]

pulse number	time (s)	zm0ai (m)	zv0ai (m)	zv0ai-zm0ai (m)	
	\[Xi]	xm(toff) (m)	zm0ai2 (m)		
1	0.02	0.00114298	0.000246973	-0.000896004	-0.329922	-
0.00028238	0.000860598				
2	0.04	0.00147225	0.000435899	-0.00103635	-0.419518	-
0.000359065	0.00111319				
3	0.06	0.00159235	0.000609326	-0.000983025	-0.38626	-
0.000330599	0.00126175				
4	0.08	0.00167244	0.000774744	-0.000897693	-0.331039	-
0.000283336	0.0013891				
5	0.1	0.00175637	0.000935091	-0.000821276	-0.279573	-
0.000239286	0.00151708				
6	0.12	0.00185379	0.00109187	-0.000761915	-0.238326	-
0.000203983	0.0016498				

7	0.14	0.00196358	0.00124599	-0.000717595	-0.206826	-
0.000177022	0.00178656					
8	0.16	0.00208236	0.00139801	-0.000684348	-0.182808	-
0.000156465	0.00192589					
9	0.18	0.00220714	0.00154834	-0.000658798	-0.164126	-
0.000140476	0.00206666					
10	0.2	0.00233585	0.00169727	-0.000638571	-0.149201	-
0.000127701	0.00220814					
11	0.22	0.00246713	0.00184503	-0.000622103	-0.136962	-
0.000117225	0.00234991					
12	0.24	0.00260015	0.00199177	-0.000608374	-0.126697	-
0.00010844	0.00249171					
13	0.26	0.00273434	0.00213764	-0.000596702	-0.117928	-
0.000100935	0.00263341					

Export["Data. xls", Data, "Table"]

Condition#2

$Clear[ton, Ppeak, pi, Tsat, x0, \xi];$

$ton = 0.001;$

$Ppeak = 4000;$

$pi = 5 * 10\^5;$

$f = 50;$

$toff = \dfrac{1}{f} - ton;$

$ti = 3.210^{-6};$

$rb = 251.8510^{-6};$

$(*ton = 0.0005s, rb = 203.5110^{-6};$

$`ton = 0.001s, rb = 251.8510^{-6};$

$ton = 0.0015s, rb = 279.4510^{-6};$

$ton = 0.0018s, rb = 290.7710^{-6};$

$ton = 0.002s, rb = 296.7210^{-6};$

$ton = 0.0025s, rb = 307.2810^{-6};$

$ton = 0.003s, rb = 313.0210^{-6}s;$

$ton = 0.0035, rb = 31510^{-6};$

$*)$

$xmi = 0;$

$Data =$

$Grid[$

$Prepend[$

$Table[$

$\{i$

$, tt = N[i(1/f)]$

$, zm0ai = zm0a[iton] + xmi$

$, zv0ai = zv0a[iton]$

$, x0 = zv0ai - zm0ai$

$, \xi i = FindRoot[LHS[\xi, toff] == RHS[\xi, toff], \{\xi, 0.1\}]$

$; \xi = \xi /. \xi i$

$, xm[toff]$

$, xmi = xmi + xm[toff]$

$; zm0ai2 = zm0ai + xm[toff]\}$

$, \{i, 1, 13\}]$

, {"pulse number", "time (s)", "zm0ai (m)", "zv0ai (m)", "zv0ai
                − zm0ai (m)", "ξ", "xm(toff) (m)", "zm0ai2 (m)"}]
, Frame → All, Background → {None, {LightGray}}]

pulse number	time (s)	zm0ai (m)	zv0ai (m)	zv0ai-zm0ai (m)	ξ	xm(toff) (m)	zm0ai2 (m)
1	0.02	0.000894386	0.000209494	-0.000684892	-0.177395	-0.000153871	0.000740516
2	0.04	0.00124191	0.000377047	-0.000864865	-0.302184	-0.000262111	0.000979802
3	0.06	0.00137482	0.000532189	-0.00084263	-0.287296	-0.000249197	0.00112562
4	0.08	0.00146553	0.000680901	-0.000784633	-0.247751	-0.000214896	0.00125064
5	0.1	0.00155565	0.000825547	-0.000730104	-0.20965	-0.000181848	0.0013738
6	0.12	0.0016543	0.000967342	-0.000686962	-0.178885	-0.000155162	0.00149914
7	0.14	0.00176129	0.00110701	-0.000654279	-0.15522	-0.000134636	0.00162665
8	0.16	0.00187444	0.00124501	-0.000629429	-0.137022	-0.000118851	0.00175559
9	0.18	0.00199178	0.00138167	-0.000610109	-0.122754	-0.000106475	0.0018853
10	0.2	0.0021119	0.00151722	-0.000594681	-0.111283	-0.0000965259	0.00201538
11	0.22	0.00223389	0.00165185	-0.000582044	-0.101839	-0.0000883342	0.00214556
12	0.24	0.00235714	0.00178567	-0.000571468	-0.0939011	-0.0000814487	0.00227569
13	0.26	0.00248127	0.00191881	-0.000562459	-0.0871137	-0.0000755614	0.00240571
14	0.28	0.00260602	0.00205135	-0.000554671	-0.0812287	-0.0000704568	0.00253556
15	0.3	0.00273121	0.00218335	-0.000547858	-0.0760668	-0.0000659794	0.00266523

REFERENCES

[1]   A.Corcoran, L.Sexton, B.Seaman, P.Ryan, and G.Byrne, "The Laser Drilling of Multi-Layer Aerospace Material Systems," *Journal of Materials Processing Technology,* vol. 123, pp. 100-106, 2002.

[2]   Th.Maiman, "Stimulated Optical Radiation in Ruby," *Nature,* vol. 187, pp. 493-494, 1960.

[3]   C.Phipps, "Overview of Laser Applications: The State of the Art and the Future Trend," in *Proceedings of SPIE*, 2003, pp. 1-10.

[4]   W.M.Steen, "Laser Material Processing-An Overview," *Journal of Optics A: Pure and Applied Optics,* vol. 5, pp. S3-S7, 2003.

[5]   S.Leigh, K.Sezer, L.Li, C.Grafton-Reed, and M.Cuttell, "Statistical Analysis of Recast Formation in Laser Drilled Acute Blind Holes in CMSX-4 Nickel Superalloy," *International Journal of Advanced Manufacturing Technology,* vol. 43, pp. 1094-1105, 2009.

[6]   W.T.Silfvast, *Laser Fundamentals 2nd ed.* Cambridge: Cambridge University Press, 2004.

[7]   N.B.Dahotre and S.P.Harimkar, *Laser Fabrication and Machining of Materials*: Springer Science+Business Media, LLC, 2008.

[8]   R.Brown, *Lasers: A Survey of Their Performance and Applications*. London: Business Books, 1969.

[9]   J.T.Luxon, D.E.Parker, and P.D.Plotkowski, *Lasers in Manufacturing: An Introduction to the Technology*. Luton: IFS Publications and Springer-Verlag, 1987.

[10]   H.Haken, *Laser Theory*. Berlin: Springer, 1983.

[11]   J.F.Ready, *Industrial Applications of Lasers*. San Diego: Academic Press, 1997.

[12]   A.E.Siegman, *Lasers*. Oxford: Oxford University Press, 1986.

[13]   O.Svelto, *Principles of Lasers*, 4th ed. New York, London: Plenum Press, 1998.

[14]   Y.P.Kathuria, "Industrial Aspects of Nd-YAG Laser Microprocessing," in *Proceedings of SPIE*, 2001, pp. 113-118.

[15]   C.E.Webb and J.D.C.Jones, *Handbook of Laser Technology and Applications: Volume III-Applications*: Institute of Physics, 2004.

[16]   K.Du, J.Biesenbach, D.Ehrlichmann, U.Habich, U.Jarosch, J.Klein, P.Loosen, J.Niehoff, and R.Wester, "Lasers for Material Processing Specifications and Trends," *Optical and Quantum Electronics,* vol. 27, pp. 1089-1102, 1995.

[17]   J.Meijer, "Laser Beam Machining (LBM), State of the Art and New Opportunities," *Journal of Materials Processing Technology,* vol. 149, pp. 2-17, 2004.

[18]   A.K.Dubey and V.Yadava, "Laser Beam Machining - A Review," *International Journal of Machine Tools and Manufacture,* vol. 48, pp. 609-628, 2008.

[19]   W.Zhang and Y.L.Yao, "Laser Materials Processing," in *Manufacturing Engineering Handbook*, H.Geng, Ed., ed: McGraw-Hill Professional, 2004.

[20]   P.Denney, "Impact of Industrial Needs on Advances in Laser Technology," in *Proceedings of SPIE*, 2005, pp. 1-10.

[21] A.Schoonderbeek, C.A.Biesheuvel, R.M.Hofstra, K.J.Boller, and J.Meijer, "The Influence of the Pulse Length on the Drilling of Metals with an Excimer Laser," *Journal of Laser Applications,* vol. 16, pp. 85-91, 2004.

[22] Y.P.Kathuria, "Laser Material Interaction Technologies for Material Processing," *Proceedings of SPIE,* vol. 3573, pp. 88-95, 1998.

[23] K.Nagarathnam and K.M.B.Taminger, "Technology Assessment of Laser-Assisted Materials Processing in Space," *AIP Conference Proceedings,* vol. 552, pp. 153-160, 2001.

[24] F.J.Duarte and L.W.Hillman, *Dye Laser Principles with Applications.* Boston: Academic Press, 1990.

[25] D.C.O'Shea, W.R.Callen, and W.T.Rhodes, *An Introduction to Lasers and Their Applications.* Reading, Massachusetts, London: Addison-Wesley Publishing Company, 1978.

[26] V.Kovalenko, "Recent Developments in Laser Material Processing," in *Proceedings of SPIE*, 2004, pp. 424-435.

[27] J.C.J.Verhoeven, J.K.M.Jansen, and R.M.M.Mattheij, "Modelling Laser Induced Melting," *Mathematical and Computer Modelling,* vol. 37, pp. 419-437, 2003.

[28] J.J.Benes, "Technology Adds a New Twist to Difficult Drilling," *American Machinist,* vol. 140, pp. 78-79, 1996.

[29] C.Y.Yeo, S.C.Tam, S.Jana, and M.W.S.Lau, "A Technical Review of the Laser Drilling of Aerospace Materials," *Journal of Materials Processing Technology,* vol. 42, pp. 15-49, 1994.

[30] K.T.Voisey and T.W.Clyne, "Laser Drilling of Cooling Holes through Plasma Sprayed Thermal Barrier Coatings," *Surface & Coatings Technology* vol. 176, pp. 296-306, 2004.

[31] D.J.Majumdar and I.Manna, "Laser Processing of Materials," *Sadhana,* vol. 28, pp. 495-562, 2003.

[32] A.Ferguson, "Comparison of Drilling Rates and Tolerances of Laser-Drilled Holes in Solicon Nitride and Polyimide Vertical Probe Cards," Oxford Lasers Industrial Division, IEEE SW Test Workshop2008.

[33] F.Dausinger, "Laser Drilling with Short Pulses," *Proceedings of SPIE,* vol. 4184, pp. 519-524, 2001.

[34] F.Dausinger, H.Hugel, and V.Konov, "Micro-Machining with Ultrashort Laser Pulses: From Basic Understanding to Technical Applications," in *Proceedings of SPIE*, 2003, pp. 106-115.

[35] C.Fohl, D.Breitling, K.Jasper, J.Radtke, and F.Dausinger, "Precision Drilling of Metals and Ceramics with Short and Ultrashort Pulsed Solid State Lasers," in *Proceedings of SPIE*, 2002, pp. 104-107.

[36] J.F.Ready and D.F.Farson, *LIA Handbook of Laser Materials Processing.* Orlando: Laser Institute of America, 2001.

[37] H.Misawa and S.Juodkazis, *3D Laser Microfabrication: Principles and Applications.* Weinheim: Wiley-VCH, 2006.

[38] K.Verhoeven, "Modelling Laser Percussion Drilling," Eindhoven University, Bladel, 2004.

[39] P.W.French, D.P.Hand, C.Peters, G.J.Shannon, P.Byrd, and W.M.Steen, "Investigation of the Nd:YAG Laser Percussion Drilling Process using High Speed Filming " in *Proceedings of the ICALEO'98*, ed. Orlando, FL, USA: Laser Institute of America, 1998, pp. SectionB-ICAI.EO 1998 1-10.

[40] W.R.Smith, "Models for Solidification and Splashing in Laser Percussion Drilling," *SIAM Journal on Applied Mathematics,* vol. 62, pp. 1899-1923, 2001.

[41] N.D.Pandey, H.S.Shan, and T.Mohandas, "A New Model of Percussion Laser Drilling," *International Journal of Computer Applications in Technology,* vol. 6, pp. 218-232, 2006.

[42] N.Sanikommu, R.Bathe, and A.S.Joshi, "Detection of Breakthrough in Laser Percussion Drilling," *Lasers in Engineering,* vol. 17, pp. 361-369, 2007.

[43] A.Sona, "Metalic Materials Processing: Cutting and Drilling," in *Applied Laser Tooling*, O.D.D.Soares and M.Perez-Amor, Eds., ed Boston: Nijhoff, 1987, pp. 105-113.

[44] S.Sommer, F.Dausinger, P.Berger, and H.Hügel, "Aerodynamic Window for High Precision Laser Drilling," in *Proceedings of SPIE*, 2007.

[45] T.J.Weiting and J.L.DeRosa, "Effects of Surface Condition on the Infrared Absorptivity of 304 Stainless Steel," *Journal of Applied Physics,* vol. 50, pp. 1071-1078, 1979.

[46] L.K.Ang, Y.Y.Lau, R.M.Gilgenbach, and H.L.Spindler, "Analysis of Laser Absorption on a Rough Metal Surface," *Applied Physics Letter,* vol. 70, pp. 696-698, 1997.

[47] A.G.Grigoryants, *Basics of Laser Material Processing*. Boca Raton, Florida: CRC Press, 1994.

[48] W.M.Steen, *Laser Material Processing 3rd Edition*. London: Springer, 2003.

[49] C.A.McNally, J.Folkes, and I.R.Pashby, "Laser Drilling of Cooling Holes in Aeroengines: State of the Art and Future Challenges," *Materials Science and Technology,* vol. 20, pp. 805-813, 2004.

[50] R.K.Ganesh, W.W.Bowley, R.R.Bellantone, and Y.Hahn, "A Model for Laser Hole Drilling in Metals," *Journal of Computational Physics,* vol. 125, pp. 161-176, 1996.

[51] S.Basu and T.DebRoy, "Liquid Metal Expulsion during Laser Irradiation," *Journal of Applied Physics,* vol. 72, pp. 3317-3322, 1992.

[52] D.K.Y.Low, L.Li, and P.J.Byrd, "Hydrodynamic Physical Modeling of Laser Drilling," *Transactions of the ASME,* vol. 124, pp. 852-862, 2002.

[53] M.V.Allmen, "Laser Drilling Velocity in Metals," *Journal of Applied Physics,* vol. 47, pp. 5460-5463, 1976.

[54] B.S.Yilbas, "Study of Liquid and Vapor Ejection Processes during Laser Drilling of Metals," *Journal of Laser Applications,* vol. 7, pp. 147-152, 1995.

[55] R.K.Ganesh and A.Faghri, "A Generalized Thermal Modeling of Laser Drilling Process-I. Mathematical Modeling and Numerical Methodology," *International Journal of Heat and Mass Transfer,* vol. 40, pp. 3351-3360, 1997.

[56] R.K.Ganesh and A.Faghri, "A Generalized Thermal Modeling of Laser Drilling Process-II. Numerical Simulation and Results," *International Journal of heat and Mass Transfer,* vol. 40, pp. 3361-3373, 1997.

[57] B.S.Yilbas, "Experimental Study into Ejected Materials during Laser-Metal Interaction at Subatmospheric Pressures of Drilling Ambients," *Turkish Journal of Engineering and Environmental Science,* vol. 12, pp. 68-73, 1988.

[58] K.T.Voisey, S.S.Kudesia, W.S.O.Rodden, D.P.Hand, J.D.C.Jones, and T.W.Clyne, "Melt Ejection during Laser Drilling of Metals," *Materials Science and Engineering,* vol. 356, pp. 414-424, 2003.

[59]   P.S.Wei and L.R.Chiou, "Molten Metal Flow around the Base of a Cavity during a High-Energy Beam Penetrating Process," *Transactions of the ASME. Journal of Heat Transfer,* vol. 110, pp. 918-923, 1988.

[60]   G.Chryssolouris, *Laser Machining : Theory and Practice*. New York: Springer-Verlag, 1991.

[61]   X.Chen and H.Wang, "A Calculation Model for the Evaporation Recoil Pressure in Laser Material Processing," *Journal of Physics D: Applied Physics,* vol. 34, pp. 2637-2642, 2001.

[62]   M.Allmen and A.Blatter, *Laser Beam Interactions with Materials: Physical Principles and Applications*, 2nd updated ed. Berlin: Springer, 1995.

[63]   B.S.Yilbas, A.Z.Sahin, and R.Davies, "Laser Heating Mechanism Including Evaporation Process Initiating Laser Drilling," *International Journal of Machine Tools and Manufacture,* vol. 35, pp. 1047-1062, 1995.

[64]   F.W.Dabby and U.C.Paek, "High-Intensity Laser Induced Vaporization and Explosion of Solid Material," *IEEE Journal of Quantum Electronics,* vol. QE-8, pp. 106-111, 1972.

[65]   W.W.Duley and J.J.Gonsalves, "Interaction of CO_2 Laser Radiation with Solids. II. Drilling of Fused Quartz " *Canadian Journal of Physics,* vol. 50, pp. 216-221, 1972.

[66]   S.S.Kudesia, W.S.O.Rodden, D.P.Hand, P.Solana, and J.D.C.Jones, "Suitability of Laser Drilling Models Containing Melt Ejection Mechanisms," in *Proceedings of the ICALEO 2000*, 2000, pp. B-68-77.

[67]   W.S.O.Rodden, P.Solana, S.S.Kudesia, D.P.Hand, P.Kapadia, J.Dowden, and J.D.C.Jones, "Melt-Ejection Processes in Single Pulse Nd:YAG Laser Drilling," in *Proceedings of the ICALEO'99*, 2000, pp. C61-C69

[68]   C.L.Chan and J.Mazumder, "One-Dimensional Steady-State Model for Damage by Vaporization and Liquid Expulsion due to Laser-Material Interaction," *Journal of Applied Physics,* vol. 62, pp. 4579-4586, 1987.

[69]   V.Semak and A.Matsunawa, "The Role of Recoil Pressure in Energy Balance during Laser Materials Processing," *Journal of Physics D: Applied Physics,* vol. 30, pp. 2541-2552, 1997.

[70]   V.V.Semak, J.G.Thomas, and B.R.Campbell, "Melting Threshold and Melt Removal Dynamics during Laser Interaction with Steel and HgCdTe in Femtosecond Regime," in *Proceedings of SPIE*, 2004, pp. 448-453.

[71]   I.I.Ashmarin, Yu.A.Bykovskii, G.I.Kozin, A.B.Kostromin, and A.A.Chistyakov, "Recoil Impulse in Laser Impact," *Soviet Physics - Technical Physics,* vol. 24, pp. 1083-1085, 1979.

[72]   S.I.Anisimov, "Vaporization of Metal Absorbing Laser Irradiation," *Soviet Physics-JETP,* vol. 27, p. 182, 1968.

[73]   L.D.Landau and E.M.Lifshitz, *Satistical Physics, Part I*. Oxford: Pergamon, 1980.

[74]   S.I.Anisimov and V.A.Khokhlov, *Instabilities in Laser-Matter Interaction*. Boca Raton, London: CRC Press 1995.

[75]   N.D.Pandey, H.S.Shan, and A.Bharti, "Percussion Drilling with Laser: Hole Completion Criterion," *International Journal of Advanced Manufacturing Technology,* vol. 28, pp. 863-868, 2006.

[76]   S.Sankaranarayanan, H.Emminger, and A.Kar, "Energy Loss in the Plasma during Laser Drilling," *Journal of Physics D: Applied Physics,* vol. 32, pp. 1605-1611, 1999.

[77] M.Li, T.P.Duffey, and J.Mazumder, "Spatially and Temporally Resolved Temperature Measurements of Plasma Generated in Percussion Drilling with a Diode-Pumped Nd:YAG Laser," *Journal of Applied Physics,* vol. 84, pp. 4122-4127, 1998.

[78] O.N.Krokhin, "Modern Physical Principles of Laser Ablation," *Proceedings of SPIE,* vol. 4065, pp. 6-16, 2000.

[79] D.Breitling, A.Ruf, P.W.Berger, F.H.Dausinger, S.M.Klimentov, P.A.Pivovarov, T.V.Kononenko, and V.I.Konov, "Plasma Effects during Ablation and Drilling Using Pulsed Solid-State Lasers," in *Proceedings of SPIE*, 2003, pp. 24-33.

[80] T.V.Kononenko, S.M.Klimentov, S.V.Garnov, V.I.Konov, D.Breitling, C.Fohl, A.Ruf, J.Radtke, and F.Dausinger, "Hole Formation Process in Laser Deep Drilling with Short and Ultrashort Pulses," in *Proceedings of SPIE*, 2002, pp. 108-112.

[81] B.Tan, "Deep Micro Hole Drilling in a Silicon Substrate Using Multi-Bursts of Nanosecond UV Laser Pulses," *Journal of Micromechanics and Microengineering,* vol. 16, pp. 109-112, 2006.

[82] X.Zeng, S.S.Mao, C.Liu, X.Mao, R.Greif, and R.Russo, "Plasma Diagnostics during Laser Ablation in a Cavity," *Spectrochimica Acta - Part B Atomic Spectroscopy,* vol. 58, pp. 867-877, 2003.

[83] S.M.Klimentov, T.V.Kononenko, P.A.Pivovarov, S.V.Garnov, V.I.Konov, A.M.Prokhorov, D.Brightling, and F. Dausinger, "The Role of Plasma in Ablation of Materials by Ultrashort Laser Pulses," *Quantum Electronics,* vol. 31, pp. 378-382, 2001.

[84] A.Luft, U.Franz, A.Emsermann, and J.Kaspar, "A Study of Thermal and Mechanical Effects on Materials Induced by Pulsed Laser Drilling," *Applied Physics,* vol. A63, pp. 93-101, 1996.

[85] C.Li, S.R.Vatsya, and S.K. Nikumb, "Effect of Plasma on Ultrashort Pulse Laser Material Processing," *Journal of Laser Applications,* vol. 19, pp. 26-31, 2007.

[86] B.S.Yilbas, "The Absorption of Incident Beams during Laser Drilling of Metals," *Optics and Laser Technology,* vol. 18, pp. 27-32, 1986.

[87] B.S.Yilbas and Z.Yilbas, "Effects of Plasma on CO_2 Laser Cutting Quality," *Optics and Lasers in Engineering,* vol. 9, pp. 1-12, 1988.

[88] B.S.Yilbas, Z.Yilbas, and N.Akcakoyun, "Investigation into Absorption of the Incident Laser Beam during Nd:YAG Laser Processing of Metals," *Optics and Laser Technology,* vol. 28, pp. 503-511, 1996.

[89] A.Kar, T.Rockstroh, and J.Mazumder, "Two-Dimensional Model for Laser-Induced Materials Damage: Effects of Assist Gas and Multiple Reflections inside the Cavity," *Journal of Applied Physics,* vol. 71, pp. 2560-2569, 1992.

[90] D.Lacroix, A.G.Jeandel, and C.Boudot, "Spectroscopic Characterization of Laser-Induced Plasma Created during Welding with a Pulsed Nd:YAG Laser," *Journal of Applied Physics* vol. 81, pp. 6599-6606, 1997.

[91] E.O.S.Noguchi, W.R.Harp, J.Tu, and Y.Hirata, "Modeling of Laser Drilling Considering Multiple Reflection of Laser, Evaporation and Melt Flow," in *Proceedings of the ICALEO 2007*, Orlando, 2007, pp. 674-683.

[92] S.Ramanathan and M.F.Modest, "CW Laser Drilling of Composite Ceramics," in *Proceedings of the ICALEO'91*, 1992, pp. 305-326.

[93] H.Ki, P.Mohanty, and J.Mazumder, "Modeling of Laser Keyhole Welding: Part I. Mathematical Modeling, Numerical Methodology, Role of Recoil

Pressure, Multiple Reflections, and Free Surface Evolution," *Metallurgical and Materials Transactions A: Physical Metallurgy and Materials Science,* vol. 33, pp. 1817-1830, 2002.

[94]   H.Ki, P.Mohanty, and J.Mazumder, "Modeling of Laser Keyhole Welding: Part II. Simulation of Keyhole Evolution, Velocity, Temperature Profile, and Experimental Verification," *Metallurgical and Materials Transactions A: Physical Metallurgy and Materials Science,* vol. 33, pp. 1831-1842, 2002.

[95]   M.F.Modest, "Effects of Multiple Reflections on Hole Formation During Short-Pulsed Laser Drilling," *Journal of Heat Transfer,* vol. 128, pp. 653-661, 2006.

[96]   W.Han and R.J.Pryputniewicz, "Investigations of Laser Percussion Drilling of Small Holes on Thin Sheet Metals," in *Proceedings of SPIE*, 2004, pp. 31-40.

[97]   W.R.Smith, "Models for Solidification and Splashing in Laser Percussion Drilling," *SIAM Journal on Applied Mathematics,* vol. 62, pp. 1899-1923, 2002.

[98]   B.F.Scott, "Laser Machining and Fabrication-A Review," *Journal of Nuclear Materials,* vol. 2, pp. 335-339D, 1976.

[99]   B.S.Yilbas and A.Aleem, "Laser Hole Drilling Quality and Efficiency Assessment," *Proceedings of the Institution of Mechanical Engineers -- Part B -- Engineering Manufacture,* vol. 218, pp. 225-233, 2004.

[100] N.D.Pandey, H.S.Shan, and T.Mohandas, "Percussion Laser-Drilled Holes: Characteristics and Characterization Procedure," *Materials and Manufacturing Processes,* vol. 21, pp. 383-391, 2006.

[101] Th.Beck, G.Bostanjoglo, N.Kugler, K.Richter, and H.Weber, "Laser Beam Drilling Applications in Novel Materials for the Aircraft Industry," in *Proceedings of the ICALEO'97*, California, 1997, pp. 93-102.

[102] M.Ghoreishi, D.K.Y.Low, and L.Li, "Comparative Statistical Analysis of Hole Taper and Circularity in Laser Percussion Drilling," *International Journal of Machine Tools & Manufacture,* vol. 42, pp. 985-995, 2002.

[103] L.Li, D.K.Y.Low, and M.Ghoreshi, "Hole Taper Characterisation and Control in Laser Percussion Drilling," *CIRP Annals - Manufacturing Technology,* vol. 51, pp. 153-156, 2002.

[104] S.Bandyopadhyay, H.Gokhale, J.K.S. Sundar, G.Sundararajan, and S.V.Joshi, "A Statistical Approach to Determine Process Parameter Impact in Nd:YAG Laser Drilling of IN718 and Ti-6Al-4V Sheets," *Optics and Lasers in Engineering,* vol. 43, pp. 163-182, 2005.

[105] M.M.Okasha, P.T.Mativenga, and L.Li, "Sequential Laser Mechanical Microdrilling of Inconel 718 Alloy," *Journal of Manufacturing Science and Engineering,* vol. 133, pp. 011008-1-011008-8, 2011.

[106] M.Ghoreishi, D.K.Y.Low, and L.Li, "Hole Taper Control in Laser Percussion Drilling using Statistical Modelling " in *Proceedings of the ICALEO 2001*, Florida, 2001, pp. 344-352.

[107] B.S.Yilbas, "Parametric Study to Improve Laser Hole Drilling Process," *Journal of Materials Processing Technology* vol. 70, pp. 264-273, 1997.

[108] G.K.L.Ng and L.Li, "An Investigation into the Role of Melt Ejection in Repeatability of Entrance and Exit Hole Diameters in Laser Percussion Drilling " in *Proceedings of the ICALEO 2001*, Florida, 2001, pp. 296-305.

[109] G.K.L.Ng and L.Li, "The Effect of Laser Peak Power and Pulse Width on the Hole Geometry Repeatability in Laser Percussion Drilling," in *Proceedings of the ICLEO 2001*, Florida, 2001, pp. 393-402.

[110] M.Ghoreishi, D.K.Y.Low, and L.Li, "Effects of Processing Parameters on Hole Circularity in Laser Percussion Drilling-A Statistical Model," in *Proceedings of the ICALEO 2001*, Florida, 2001, pp. 326-333.

[111] H.K.Sezer, L.Li, M.Schmidt, A.J.Pinkerton, B.Anderson, and P.Williams, "Effect of Beam Angle on HAZ, Recast and Oxide Layer Characteristics in Laser Drilling of TBC Nickel Superalloys," *International Journal of Machine Tools & Manufacture,* vol. 46, pp. 1972-1982, 2006.

[112] S.Bandyopadhyay, J.K.S. Sundar, G.Sundararajan, and S.V.Joshi, "Geometrical Features and Metallurgical Characteristics of Nd:YAG Laser Drilled Holes in Thick IN718 and Ti-6Al-4V Sheets," *Journal of Materials Processing Technology,* vol. 127, pp. 83-95, 2002.

[113] C.Y.Chien and M.C.Gupta, "Pulse Width Effect in Ultrafast Laser Processing of Materials," *Applied Physics,* vol. A81, pp. 1257-1263, 2005.

[114] D.K.Y.Low, L.Li, and A.G.Corfe, "Effects of Assist gas on the Physical Characteristics of Spatter during Laser Percussion Drilling of Nimonic 263 Alloy," *Applied Surface Science,* vol. 154, pp. 689-695, 2000.

[115] D.K.Y.Low, L.Li, and P.J.Byrd, "The Effects of Process Parameters on Spatter Deposition in Laser Percussion Drilling," *Optics and Laser Technology,* vol. 32, pp. 347-354, 2000.

[116] D.K.Y.Low, L.Li, and A.G.Corfe, "The Influence of Assist Gas on the Mechanism of Material Ejection and Removal during Laser Percussion Drilling," *Proceedings of the Institution of Mechanical Engineers: Part B,* vol. 214, pp. 521-527, 2000.

[117] M.Ghoreishi and O.B.Nakhjavani, "Optimisation of Effective Factors in Geometrical Specifications of Laser Percussion Drilled Holes," *Journal of Materials Processing Technology,* vol. 196, pp. 303-310, 2008.

[118] W.K.Hamoudi and B.G.Rasheed, "Parameters Affecting Nd:YAG Laser Drilling of Metals," *International Journal for the Joining of Materials,* vol. 7, pp. 63-69, 1995.

[119] R.S.Patel and M.Q.Brewster, "Gas-Assisted Laser-Metal Drilling: Theoretical Model," *Journal of Thermophysics and Heat Transfer,* vol. 5, pp. 32-39, 1991.

[120] S.M.Klimentov, T.V.Kononenko, P.A.Pivovarov, S.V.Garnov, V.I.Konov, D.Breitling, and F.Dausinger, "Role of Gas Environment in the Process of Deep Hole Drilling by Ultra-Short Laser Pulses," in *Proceedings of SPIE*, 2003, pp. 515-519.

[121] G.K.L.Ng, P.L.Crouse, and L.Li, "An Analytical Model for Laser Drilling Incorporating Effects of Exothermic Reaction, Pulse Width and Hole Geometry," *International Journal of Heat and Mass Transfer,* vol. 49, pp. 1358-1374, 2006.

[122] L.M.Heglin, "Laser Drilling," in *The Industrial Laser Annual Handbook*, D.Belforte and M.Levitt, Eds., ed: Penn Well 1986, pp. 116-120.

[123] J.Powell, D.Petring, R.V.Kumar, S.O.Al-Mashikhi, A.F.H.Kaplan, and K.T.Voisey, "Laser-Oxygen Cutting of Mild Steel: the Thermodynamics of the Oxidation Reaction," *Journal of Physics D: Applied Physics,* vol. 42, pp. 1-11, 2009.

[124] J.N.Gonsalves and W.W.Duley, "Interaction of CO_2 Laser Radiation with Solids, I. Drilling of Thin Metallic Sheets," *Canadian Journal of Physics,* vol. 49, pp. 1708-1713, 1971.

[125] R.S.Patel and M.Q.Brewster, "Plume Formation and Low Power Nd:YAG Laser Metal Interaction," *Journal of Heat Transfer,* vol. 112, pp. 170-177, 1990.

[126] W.S.O.Rodden, S.S.Kudesia, D.P.Hand, and J.D.C.Jones, "Use of Assist Gas in the Laser Drilling of Titanium," *Journal of Laser Applications,* vol. 13, pp. 204-208, 2001.

[127] A.H.Khan, S.Celotto, L.Tunna, W.O'Neill, and C.J.Sutcliffe, "Influence of Microsupersonic Gas Jets on Nanosecond Laser Percussion Drilling," *Optics and Laser in Engineering,* vol. 45, pp. 709-178, 2007.

[128] X.Chen, W.T.Lotshaw, A.L.Ortiz, P.R.Staver, C.E.Erikson, and M.H.McLaughlin, "Laser Drilling of Advanced Materials: Effects of Peak Power, Pulse Format, and Wavelength," *Journal of Laser Applications,* vol. 8, pp. 233-239, 1996.

[129] X.Chen, A.L.Ortiz, P.R.Staver, W.T.Lotshaw, T.J.Rockstroh, and M.H.McLaughlin, "Improved Hole Drilling Using a High Peak Power Nd:YAG Laser at the Second Harmonic Wavelength," *Journal of Laser Applications,* vol. 9, pp. 287-290, 1997.

[130] J.James and P.Mike, "Deep Hole Drilling with Lasers," *Modern Machine Shop,* vol. 62, pp. 53-63, 1989.

[131] X.Chen, X.Liu, and W.T.Lotshaw, "Machining with Ultrashort Laser Pulses," in *Proceedings of the ICALEO'96*, 1996, pp. 64-71.

[132] T.J.Rockstroh, X.Chen, and W.T.Lotshaw, "Influence of Laser Pulse Duration on Laser Drilled Hole Quality in Nickel Based Super Alloy " in *Proceedings of the ICALEO'96*, Orlando, 1996, pp. 113-122.

[133] A.H.Wang, W.Y.Wang, Z.K.Bai, C.S.Xie, D.W.Zeng, and W.L.Song, "YAG Laser Percussion Drilling of a Functional Multi-Layer Thin Plate," *Optics and Laser Technology,* vol. 39, pp. 840-845, 2007.

[134] R.T.Brown and R.W.Frye, "High-Brightness Laser Cutting and Drilling of Aerospace Materials," in *Proceedings of the ICALEO'96*, Orlando, 1996, pp. 78-85.

[135] M.Ghoreishi, "Statistical Analysis of Repeatability in Laser Percussion Drilling," *International Journal of Manufacturing Technology,* vol. 29, pp. 70-78, 2006.

[136] K.Salonitis, A.Stournara, G.Tsoukantas, P.Stavropoulos, and G.Chryssolouris, "A Theoretical and Experimental Investigation on Limitations of Pulsed Laser Drilling," *Journal of Materials Processing Technology,* vol. 183, pp. 96-103, 2007.

[137] D.C.Hamilton and I.R.Pashby, "Hole Drilling Studies with a Variable Pulse Length CO_2 Laser," *Optics and Laser Technology,* vol. 8, pp. 183-188, 1979.

[138] S.O.Roos, "Laser Drilling with Different Pulse Shapes," *Journal of Applied Physics,* vol. 51, pp. 5061-5063 1980.

[139] M.Dimitrijevic and N.Konjevic, "The Importance of the Pulse Shape for the Laser-Beam Target Interaction," *Optics and Laser Technology,* vol. 12, pp. 145-147, 1980.

[140] J.Chen, F.J.Kahlen, and A.Kar, "Effects of Intrapulse Structure on Hole Geometry in Laser Drilling," *Journal of Laser Applications,* vol. 12, pp. 232-238, 2000.

[141] D.K.Y.Low, L.Li, and P.J.Byrd, "The Influence of Temporal Pulse Train Modulation during Laser Percussion Drilling," *Optics and Lasers in Engineering,* vol. 35, pp. 149-164, 2001.

[142] D.K.Y.Low and L.Li, "Effects of Inter-Pulse and Intra-Pulse Shaping during Laser Percussion Drilling," in *Proceedings of SPIE,* 2002, pp. 191-194.

[143] V.I.Mazhukin, M.G.Lobok, and I.Smurov, "Transient Effects in Pulsed Laser Irradiation," *Applied Surface Science,* vol. 253, pp. 7744-7748, 2007.

[144] A.C.Forsman, P.S.Banks, M.D.Perry, E.M.Campbell, A.L.Dodell, and M.S.Armas, "Double-Pulse Machining as a Technique for the Enhancement of Material Removal Rates in Laser Machining of Metals," *Journal of Applied Physics,* vol. 98, pp. 033302-1-6, 2005.

[145] C.Hartmann, A.Gillner, U.Aydin, R.Noll, T.Fehr, C.Gehlen, and R.Poprawe, "Investigation on Laser Micro Ablation of Metals Using Ns-Multi-Pulses," *Journal of Physics : Conference Series,* vol. 59, pp. 440-444, 2007.

[146] K.Walther, M.Brajdic, and E.W.Kreutz, "Enhanced Processing Speed in Laser Drilling of Stainless Steel by Spatially and Temporally Superposed Pulsed Nd:YAG Laser Radiation," *International Journal of Advance Manufacturing Technology,* vol. 35, pp. 895-899, 2008.

[147] M.Ostermeyer, P.Kappe, R.Menzel, S.Sommer, and F.Dausinger, "Laser Drilling in Thin Materials with Bursts of Ns-Pulses Generated by Stimulate Brillouin Scattering (SBS)," *Applied Physics A: Materials Science and Processing,* vol. 81, pp. 923-927, 2005.

[148] Y.F.Tzeng and F.C.Chen, "Effects of Operating Parameters on the Static Properties of Pulsed Laser Welded Zinc-Coated Steel," *International Journal of Advance Manufacturing Technology,* vol. 18, pp. 641-647, 2001.

[149] Y.Lin and G.G.Shi, "Minimization of Welding-Induced Alignment Distortion in Butterfly Laser Module Packages: a Study of Laser Pulse Shape," *Optical Engineering,* vol. 46, pp. 044302:1-5 2007.

[150] M.Ross, *Laser Applications: Volume 1.* New York: Academic Press, New York., 1971.

[151] S.V.Govorkov, E.V. Slobodtchikov, A.O. Wiessner, and D. Basting, "Effect of the Wavelength on High-Aspect Ratio Microdrilling of Steel with an All-Solid-State Laser," in *Proceedings of the ICLEO 2000: Postconference Edition*, 2000, pp. 580-581.

[152] M.Heglin, S.V.Govorkov, M.Scaggs, H.Theoharidis, and T.Schoelzel, "Short Pulse Width Micromachining of Hard Materials Using DPSS Nd:YAG Lasers," in *Proceedings of SPIE*, 2002, pp. 386-396.

[153] J.Wilson and J.F.B.Hawkes, *Lasers Principles and Applications.* Hertfordshire: Prentice Hall, 1987.

[154] R.W.Olson and W.C.Swope, "Laser Drilling with Focused Gaussian Beams," *Journal of Applied Physics,* vol. 72, pp. 3686-3696, 1992.

[155] S.Lazare and V.N.Tokarev, "A Laser Beam Model for High Performance Microdrilling," *Journal of Physics: Conference Series,* vol. 59, pp. 32-35, 2007.

[156] A.Gorur, C.Ciftlikli, and B.S.Yilbas, "Focusing for Laser Hole Drilling," *Optics and Lasers in Engineering,* vol. 18, pp. 349-369, 1993.

[157] J.C.Ion, *Laser Processing of Engineering Materials.* Oxford: Elsevier Butterworth-Heinemann, 2005.

[158] M.Polak, H.Chmelickova, M.Stranyanek, and L.Vasicek, "Modeling of Laser Cutting and Drilling," in *Proceedings of SPIE*, 2002, pp. 146-151.

[159] M.Schneider, L.Berthe, R.Fabbro, and M.Muller, "Measurement of Laser Absorptivity for Operating Parameters Characteristic of Laser Drilling Regime," *Journal of Physics D: Applied Physics,* vol. 41, pp. 1-6, 2008.

[160] J.F.Ready, "Material Processing-An Overview," in *Proceedings of the IEEE*, 1982, pp. 533-544.

[161] E.M.R.Silva, W.A.Monteiro, and W.Rossi, "Absorption of Nd:YAG Laser Beam by Metallic Alloys," *Journal of Materials Science Letters,* vol. 19, pp. 2095-2097, 2000.

[162] S.V.Garnov, V.I.Konov, A.S.Silenok, O.G.Tsarkova, and V.N.Tokarev, "Experimental Study of Temperature Dependence of Reflectivity and Heat Capacity of Steels and Alloys at Continous Wave Nd:YAG Laser Heating," in *Proceedings of SPIE*, 1997, pp. 160-175.

[163] Z.H.Shen, S.Y.Zhang, J.Lu, and X.W.Ni, "Mathematical Modeling of Laser Induced Heating and Melting in Solids," *Optics and Laser Technology,* vol. 33, pp. 533-537, 2001.

[164] H.Chmelickova and M.Polak, "Material Processing with Pulsed Nd:YAG Laser," in *Proceedings of SPIE*, 2001, pp. 358-363.

[165] H.S.Carslaw and J.C.Jaeger, *Conduction of Heat in Solids*. Newyork: Oxford University Press, 1959.

[166] Y.Zhang and A.Faghri, "Vaporization, Melting and Heat Conduction in the Laser Drilling Process," *International Journal of Heat and Mass Transfer,* vol. 42, pp. 1775-1790, 1999.

[167] Z.H.Shen and S.Y.Zhang, "Laser Heating of Thin Plate with Time-Dependent Absorptance " *Microwave and Optical Technology Letters,* vol. 28, pp. 364-367, 2001.

[168] M.K.El-Adawi, "Laser Melting of Solids-An Exact Solution for Time Intervals Less or Equal to the Transit Time," *Journal of Applied Physics,* vol. 60, pp. 2256-2259, 1986.

[169] J.Xie and A.Kar, "Mathematical Modeling of Melting during Laser Materials Processing," *Journal of Applied Physics,* vol. 81, pp. 3015-3022, 1997.

[170] I.Yu.Smurov, A.A.Uglov, A.M.Lashin, P.Matteazzi, V.Tagliaferri, and L.Covelli, "Movement of Phase Boundaries of Metals Subjected to Surface Periodic Energy Pulses," *Journal of Applied Physics,* vol. 69, pp. 8031-8036, 1991.

[171] C.Zhang, I.S.Salama, N.R.Quick, and A.Kar, "One-Dimensional Transient Analysis of Volumetric Heating for Laser Drilling," *Journal of Applied Physics,* vol. 99, pp. 113530-1-113530-10, 2006.

[172] P.Solana, P.Kapadia, J.M.Dowden, and P.J.Marsden, "An Analytical Model for the Laser Drilling of Metals with Absorption within the Vapour," *Journal of Physics D: Applied Physics,* vol. 32, pp. 942-952, 1999.

[173] J.P.Holman, *Heat Transfer*, 9th ed. Boston: McGraw-Hill, 2002.

[174] E.F.Obert, *Boundary Value Problems of Heat Conduction*: Scranton: International Textbook Company, 1968.

[175] E.Kreyszig, *Advanced Engineering Mathematics*, 9th ed. New York: Wiley, 2006.

[176] V.Alexiades and A.D.Solomon, *Mathematical Modeling of Melting and Freezing Processes*. Washington: Hemisphere Publishing Corporation, 1993.

[177] V.N.Tokarev and A.F.H.Kaplan, "An Analytical Modeling of Time Dependent Pulsed Laser Melting," *Journal of Applied Physics,* vol. 86, 1999.

[178] Z.Ling, Z.Zhi-Rong, and L.Jianglong, "Heat and Mass Transfer Model during Melting of Metal Induced by CW CO_2 Laser Irradiation," *Key Engineering Materials,* vol. 46-47, pp. 497-504, 1990.

[179] A.Kar and J.Mazumder, "Two-Dimensional Model for Material Damage due to Melting and Vaporization during Laser Irradiation," *Journal of Applied Physics,* vol. 68, pp. 3884-3891, 1990.

[180] B.Basu and J.Srinivasan, "Numerical Study of Steady-State Laser Melting Problem," *International Journal of Heat and Mass Transfer,* vol. 31, pp. 2331-2338, 1988.

[181] S.Shin and H.Chung, "Modeling of Melting, Evaporating, and Resolidifying Procedure in Laser-Induced Metal Processing," *Transactions of the ASME,* vol. 131, pp. 024501-1-024501-5, 2009.

[182] M.I.Cohen and J.P.Epperson, "Application of Lasers to Microelectronic Fabrication," *Advances in Electronics and Electron Physics,* pp. 139-186, 1968.

[183] J.M.Dowden, *The Mathematics of Thermal Modeling: An Introduction to the Theory of Laser Material Processing*. Florida: Chapman & Hall/CRC, 2001.

[184] D.Zeng, W.P.Latham, and A.Kar, "Two-Dimensional Model for Melting and Vaporization during Optical Trepanning," *Journal of Applied Physics,* vol. 97, pp. 104912-1-7, 2005.

[185] B.S.Yilbas, S.B. Mansoor, S.Z.Shuja, and H.Abualhamayel, "Laser Pulse Heating and Vapor Front Generation," *AIChE Journal,* vol. 54, pp. 627-638, 2008.

[186] S.Shin and H.Chung, "Modeling of Melting, Evaporating, and Resolidifying Procedure in Laser-Induced Metl Processing," *Journal of Manufacturing Science and Engineering,* vol. 131, pp. 024501-1-024501-5, 2009.

[187] V.V.Semak, B.R.Campbell, and J.G.Thomas, "On the Possible Effect of Pedestal Pulse on Material Removal by Ultrahigh Intensity Laser Pulses," *Journal of Physics D: Applied Physics,* vol. 39, pp. 3440-3449, 2006.

[188] S.E.S.A. El-Ghany, "On the Evaporation of a Semi-Infinite Target Induced by a Pulsed Laser," *Optics & Laser Technology,* vol. 38, pp. 77-86, 2006.

[189] D.A.McQuarrie and J.D.Simon, *Physical Chemistry - A Molucular Approach*. Sausalito, Calif: University Science Books, 1997.

[190] P.W.Atkins, *Physical Chemistry*, 7th ed. Oxford: Oxford University Press, 2002.

[191] J.Collins and P.Gremaud, "A Simple Model for Laser Drilling," *Mathematics and Computers in Simulation,* vol. 81, pp. 1541-1552, 2011.

[192] J.F.Ready, "Effects due to Absorption of Laser Radiation," *Journal of Applied Physics,* vol. 36, pp. 462-468, 1965.

[193] R.E.Wagner, "Laser Drilling Mechanics," *Journal of Applied Physics,* vol. 45, pp. 4631-4637, 1974.

[194] A.Ruf, P.Berger, F.Dausinger, and H.Hugel, "Analytical Investigations on Geometrical Influences on Laser Drilling," *Journal of Physics D: Applied Physics,* vol. 34, pp. 2918-2925, 2001.

[195] J.Dowden and P.Kapadia, "The Penetration Depth in Keyhole Welding with Pseudo-Continuous Nd-YAG and CO Lasers Investigated Mathematically," *Applied Surface Science,* vol. 106, pp. 235-239, 1996.

[196] I.Barin, *Thermochemical Data of Pure Substances*, 3rd ed. WeinHeim and New York: VCH, 1995.

[197]   Y.S.Toulokian, P.E.Liley, and S.C.Saxena, "Thermophysical Properties of Matter: Thermal Conductivity ". vol. 3, Y.S.Touloukian and C.Y.Ho, Eds., ed New York: IFI/Plenum, 1970.

[198]   Y.S.Toulokian, S.C.Saxena, and P.Hestermans, "Thermophysical Properties of Matter: Viscosity." vol. 11, Y.S.Touloukian and C.Y.Ho, Eds., ed New York: IFI/Plenum, 1970.

[199]   P.E.Liley, *Properties of Nonmetallic Fluid Elements, McGraw-Hill/CINDAS Data Series on Material Properties* vol. III-2. New York: McGraw-Hill, 1981.

[200]   D.Zipperian, "Chemical Etching," *PACE Technologies,* vol. 2, pp. 1-3, 2003.